

# **Layered and Composite Biopolymers: Mechanical, Physical and Antimicrobial Properties**

vorgelegt von

M.Sc.

**Hakan Kaygusuz**

geboren in Fatih, Türkei

von der Fakultät II - Mathematik und Naturwissenschaften  
der Technischen Universität Berlin  
zur Erlangung des akademischen Grades  
Doktor der Naturwissenschaften  
(Dr. rer. nat.)

genehmigte Dissertation

Promotionsausschuss:

Vorsitzender: Prof. Dr. Önder Pekcan (Kadir Has Universität)

Gutachterin: Prof. Dr. F. Bedia Erim Berker (Technische Universität Istanbul)

Gutachterin: Prof. Dr. Regine von Klitzing (Technische Universität Darmstadt)

Gutachter: Prof. Dr. Michael Gradzielski

Gutachter: Prof. Dr. Arne Thomas

Gutachterin: Prof. Dr. Huceste Giz (Technische Universität Istanbul)

Gutachterin: Assoc. Prof. Dr. Nevin Öztekin (Technische Universität Istanbul)

Tag der wissenschaftlichen Aussprache: 6. Juni 2017

**Berlin 2017**



*To my family,*



## **FOREWORD**

I would like to express my gratitude to my supervisors, Prof. Dr. F. Bedia Erim Berker and Prof. Dr. Regine von Klitzing for giving me the opportunity to work in their research groups. I am grateful for their academic guidance and motivation.

I thank Prof. Dr. Önder Pekcan, Prof. Dr. Michael Gradzielski, Prof. Dr. Arne Thomas, Prof. Dr. Huceste Giz and Assoc. Prof. Dr. Nevin Öztekin for evaluating this thesis. I also thank Dr. Gülşen Akin Evingür for her scientific support.

I would like to thank Dr. Hakan Bildirir, Dr. Züleyha Yenice Campbell, Dr. Samantha Micciulla, Dr. Salomé Vargas Ruíz, Dr. Maximilan Zerbball, Burcu Altın, Esra Oğuztürk, Dimitri Stehl, Sebastian Schön, Weina Wang, Ceyhun Yalçın, Dr. Tolga Müderrisoğlu, Thami Elboukhari, Ahmet Durmaz, Kerem Turhan, Zeynep Kalaycıoğlu, Nilay Kahya, Semira Bener, Sirun Özçelik, Dr. Ali Türkoğlu, Özgür Beyazıt and all other of my friends and colleagues in ITU Erim Lab and Stranski-Laboratorium TU Berlin for creating a pleasant atmosphere. I thank Lara Schäfer, Petra Erdmann, Maria Bülth and Fatih Şimşit for their help in bureaucratic paperwork.

I would like to acknowledge the support from The Scientific and Technological Research Council of Turkey (TÜBİTAK) – BİDEB 2214/B joint doctoral scholarship programme.

Finally, my special thanks go to my family, Üstün and Emel Kaygusuz for their love and support.

March 2017

Hakan KAYGUSUZ





## TABLE OF CONTENTS

	<u>Page</u>
<b>FOREWORD</b> .....	<b>ix</b>
<b>TABLE OF CONTENTS</b> .....	<b>viii</b>
<b>ABBREVIATIONS AND SYMBOLS</b> .....	<b>x</b>
<b>LIST OF TABLES</b> .....	<b>xii</b>
<b>LIST OF FIGURES</b> .....	<b>xiv</b>
<b>SUMMARY</b> .....	<b>xviii</b>
<b>ZUSAMMENFASSUNG</b> .....	<b>xx</b>
<b>ÖZET</b> .....	<b>xxii</b>
<b>1. INTRODUCTION</b> .....	<b>1</b>
1.1 Motivation .....	1
1.2 Outline .....	1
<b>2 SCIENTIFIC BACKGROUND</b> .....	<b>3</b>
2.1 Chitosan.....	3
2.2 Alginate.....	4
2.2.1 Drug delivery .....	7
2.2.2 Modeling of delivery.....	8
2.2.3 Waste removal .....	9
<b>3 EFFECTS OF SURFACTANTS AND CROSSLINKERS ON MECHANICAL PROPERTIES OF ALGINATE HYDROGELS</b> .....	<b>11</b>
3.1 Introduction.....	11
3.2 Materials and Methods .....	12
3.2.1 Preparation of gel beads .....	12
3.2.2 Compression measurements.....	13
3.2.3 Calculations .....	13
3.3 Results .....	14
3.4 Discussion .....	19
<b>4 EFFECT OF ANIONIC SURFACTANT ON ALGINATE-CHITOSAN POLYELECTROLYTE MULTILAYERS</b> .....	<b>22</b>
4.1 Introduction.....	22

4.2	Materials and Methods .....	23
4.2.1	Preparation of polyelectrolyte multilayers .....	24
4.2.2	Characterization .....	25
4.3	Results .....	30
4.4	Discussion .....	37
<b>5</b>	<b>PREPARATION OF CERIUM ALGINATE–CHITOSAN FILMS AS POTENT WOUND DRESSING AGENTS .....</b>	<b>39</b>
5.1	Introduction.....	39
5.2	Materials and Methods .....	40
5.2.1	Preparation of the film samples .....	40
5.2.2	Preparation of inoculums .....	42
5.2.3	Characterization .....	42
5.2.4	Antibacterial activity.....	44
5.3	Results and Discussion .....	44
5.3.1	Characterization .....	44
5.3.2	Antibacterial activities .....	47
<b>6</b>	<b>BIBLIOGRAPHY .....</b>	<b>49</b>
	<b>APPENDICES .....</b>	<b>58</b>
	APPENDIX A: SUPPORTING INFORMATION FOR CHAPTER 3.....	58
	APPENDIX B: SUPPORTING INFORMATION FOR CHAPTER 4.....	73
	APPENDIX C: SUPPORTING INFORMATION FOR CHAPTER 5.....	81

## ABBREVIATIONS AND SYMBOLS

<b>Alg</b>	: Alginate
<b>Chi</b>	: Chitosan
<b>PEI</b>	: Polyethyleneimine
<b>SDS</b>	: Sodium dodecyl sulfate
<b>cmc</b>	: Critical micelle concentration
<b>LbL</b>	: Layer by layer
<b>PE</b>	: Polyelectrolyte
<b>PEM</b>	: Polyelectrolyte multilayer
<b>SR</b>	: Swelling ratio
<b>DL</b>	: Double layer
<b>F</b>	: Force
<b>C</b>	: Concentration
<b>t</b>	: Time
<b>f</b>	: Frequency
<b>m</b>	: Mass
<b>R</b>	: Radius
<b>H</b>	: Displacement
<b>v</b>	: Poisson's ratio
<b>D</b>	: Dissipation



## LIST OF TABLES

	<u>Page</u>
<b>Table 3.1:</b> Effects of crosslinker, alginate and surfactant concentrations on bead diameter. Concentrations are given in <i>times cmc</i> . .....	16
<b>Table 4.1 :</b> Effect of sodium chloride concentration on thickness. ....	32
<b>Table 4.2 :</b> Effect of SDS concentration on thickness of the 6-DL samples. $C_{\text{NaCl}} = 100$ mmol/L. ....	32
<b>Table 5.1</b> Mechanical properties and <i>SR</i> values of the samples .....	44
<b>Table B.1 :</b> Thickness values of the all PEM samples (calculated from ellipsometry data).....	73
<b>Table B.2 :</b> Parameters of XRR fits.....	74
<b>Table B.3 :</b> Swelling ratio (SR) values of the PEM samples .....	74



## LIST OF FIGURES

	<u>Page</u>
<b>Figure 2.1</b> : Structures of N-Acetylglucosamine and chitin (top) and chitosan (bottom).....	3
<b>Figure 2.2</b> : Structures of alginic acid (top) and sodium alginate (bottom) .....	5
<b>Figure 2.3</b> : Egg-box model of crosslinked alginate. ....	6
<b>Figure 2.4</b> : Calcium alginate spherical beads .....	6
<b>Figure 3.1</b> : Schematic illustration of compression measurement setup. ....	14
<b>Figure 3.2</b> : Force (N) versus $(H)^{3/2}$ curves for beads with 4% (w/v) alginate beads crosslinked with 3% (w/v) $Ba^{2+}$ (a) with Brij 35 (b) SDS. ....	15
<b>Figure 3.3</b> : Effects of (a) Brij 35 and (b) SDS concentrations on the Young's modulus of the calcium alginate beads. ....	17
<b>Figure 3.4</b> : Effects of (a) Brij 35 and (b) SDS concentrations on the Young's modulus of the barium alginate beads.....	18
<b>Figure 3.5</b> : Effect of crosslinker cation concentration on the Young's modulus of 2% (w/v) alginate beads containing 50 cmc of SDS.....	19
<b>Figure 3.6</b> : Proposed structure for the interaction between surfactants and alginate chain (a) calcium alginate, (b) calcium alginate with SDS, (c) calcium alginate with Brij 35.....	20
<b>Figure 4.1</b> : Preparation of PEMs with LbL technique .....	22
<b>Figure 4.2</b> : Schematic representation of LbL procedure.....	25
<b>Figure 4.3</b> : Schematic representation of ellipsometry.....	26
<b>Figure 4.4</b> : Schematic representation of X-ray reflectometry.....	27
<b>Figure 4.5</b> : Schematic representation of an AFM scan. The surface morphology is obtained from the change of the position of the reflected laser beam on the detector. Adapted from reference [82]. ....	28
<b>Figure 4.6</b> : Principle of QCM-D. Potential excites the crystal to oscillate at its resonance frequency and higher overtones. When the potential is cut off, the damping amplitude of oscillation (A) is monitored in time (t). Adapted from reference [82]. ....	29
<b>Figure 4.7</b> : Schematic representation of QCM-D measurement setup. ....	30
<b>Figure 4.8</b> : Representation of (a) etched Si wafer, (b) alginate-chitosan PEMs with Brij 35, (c) alginate-chitosan PEMs with and without SDS, (d) alginate-chitosan PEMs crosslinked with cations. ....	31
<b>Figure 4.9</b> : Thickness profiles of PEMs. Left: without SDS, Right: with 0.1 mmol/L SDS. Open symbols represent chitosan-terminated PEMs; filled symbols represent alginate-terminated PEMs. Black and red points indicate the thicknesses.....	33
<b>Figure 4.10</b> : Refractive indices of the samples, calculated from ellipsometry data. Left: without SDS, Right: with 0.1 mmol/L SDS. Open symbols represent chitosan-terminated PEMs; filled symbols represent alginate-terminated PEMs. ....	35

<b>Figure 4.11</b> : Roughness values of the samples, calculated from Left: XRR, Right: AFM. Open symbols represent chitosan-terminated PEMs; filled symbols represent alginate-terminated PEMs.....	<b>35</b>
<b>Figure 4.12</b> : AFM images of 18 DL samples (A) without SDS, (B) with 0.1 mmol/L SDS. ....	<b>36</b>
<b>Figure 4.13</b> : Adsorbed mass vs number of layers, calculated from QCM-D data...	<b>36</b>
<b>Figure 4.14</b> : AFM images of PEM samples crosslinked with 1 mol/L Ca <sup>2+</sup> , A: 49.5 double layers, B: 50 double layers, without SDS.....	<b>37</b>
<b>Figure 5.1</b> : Application of a wound dressing on a wound. Wound dressing should be flexible and cover the lesion.....	<b>39</b>
<b>Figure 5.2</b> : Sodium alginate film .....	<b>41</b>
<b>Figure 5.3</b> : Crosslinked cerium alginate-chitosan film.....	<b>41</b>
<b>Figure 5.4</b> : Illustration of experimental setup for stretching measurements. Film sample was carefully held by pneumatic holders.....	<b>43</b>
<b>Figure 5.5</b> : Wet-cup method for WVTR determination. A vessel is filled with water and the cup is completely sealed with film sample. The loss of the mass due to escaped vapor through film is recorded over time.....	<b>43</b>
<b>Figure 5.6</b> : FTIR spectra of Ce and Ce-Chi samples.....	<b>45</b>
<b>Figure 5.7</b> : Surface images of Ce and Ce-Chi samples.....	<b>45</b>
<b>Figure 5.8</b> : Cross-section images of Ca, Ca-Chi, Ce and Ce-Chi samples.....	<b>46</b>
<b>Figure 5.9</b> : UV-VIS transmittance spectra of the Ce, Ce-Chi, Ca and Ca-Chi samples.....	<b>47</b>
<b>Figure 5.10</b> : Antibacterial activity (log CFU/g sample vs exposure time in h) of the samples and polypropylene film (PP) against <i>E. coli</i> and <i>S. aureus</i> .....	<b>47</b>
<b>Figure A.1</b> : Force (N) versus (H) <sup>3/2</sup> curves for beads with 1% (w/v) alginate beads crosslinked with 3% (w/v) Ca <sup>2+</sup> ; doped with Brij 35.....	<b>58</b>
<b>Figure A.2</b> : Force (N) versus (H) <sup>3/2</sup> curves for beads with 2% (w/v) alginate beads crosslinked with 3% (w/v) Ca <sup>2+</sup> ; doped with Brij 35.....	<b>59</b>
<b>Figure A.3</b> : Force (N) versus (H) <sup>3/2</sup> curves for beads with 3% (w/v) alginate beads crosslinked with 3% (w/v) Ca <sup>2+</sup> ; doped with Brij 35.....	<b>60</b>
<b>Figure A.4</b> : Force (N) versus (H) <sup>3/2</sup> curves for beads with 4% (w/v) alginate beads crosslinked with 3% (w/v) Ca <sup>2+</sup> ; doped with Brij 35.....	<b>61</b>
<b>Figure A.5</b> : Force (N) versus (H) <sup>3/2</sup> curves for beads with 1% (w/v) alginate beads crosslinked with 3% (w/v) Ca <sup>2+</sup> ; doped with SDS.....	<b>62</b>
<b>Figure A.6</b> : Force (N) versus (H) <sup>3/2</sup> curves for beads with 2% (w/v) alginate beads crosslinked with 3% (w/v) Ca <sup>2+</sup> ; doped with SDS.....	<b>63</b>
<b>Figure A.7</b> : Force (N) versus (H) <sup>3/2</sup> curves for beads with 3% (w/v) alginate beads crosslinked with 3% (w/v) Ca <sup>2+</sup> ; doped with SDS.....	<b>64</b>
<b>Figure A.8</b> : Force (N) versus (H) <sup>3/2</sup> curves for beads with 4% (w/v) alginate beads crosslinked with 3% (w/v) Ca <sup>2+</sup> ; doped with SDS.....	<b>65</b>
<b>Figure A.9</b> : Force (N) versus (H) <sup>3/2</sup> curves for beads with 1% (w/v) alginate beads crosslinked with 3% (w/v) Ba <sup>2+</sup> ; doped with Brij 35.....	<b>66</b>
<b>Figure A.10</b> : Force (N) versus (H) <sup>3/2</sup> curves for beads with 2% (w/v) alginate beads crosslinked with 3% (w/v) Ba <sup>2+</sup> ; doped with Brij 35.....	<b>67</b>
<b>Figure A.11</b> : Force (N) versus (H) <sup>3/2</sup> curves for beads with 3% (w/v) alginate beads crosslinked with 3% (w/v) Ba <sup>2+</sup> ; doped with Brij 35.....	<b>68</b>
<b>Figure A.12</b> : Force (N) versus (H) <sup>3/2</sup> curves for beads with 4% (w/v) alginate beads crosslinked with 3% (w/v) Ba <sup>2+</sup> ; doped with Brij 35.....	<b>69</b>
<b>Figure A.13</b> : Force (N) versus (H) <sup>3/2</sup> curves for beads with 2% (w/v) alginate beads crosslinked with 3% (w/v) Ba <sup>2+</sup> ; doped with SDS.....	<b>70</b>

<b>Figure A.14</b> : Force (N) versus $(H)^{3/2}$ curves for beads with 3% (w/v) alginate beads crosslinked with 3% (w/v) $Ba^{2+}$ ; doped with SDS .....	<b>71</b>
<b>Figure A.15</b> : Force (N) versus $(H)^{3/2}$ curves for beads with 4% (w/v) alginate beads crosslinked with 3% (w/v) $Ba^{2+}$ ; doped with SDS .....	<b>72</b>
<b>Figure B.1</b> : XRR data and fit of PEM samples measured at ambient conditions. Dots indicate fits and lines are experimental data.....	<b>75</b>
<b>Figure B.2</b> : XRR data and fit of PEM samples measured at ambient conditions. Dots indicate fits and lines are experimental data.....	<b>76</b>
<b>Figure B.3</b> : XRR data and fit of PEM samples measured at ambient conditions. Dots indicate fits and lines are experimental data.....	<b>77</b>
<b>Figure B.4</b> : XRR data and fit of PEM samples measured at ambient conditions. Dots indicate fits and lines are experimental data.....	<b>78</b>
<b>Figure B.5</b> : XRR data and fit of PEM samples measured at ambient conditions. Dots indicate fits and lines are experimental data.....	<b>79</b>
<b>Figure B.6</b> : Surface of a chitosan PEM film, imaged by AFM. Right hand side of the image is the Si wafer, left side is the PEM.....	<b>80</b>
<b>Figure C.1</b> : Stress-strain curves for equally shaped film samples.....	<b>81</b>



## **LAYERED AND COMPOSITE BIOPOLYMERS: MECHANICAL, PHYSICAL AND ANTIMICROBIAL PROPERTIES**

### **SUMMARY**

In this thesis, two oppositely charged biopolyelectrolytes –alginate and chitosan– were focused on. The interactions between these biopolymers and the effect of surfactants on these biopolymers were studied. Thesis is composed of three chapters.

In first chapter. The changes in mechanical properties of the calcium and barium crosslinked alginate hydrogel beads, when sodium dodecyl sulfate (SDS) and Brij 35 were incorporated into the gel structure, were studied. SDS and Brij 35 are negatively charged and nonionic surfactants, respectively. Alginate concentration, types and concentrations of crosslinker and surfactant were found as parameters which affect the elastic properties of alginate hydrogel beads. Modulus of elasticity of the alginate gels increased when SDS was added and decreased in the presence of Brij 35. Therefore it is considered that SDS increases the negative charge density on alginate chain by binding to the chain via hydrophobic interactions. On the other hand, Brij 35 decreased the charge density. Second chapter focuses on the preparation of the alginate – chitosan polyelectrolyte multilayer (PEM) films and the effect of surfactants on them by characterizing the samples using ellipsometry, X-ray reflectometry and atomic force microscopy. Results showed that SDS increased the thickness of the PEM films by increasing the adsorbed amount of mass of the alginate – chitosan system. In third chapter, it was aimed to develop a potent wound dressing agent by preparing cerium(III) crosslinked alginate-chitosan films. Mechanical and antimicrobial characterization of the samples indicated the potential of cerium(III) crosslinked alginate-chitosan as wound dressings.

This graduate thesis project was derived from the results of the experiments and measurements, which were conducted within the scope of joint doctoral agreement between *İstanbul Teknik Üniversitesi* and *Technische Universität Berlin*. Graduate student was supported by Scientific and Technical Research Council of Turkey (TÜBİTAK) BİDEB 2214/B joint doctoral scholarship program.



# **SCHICHT- UND VERBUNDBIOPOLYMERE: MECHANISCHE, PHYSIKALISCHE UND ANTIMIKROBIELLE EIGENSCHAFTEN**

## **ZUSAMMENFASSUNG**

Die vorliegende Arbeit konzentriert sich auf die beiden entgegengesetzt geladenen Biopolyelectrolyte, Alginate und Chitosan. Die Wechselwirkungen zwischen diesen Biopolymeren und die Wirkung von Tensiden auf diese Biopolymere wurden untersucht. Die Arbeit besteht aus drei Teilen:

Im ersten Teil der Dissertation wird die Änderungen der mechanischen Eigenschaften der Calcium- und Barium-vernetzten Alginat-Hydrogelperlen, wenn Natriumdodecylsulfat (SDS) und Brij 35 in die Gelstruktur eingearbeitet wurden, präsentiert. SDS und Brij 35 sind anionisches bzw. Nichtionisches Tensiden. Alginatkonzentration, Typen und Konzentrationen von Vernetzter und Tensid wurden als Parameter gefunden, die elastischen Eigenschaften von Alginat-Hydrogelperlen beeinflussen. Der Elastizitätsmodul der Alginatgele nahm zu, wenn SDS zugegeben und in Gegenwart von Brij 35 vermindert wurde. Daher wird davon ausgegangen, dass SDS die negative Ladungsdichte an der Alginatkette durch Bindung an die Kette über hydrophobe Wechselwirkungen erhöht. Der zweite Teil beschreibt auf die Herstellung der Alginat – Chitosan – Polyelektrolyt-Multischichten (PEMs) und die Wirkung von Tensiden auf sie durch die Charakterisierung der Proben mittels Ellipsometrie, Röntgenreflektometrie und Atomkraftmikroskop. Die Ergebnisse zeigten, dass SDS die Filmdicke der PEMs erhöhte, indem die adsorbierte Massenmenge des Alginat – Chitosansystems erhöht wurde. Im dritten Teil wurde darauf hingewiesen, ein potentieller Wundverband durch die Herstellung von Cer(III) vernetzten Alginat-Chitosan-Filmen zu entwickeln. Die mechanische und antimikrobielle Charakterisierung der Proben zeigte das Potential von Cer(III) vernetzten Alginat-Chitosan als Wundverbände an.

Diese Dissertation wurde aus den Ergebnissen der Experimente und Messungen abgeleitet, die im Rahmen der gemeinsamen Promotionsvereinbarung zwischen der Technischen Universität Berlin und Technische Universität Istanbul durchgeführt wurden. Der Doktorand wurde von die Die Türkische Anstalt für Wissenschaftliche und Technologische Forschung (*TÜBİTAK*) BİDEB 2214/B gemeinsamen Doktorandenstipendium Programm unterstützt.



## KATMANLI VE KOMPOZİT BİYOPOLİMERLER: MEKANİK, FİZİKSEL VE ANTİMİKROBİYAL ÖZELLİKLERİ

### ÖZET

Bu tez çalışmasında karşıt yüklü biyopolielektrolitler olan aljinat ve kitosanın, birbirleri ile ve yüzey aktif maddelerle olan etkileşimleri yapısal olarak aydınlatılmaya çalışılmış ve üç ayrı aşamada deneyler yapılmıştır.

Birinci bölümde kalsiyum ve baryum katyonlarıyla çapraz bağlanmış aljinat hidrojellerinin, sırasıyla eksi yüklü ve yüksüz yüzey aktif maddeler olan sodyum dodesil sülfat (SDS) ve Brij 35 ile katkılandırıldığında mekanik özelliklerinin değişimini konu almaktadır. Bu kısımda, hidrojel kürelerinin esneklik katsayısına aljinat derişiminin, katyon derişiminin, yüzey aktif madde türünün ve derişiminin etkileri incelenmiş ve yüzey aktif maddelerin esneklik katsayısını ayarlanabilir biçimde değiştirdiği görülmüştür. SDS'nin aljinat zincirine hidrofobik etkileşimle bağlandığı ve yüzeydeki yük yoğunluğunu yükselterek, çapraz bağlanmayı artırdığı düşünülmektedir. Brij 35 ise ters etki göstererek yük yoğunluğunu azalttığı, dolayısıyla çapraz bağlanma yüzdesinin düştüğü anlaşılmaktadır. İkinci aşamada aljinat ve kitosan çoklu polielektrolit katmanları (PEM) hazırlanmış ve yüzey aktif maddelerin bu yapılara etkisi incelenmiştir. Deneysel olarak elipsometri, X-ışını yansıma ölçümü, atomik kuvvet mikroskopu ve kuvars kristal mikrodenge yöntemleri kullanılmıştır. Elde edilen sonuçlar, SDS varlığında filmlerin daha kalın olduğunu göstermektedir. SDS, aljinat – kitosan katmanlarının etkileşimini artırmaktadır. Elde edilen sonuçlar, SDS'nin aljinata hidrofobik etkileşimle bağlandığı savını desteklemektedir. Çalışmanın üçüncü bölümünde ise, potansiyel bir uygulama alanı olarak aljinat – kitosan filmleri seryum(III) iyonlarıyla çapraz bağlanmış, elde edilen filmlerin mekanik ve antimikrobiyal özellikleri incelenmiştir. Bu aşamadaki sonuçlar da yara örtüsü olarak kullanılabileceğini göstermektedir.

Bu doktora tez çalışması, İstanbul Teknik Üniversitesi ve Berlin Teknik Üniversitesi arasında ortak doktora programı çerçevesinde her iki üniversitede yapılan deney ve ölçümlerin sonuçlarına dayanmaktadır. Doktora öğrencisi, Türkiye Bilimsel ve Teknolojik Araştırma Kurumu (TÜBİTAK) – BİDEB 2214-B yurtdışı müşterek doktora burs programı ile desteklenmiştir.

## **1. INTRODUCTION**

### **1.1 Motivation**

Biopolymers constitute a large part of the materials in our world. These polymers have found many uses. Besides daily life products like wood and paper, they are also of great scientific interest because of their biodegradable, non-toxic and easily modifiable nature. Biopolymer based controlled drug delivery systems, coatings, waste removal agents, food additives and medicinal formulations are some of the prominent research areas of these materials.

Biopolymers is a large group of subcategories, where polysaccharides are most abundant ones. Among the polysaccharides, alginate and chitosan were popular subjects in biopolymer based research and application development for several decades thanks to their interesting polyelectrolyte and gel-forming characteristics.

In order to improve the mechanical and chemical properties of alginate and/or chitosan, two main approaches have been adopted in literature. First is the chemical modifying and second one is the incorporation of a dopant (or additive) to the polymer gel matrix. Second method is easier since it does not require any chemical reaction and generate no toxicity. Understanding the mechanism and behavior of these gel systems in the presence of additives is vital in development of drug delivery and other biological & pharmaceutical research. As both alginate and chitosan is known as polyelectrolytes, the characterization of interactions between these polymers and surfactants is a challenge.

### **1.2 Outline**

This thesis focuses on alginate and chitosan in three different chapters and studies. After the discussion on scientific background of alginate, chitosan and their applications; Chapter 3 describes the effect of negative (sodium dodecyl sulfate) and nonionic (Brij 35) surfactants on crosslinked alginate gel beads. Alginate was ionically crosslinked with calcium or barium cations, and the effects of cation type,

cation concentration, surfactant type, surfactant concentration, alginate concentration were examined in detail.

Based on the findings of this part of the thesis, next study was to prepare alginate and chitosan polyelectrolyte multilayer (PEM) films and the influence of same surfactants on these multilayered film samples. This part was assumed to give more information regarding the alginate – surfactant interaction and take the one step further, including cationic biopolymer chitosan to this system. This part was discussed in Chapter 4.

Last study within the scope of this thesis was to develop an application of alginate and chitosan films (Chapter 5). In this direction, alginate films were crosslinked with chitosan and cerium(III) and novel film structures with good antibacterial properties were obtained. Besides antibacterial activity, these films showed good flexibility and water vapor permeability. Due to these results , cerium alginate-chitosan films are suggested as potential wound dressing material.

Experimental techniques for these three chapters are described in detail in their respective sections.

## 2 SCIENTIFIC BACKGROUND

### 2.1 Chitosan

Biopolymers are defined as the polymers synthesized by organisms. Besides synthetic organic compounds and all types of inorganic materials, they constitute an important part of the materials. Three main categories of biopolymers are polysaccharides, polypeptides and polynucleotides. In many areas of science, technology, industry and even daily life, biopolymers are commonly used. Cellulose, starch and pectin are familiar biopolymers for daily life; DNA consists of two polynucleotide biopolymer strands.

Polysaccharides, or polymeric carbohydrates, are well known for their in materials science. Besides cellulose, starch and pectin; glycogen, chitin, chitosan, alginate, arabinoxylan, dextran and xanthan gum are other examples to polysaccharides.

Chitin is an abundant biopolymer and is the polymerized form of N-acetylglucosamine. Chitin is extracted from exoskeletons of arthropods, mostly crabs and shrimps. Other sources include prawns, ants, spiders, scorpions, cockroaches, algae and fungi [1]. N-acetylglucosamine is a derivative of glucose, hence chitin is similar to cellulose. Many scientific and technological application areas of chitin is possible, but in this thesis it was focused on a derivative of chitin, namely chitosan. Chitosan is simply the deacetylated form of chitin, and it consists of randomly distributed  $\beta$ -(1 $\rightarrow$ 4)-linked D-glucosamine and N-acetyl-D-glucosamine. Structures of these compounds are given in Figure 2.1.

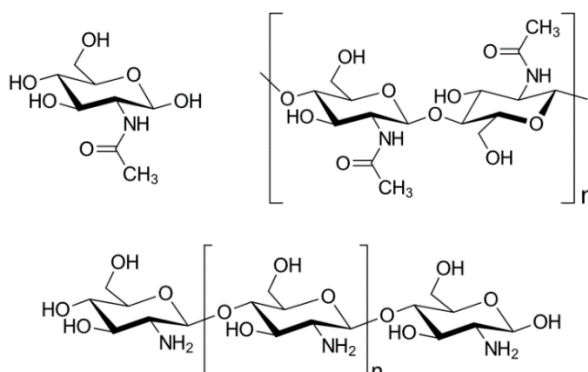


**Figure 2.1 :** Structures of N-Acetylglucosamine and chitin (top) and chitosan (bottom)

History of chitin goes back to 1818 and was discovered by French chemist Braconnot as fungine [2,3]. Further experiments were conducted by Odier and Rouget, and Rouget discovered that treating chitin with concentrated potassium hydroxide resulted in a product which is soluble in diluted organic acids [4]. Later, in 1984 Hoppe-Seyler renamed this product as chitosan [1,5]. Further experiments in following years revealed the structure of both biopolymers.

Chitosan is a pale yellow powder and it is soluble under acidic conditions. The solubilization of chitosan is due to the protonation of amino group, which has a  $pK_a$  value around 6.5. When dissolved in acidic media, chitosan forms a yellow viscous solution. Solubility of chitosan is of scientific interest because it forms a positively charged polyelectrolyte when dissolved. Most common solvent for chitosan is 1% (v/v) acetic acid solution. It is also soluble in hydrochloric and nitric acid, but insoluble in phosphoric and sulfuric acid [6]. Besides solubility, another important advantage of chitosan over synthetic polymers is its naturally abundant, biodegradable and nontoxic properties. It is also antimicrobial. Molecular weight of commercially available chitosan is in the range of 50,000 to 200,000 g/mol.

Depending on the aim, chitosan based materials can be prepared in many forms such as gels [2], microparticles [7], nanoparticles [8], membranes [9] and coatings [10]. Besides its scientific uses, industrial applications of chitosan are also numerous. It is used in agriculture as pesticides, textile industry, paper industry, water filtration and medicine. In food industry, it is both used as a preservative and thickener. Chitosan containing food additives are commercially available and is currently used for drug delivery systems.

## **2.2 Alginate**

One of the most abundant polysaccharides in nature is alginic acid, and its anionic form is called as alginate. Alginic acid is extracted from the cell walls of brown algae (seaweed) species and converted into anionic salts. This biopolymer was first introduced as “algic acid” in 1881 by Stanford (British Patent #142 1881). Several other groups examined the structure of alginic acid between 1925 and 1940 [11], however Fischer and Dörfel successfully determined the presence of L-guluronic acid in 1955 [12].

Today, structure of alginate is well known. Alginic acid is composed of homopolymeric blocks of (1–4) linked  $\beta$ -D-mannuronate (M) and  $\alpha$ -L-guluronate (G), where the sequences and the proportions of mainly depend on the source and the species of the algae. The order of alternating M and G homoblocks can vary. The blocks can be composed of consecutive residues of M and G or alternating M and G residues. Molecular weight of commercial sodium alginate is in a range of 32,000 to 400,000 g/mol [13]. Numerous sources of alginate include *Laminaria hyperborea*, *acrocystis pyrifera*, *Ascophyllum nodosum* and *Lessonia nigrescens* [11].

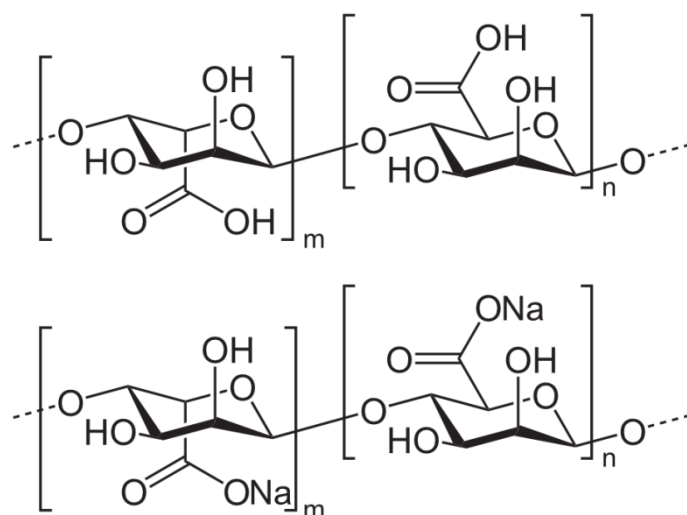
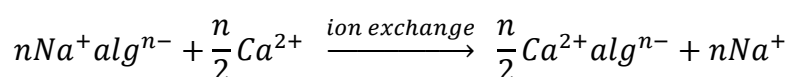


**Figure 2.2 :** Structures of alginic acid (top) and sodium alginate (bottom)

This non-toxic biopolymer is a yellow-white powder, with a similar appearance to corn starch. Alginate is soluble in water, and when dissolved, it is assumed to form an anionic polyelectrolyte. It forms a viscous solution with increasing concentration. The viscosity of the solution depends on the molecular weight of alginate and pH of medium. The mechanical strength of alginate and alginate based materials is known to increase with G content, and flexibility of the chain decreases with increasing G content.

One of most important feature of alginate is its ability to form crosslinked gels in the presence of di- or trivalent cations. The reaction between a divalent cation (e.g  $\text{Ca}^{2+}$ ) and sodium alginate can be summarized as follows:



Of course this is an *extremely simplified* approach, however is useful to explain the reaction. Most common model for explanation of this phenomenon was done by Grant et al. in 1973. In their “egg-box” model, a divalent cation is entrapped between “cavities” of two alginate chain [14]. Kvam et al. examined the probable binding site using NMR studies, and found that the binding is due to the interactions between cation and electronegative centers (O) in a single guluronate-guluronate block [11,15].

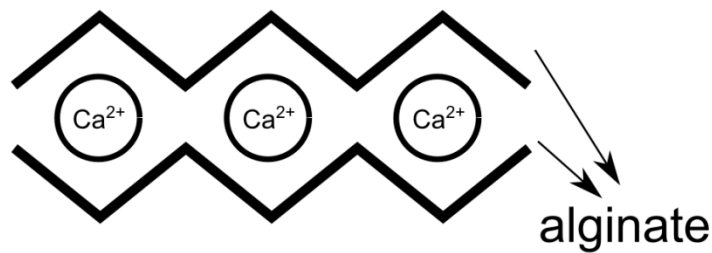


**Figure 2.3 :** Egg-box model of crosslinked alginate.

The formation of crosslinked gel is usually very fast, and formed gels are hydrophilic. The hydrogel can be dried, and can be swollen for several times. The mechanical strength of the gel varies with molecular weight of alginate, and can be improved by addition of dopants into gel structure. The shape of the gel be in form of macro- and micro- spherical beads, films and discs.

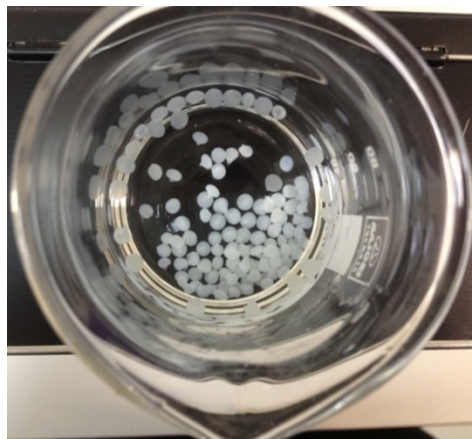


**Figure 2.4 :** Calcium alginate spherical beads

Due to its abundance, nontoxic nature, easily modifiable gel structure; alginate has wide application areas. It is used in food and textile industries as a thickener, antacid formulations, sustained release tablets and dental molds. Based on our previous experience with alginate, some of studies based on alginate are discussed in the following sections.

### 2.2.1 Drug delivery

Since alginate is extracted from brown seaweed and has no toxicity, it is commonly used and being researched in drug formulations [16–20] and food additives [21]. Although alginate has these advantages, one major disadvantage of crosslinked alginate gels is their low resistance to mechanical stimuli and chemical erosion. In addition to these, porous structure of alginate causes a burst release of the drug molecule. For this purpose, alginate gel matrices are often reinforced by chemical modification of the chain or addition of dopants. Chemical modifications include covalent crosslinking and functionalizing the chain; however these methods require chemical reactions and have the risk of increasing the toxicity. Reinforcing the material with dopants is the second method. Here, alginate gels are doped with other biopolymers such as starch, or non-toxic inorganic additives can be used. Clay materials are one of these and known for their natural abundance.

In our previous paper [22], calcium alginate-montmorillonite based composite hydrogel beads for oral protein delivery was developed. Model protein was bovine serum albumin (BSA) and experiments were done in simulated gastric fluid (SGF, pH = 1.2) and simulated intestinal fluid (SIF, pH = 7.4 phosphate buffer) media. Beads were prepared by ionic crosslinking of alginate and calcium cations. Since calcium alginate itself is a weak matrix for drug entrapment, montmorillonite (MMT) was used for improving the drug entrapment and diffusion characteristics. Beads were characterized using scanning electron microscopy (SEM), X-ray diffraction (XRD) and gravimetric swelling measurements. Delivery of BSA was spectrometrically measured by a batch method.

Results showed that mixing MMT with BSA before the alginate addition leads to exfoliation of clay layers. This was confirmed by XRD results. BSA molecules entered between the MMT layers, which significantly increased the drug entrapment efficiency. Without MMT, BSA molecules easily escaped into gelling solution during crosslinking. Addition of alginate into MMT-BSA dispersion caused the clay layers to completely exfoliate.

Release of BSA from calcium alginate beads were fast, showing almost burst release behavior. Incorporation of MMT into the structure significantly slowed the release. Moreover, release percentage of BSA was much slower in SGF when compared to

the one in SIF. This results in a route-specific release, avoiding the protein based drug to be released in acidic medium of stomach. In conclusion, calcium alginate-MMT composite beads have a high drug entrapment efficiency and thanks to their low toxicity, are candidates for intestinal controlled delivery of protein based drugs.

Not only proteins, but also smaller molecules such as riboflavin are also used for drug delivery from alginate beads. The difficulty in this case is the escape of the drug molecule during gelation step and burst release behavior. In another report, beads were reinforced with MMT to counterbalance this problem [23]. Beads were crosslinked with calcium and barium in order to see the differences. The model small drug riboflavin is also known as vitamin B2 and is an important nutritional component for human metabolism.

Preparation of drug-loaded beads was done in a very similar method to that of BSA study. One major difference was the crosslinker, barium chloride was also used in this report. Release of drug was done in a batch method. SGF and SIF were used as the release media. Beads were characterized using FTIR, SEM and gravimetric swelling measurements. Results indicated that changing the crosslinker had no major effect on release behavior. Release kinetics of riboflavin is not changed by the medium, almost 50% of riboflavin were delivered in 6 hours. Addition of MMT into the structure significantly increased the encapsulation efficiency of MMT from ~50% to ~94% and slowed the drug delivery.

### **2.2.2 Modeling of delivery**

In previous section, the reports on release of proteins and small molecules were discussed. Encapsulation efficiencies and release kinetics were improved by incorporating MMT into the alginate structure. Here, a detailed focus on the release from alginate is discussed. Two papers reported the effects of cation type and the concentration of cation on drug release [24,25]. The behavior was investigated by online fluorescence monitoring. A model fluorescent dye, pyranine was used and the release kinetics was modeled Fickian diffusion model. Pyranine-loaded alginate beads were carefully placed into the bottom of quartz fluorescence cuvettes. For 6 hours, release of pyranine into deionized water was monitored by recording the increase in intensity of fluorescence emission at 512 nm, the maximum emission wavelength of pyranine in water.

Results of these studies indicated that the slow release coefficients of the beads follow this order: Aluminum alginate > calcium alginate > barium alginate. Regarding the concentration, it is found that desorption coefficient increased up to 3% (w/v) of  $\text{Ca}^{2+}$  and decreased with the further  $\text{Ca}^{2+}$  concentrations. Also it is reported that increasing the  $\text{Ca}^{2+}$  concentration extends the incubation time, i.e. the start of release.

### **2.2.3 Waste removal**

Porous nature of alginate matrix was employed for removal of many kinds of pollutants from water [26–28]. Excess amounts of fluoride in drinking water is a problem in underdeveloped and developed countries, which may develop several health problems such as fluorosis [29]. Among the removal of fluoride from water sources studies, adsorption is the most advantageous method due to its economic advantages [30]. There are numerous reports on adsorbents for removal of fluoride. These adsorbents include iron based materials, nano and micro sized metal oxides, household wastes and biopolymers [31]. Among the adsorbent materials for this purpose, biopolymer based adsorbents are one of the most promising materials thanks to their environmentally green properties.

Aluminum and aluminum compounds are known for their affinity for fluoride anion. This property of aluminum is already used for developing defluoridation agents [32,33]. Based on this knowledge, aluminum alginate and aluminum alginate-MMT composite gel beads were reported [34,35]. Similarly to calcium in BSA delivery study, here aluminum acted as the crosslinker. In order to prepare the gel beads, MMT was dispersed in deionized water at a concentration of 1% (w/v) and necessary amounts of alginate was added to this dispersion to give a 2% (w/v) solution. Formulations without MMT, alginate was dissolved to give a 2% (w/v) solution. After dissolution of alginate, the mixture was added dropwise into a 0.2 mol/L aluminum chloride solution. Crosslinked beads were washed with deionized water, filtered and dried before adsorption experiments. Adsorption studies were performed by a match method and in preliminary studies the following parameters were optimized: pH of the solution, effect of initial fluoride concentration, and adsorbent dose. After the optimization step, experimental data was modeled using adsorption isotherms, kinetic and thermodynamic models.

Results of these studies show that aluminum alginate based adsorbent beads are effective candidates for defluoridation of water, reaching up to 93.6 mg/g adsorption capacity. Adsorption mechanism was found to be physisorption and exothermic. Moreover, they were reported as resistant to interference of other anions, i.e. the affinity towards fluoride is not affected. Incorporation of MMT into aluminum alginate beads increased their mechanical strength, as expected.

### **3 EFFECTS OF SURFACTANTS AND CROSSLINKERS ON MECHANICAL PROPERTIES OF ALGINATE HYDROGELS**

#### **3.1 Introduction**

Chemical and physical stability of the alginate gels can be improved by adding dopants to the alginate gel structure. Among the numerous dopants; other biopolymers, synthetic polymers, clays and metal oxides can be used to improve the mechanical strength. On the other hand, if the dopant has a characteristic functionality, the gel gains this functionality too. One example to this is the entrapment of magnetic iron oxide particles, which results in formation of magnetic alginate gels [36,37]. Another example to dopants is carbon nanotubes and silica nanotubes, which remarkably reinforced the mechanical properties [38]. Mongkolkajit et al. doped alginate gels with alumina and obtained good mechanical strength and improved immobilization yield [39]. Most recent dopants include graphene oxide, which significantly improved mechanical and thermal properties of alginate material [40]. Graphene oxide also improved the swelling behavior the adsorption capacity of alginate hydrogels [41,42]. Among the most-cited studies in literature, Sultana et al. improved the survival of probiotic bacteria when they included prebiotic resistant starch into alginate [43]. Other polymer additives to improve properties of alginate include poly(vinyl alcohol) [44], poly(vinyl pyrrolidone) [45], pectin [46] and, of course chitosan [47].

The effects of different structural parameters on alginate gels are reported in literature. For example, the effect of crosslinker cation type on Young's modulus values of alginate beads [48,49], speed of compression [50], ratio of M/G of alginate [51] are among these parameters.

Alginate can interact with negatively, positively or nonionic surfactants. Depending on the type of the surfactant, different types of behavior is observed. Yang et al. calorimetrically studied the interaction between alginate and a negatively charged surfactant, sodium dodecyl sulfate (SDS) [52]. They detected an aggregation between SDS and alginate when pH was lowered from 5 to 3 and the interaction was defined as the interactions between hydrophobic segments of both molecules. Öztekin et al. also reported the hydrophobic interaction between alginate and SDS for higher pH values [53]. A similar study was conducted for positively charged

surfactant, cetyltrimethylammonium bromide (CTAB). It is found that the strong interaction between CTAB and alginate occurs due to the electrostatic attraction at pH values above 5. When pH was lowered from 5, an additional attraction takes place due to the interactions between hydrophobic parts of the molecules [54,55]. The study by Bu et al. [56] also compares CTAB and SDS with a nonionic surfactant, Brij 35. They studied the interactions between alginate and the surfactants by rheological and turbidity measurements. Addition of SDS produced the least effect on solution viscosity, whereas CTAB showed a strong interaction. Nonionic Brij 35 decreased the viscosity of solution.

The importance of the alginate materials in biomedical applications such as drug release studies and scaffolds for tissue engineering requires mechanical strength of these gels. Surfactants play an important role for the uptake and release of drugs. According to our knowledge, so far the effect of surfactant on the mechanical properties of alginate gel beads hasn't been studied. This paper reports for the first time, the effect of surfactant incorporation into alginate gels on the Young's modulus of alginate beads. Two different types of surfactants (nonionic: Brij 35 and anionic: sodium dodecyl sulfate) were used. Surfactant added alginates were crosslinked by calcium or barium ions. The effect of crosslinking ions on Young's modulus was also studied.

## **3.2 Materials and Methods**

All chemicals were commercially available and used without further purification. The surfactants, Brij® 35 and sodium dodecyl sulphate (SDS), were obtained from Merck. Alginic acid sodium salt (viscosity of 2% solution ~250 cps) was purchased from Sigma-Aldrich. Calcium chloride dihydrate was purchased from J.T. Baker and barium chloride dehydrate was from Merck.

### **3.2.1 Preparation of gel beads**

In order to prepare the beads, alginate was dissolved in deionized water and necessarily amounts of surfactants were added into the alginate solutions. The solution was carefully stirred in order to avoid bubbles and foams on the solution surface. If the mixture is stirred too fast, a floating foam-like structure forms on the surface due to the presence of surfactants.

The pH of the solution was controlled in every step. The pH values of the 1% (w/v) alginate solutions with and without SDS were ~6.7. Addition of Brij 35 decreases the pH value to 6.4.

After complete dissolution, the solution was added dropwise into the gelling (crosslinking) solution. From a constant height, using a syringe of 0.8 cm inner diameter. The gelling solution consists of calcium chloride or barium chloride. The concentrations were 2, 3 and 5% (w/v) cation. Following the addition, the crosslinking reaction occurs immediately. The beads were kept at the solution for 12 hours in order to complete crosslinking.

The critical micelle concentrations (cmc) of Brij 35 and SDS are 0.09 mmol/L and 8 mmol/L, respectively. Therefore both surfactants were used above their cmc values.

Beads were of spherical shape and have colors ranging from pale yellow to white.

### 3.2.2 Compression measurements

Compression measurements were conducted using an Instron 3345 universal testing machine attached with a 10 N force transducer. The method to measure is as follows: A single bead was placed onto the platform and it was compressed with a flat-end probe at a speed of 0.5 mm/min. The measurement was stopped at a deformation ratio of 40%. Since the diameter of the compressed material is required in the calculations, the diameter of each bead was measured using a digital caliper before every measurement. All of the measurements were done at 25<sup>0</sup>C and conducted at least in triplicate. Figure 3.1 shows the schematic illustration of the measurement setup.

### 3.2.3 Calculations

Young's modulus values were obtained using the Hertz Theory [57].

$$F = \frac{4R^{0.5}}{3} \frac{E}{1 - \nu^2} \left(\frac{H}{2}\right)^{3/2} \quad (3.1)$$

Here;  $F$  is the force,  $H$  is the displacement,  $R$  is the radius of a bead,  $E$  is the Young's modulus and  $\nu$  is the Poisson's ratio.  $\nu$  was taken as 0.5 for 0.5 mm/min compression speed applied, since this value was set as 0.5 for a speed range of 0.075 [58] and 60

mm/min [50], respectively. After plotting  $F$  versus  $(H/2)^{3/2}$ , Young's modulus was obtained from the slope of linear region.

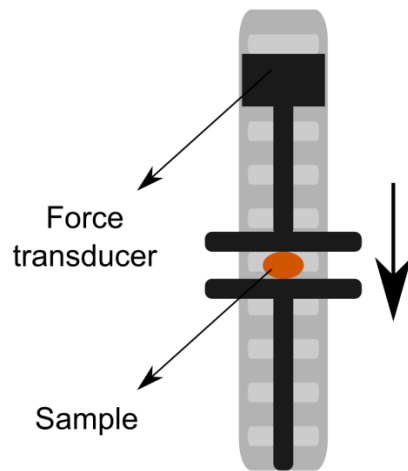


**Figure 3.1 :** Schematic illustration of compression measurement setup.

Since the data might contain statistically not significant difference, a single factor analysis of variance (ANOVA) test with a 0.05 level of significance was conducted. The calculations were done using R statistical software v. 3.02 [59].

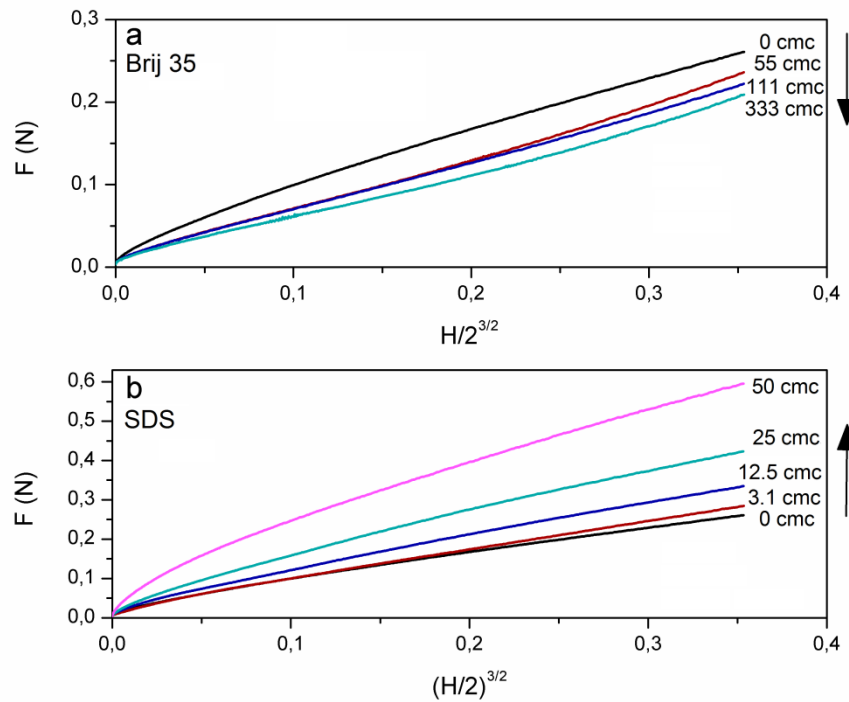
### 3.3 Results

Table 3.1 shows the effect of crosslinker, concentrations of alginate (w/v %) and surfactants (cmc) on bead diameter. Diameter values of the beads are required on elasticity calculations.

It can be seen that sizes of the beads increased with increasing alginate concentrations. Addition of surfactants decreased the sizes at low concentrations when compared to beads without surfactant. Since the viscosity increases with the concentration of alginate, an increased size can be expected. At the same time, a bigger drop will be produced for higher concentrations of alginate when compared to lower concentrations of alginate. Another interesting result is the higher diameter of barium alginate beads when compared to calcium alginate ones.

An example to Force (N) versus  $(H)^{3/2}$  curves (for beads with 4% (w/v) alginate and crosslinked with 3% (w/v)  $Ba^{2+}$ ) were given on Figure 3.2. Young's modulus of the

beads were calculated from the linear region of the force (N) versus  $(H)^{3/2}$  curves and the results were taken as averages of at least three different beads.



**Figure 3.2 :** Force (N) versus  $(H)^{3/2}$  curves for beads with 4% (w/v) alginate beads crosslinked with 3% (w/v)  $Ba^{2+}$  (a) with Brij 35 (b) SDS.

Figure 3.3 shows the effect of alginate concentration, effects each surfactant and their concentrations on the Young's modulus of the calcium alginate beads. Pure calcium alginate beads have a Young's modulus values between 60 to 300 kPa. These values are in accordance with the literature. Kaklamani et al. reported that the Young's modulus of disc-shaped alginate hydrogels in a similar range [49]. Increasing the alginate concentration from 1 to 4% (w/v) increased the Young's modulus from about 60 kPa to almost 300 kPa. This effect is expected since increasing the concentration of alginate dramatically increases the density of the solution. Regarding the effect of surfactant, Young's modulus of the beads decreased with addition of nonionic Brij 35 concentration, especially for higher alginate concentrations. For On the other hand, increasing SDS concentrations results in increasing Young's modulus values, opposite to Brij 35.

**Table 3.1:** Effects of crosslinker, alginate and surfactant concentrations on bead diameter. Concentrations are given in *times cmc*.

	Calcium alginate				Barium alginate			
	Bead diameter (cm)				Bead diameter (cm)			
	1% Alg	2% Alg	3% Alg	4% Alg	1% Alg	2% Alg	3% Alg	4% Alg
Without surfactant	3.1 ± 0.1	3.3 ± 0.2	3.4 ± 0.2	3.8 ± 0.1	3.0 ± 0.1	3.5 ± 0.1	3.8 ± 0.1	3.9 ± 0.1
Brij 35								
55 cmc	2.8 ± 0.5	3.2 ± 0.1	3.1 ± 0.1	3.2 ± 0.1	2.6 ± 0.1	3.0 ± 0.1	3.5 ± 0.1	3.8 ± 0.1
111 cmc	2.7 ± 0.2	2.7 ± 0.2	3.2 ± 0.2	3.0 ± 0.1	2.7 ± 0.1	3.3 ± 0.1	3.5 ± 0.1	4.0 ± 0.1
333 cmc	2.7 ± 0.2	3.6 ± 0.2	3.2 ± 0.2	3.3 ± 0.1	2.8 ± 0.1	3.3 ± 0.1	3.7 ± 0.1	4.2 ± 0.2
SDS								
3.1 cmc	2.6 ± 0.3	2.7 ± 0.1	3.1 ± 0.1	3.2 ± 0.6	No spherical gel formation	3.1 ± 0.2	3.3 ± 0.1	3.2 ± 0.2
12.5 cmc	3.0 ± 0.2	3.2 ± 0.1	3.1 ± 0.1	3.2 ± 0.1		3.1 ± 0.2	3.4 ± 0.1	3.8 ± 0.2
25 cmc	3.1 ± 0.5	3.4 ± 0.1	3.2 ± 0.1	3.8 ± 0.3		3.3 ± 0.1	3.7 ± 0.2	3.6 ± 0.1
50 cmc	3.2 ± 0.2	3.5 ± 0.2	3.2 ± 0.1	4.0 ± 0.2		3.4 ± 0.3	3.8 ± 0.1	4.1 ± 0.5

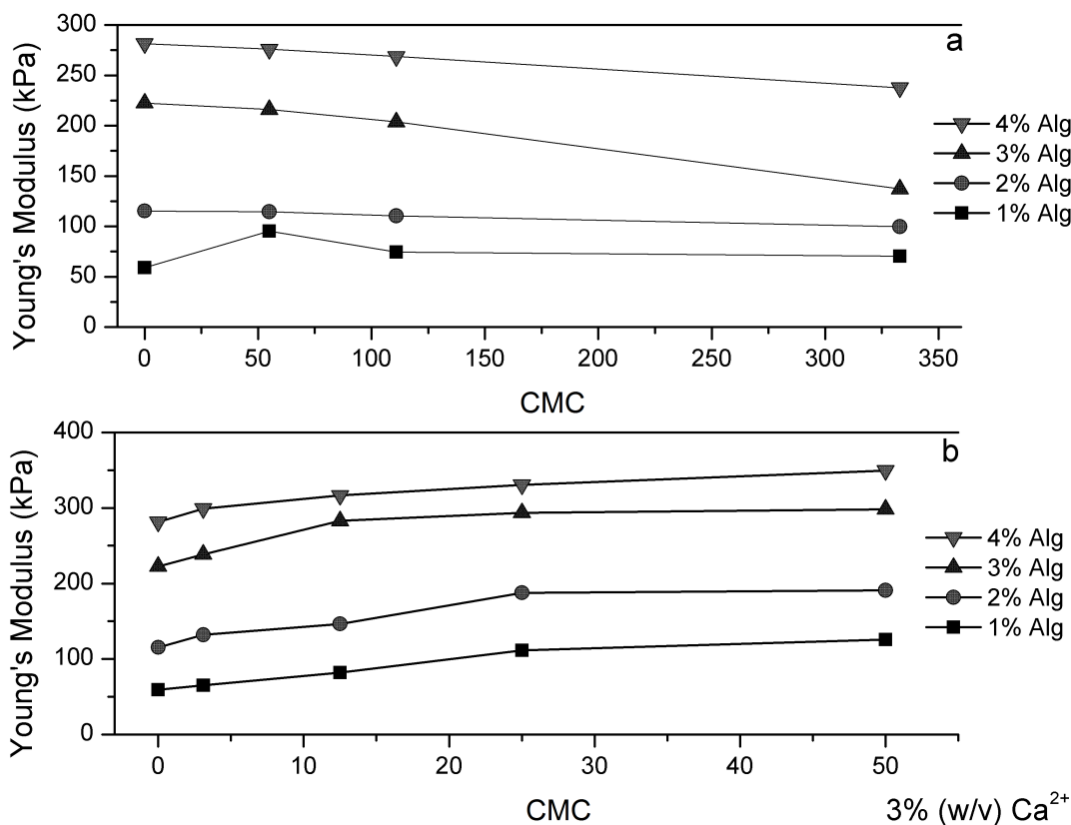


**Figure 3.3 :** Effects of (a) Brij 35 and (b) SDS concentrations on the Young's modulus of the calcium alginate beads.

The results for barium alginate beads exhibit similar behavior. Figure 3.4 shows the effect of alginate concentration, effects each surfactant and their concentrations on the Young's modulus of the barium alginate beads. The increase in the Young's modulus with presence of SDS is significant when barium alginate beads are compared with calcium alginate. The Young's modulus of barium alginate beads with 50 cmc SDS was approximately two times higher than pure barium alginate beads. Similar to calcium alginate, addition of Brij 35 slightly decreased the Young's modulus values of barium alginate beads.

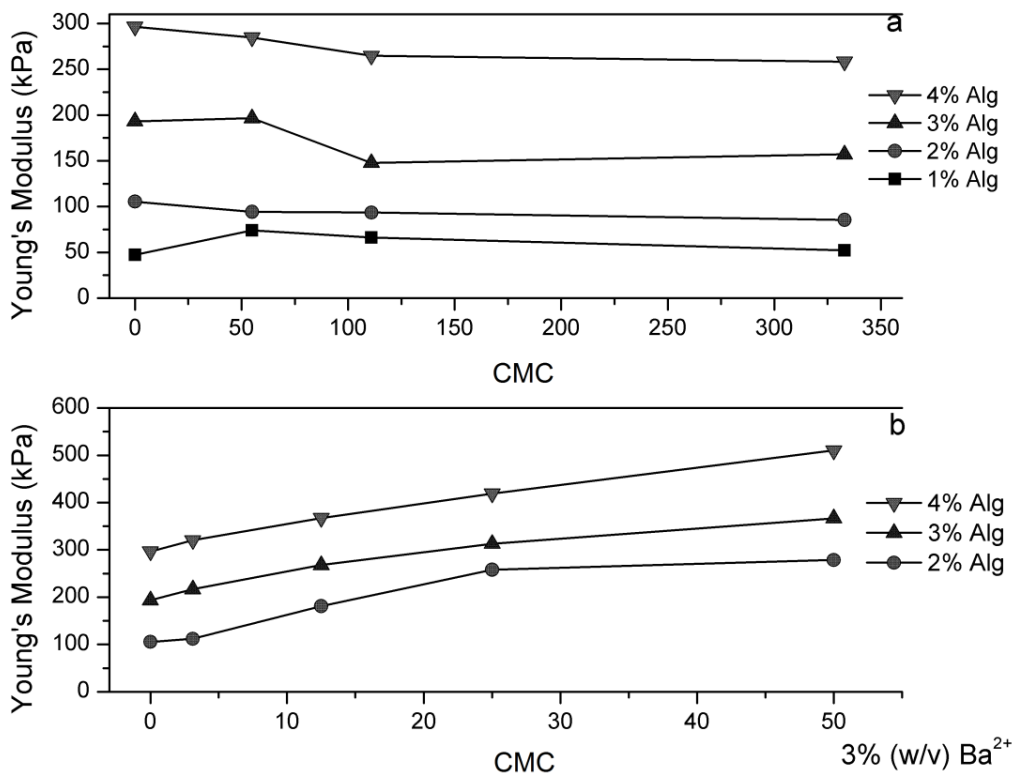


**Figure 3.4 :** Effects of (a) Brij 35 and (b) SDS concentrations on the Young's modulus of the barium alginate beads.

An interesting result was obtained for formulations containing SDS and 1% (w/v) alginate. In this case, gels were flat and no spherical beads were obtained. This was not observed for beads crosslinked with higher alginate concentrations. Thus, SDS-containing 1% alginate gels (crosslinked with barium) were not used for compression measurements.

Last parameter was the effect of cation concentration. Since the most significant change was obtained for the beads with SDS, the alginate and SDS concentrations were kept constant as 2% and 50 cmc, respectively. In order to observe the effect of cation concentration, concentrations of  $\text{Ca}^{2+}$  and  $\text{Ba}^{2+}$  were chosen as 2, 3, 4 and 5% (w/v). Figure 3.5 shows the effect of cation concentration on Young's modulus. The Young's modulus values of calcium alginate beads slightly decreased with increasing cation concentration, on contrary, the Young modulus of barium alginate beads dramatically increased. Therefore it can be concluded that increasing the concentration of  $\text{Ba}^{2+}$  increases the Young's modulus of barium alginate beads.

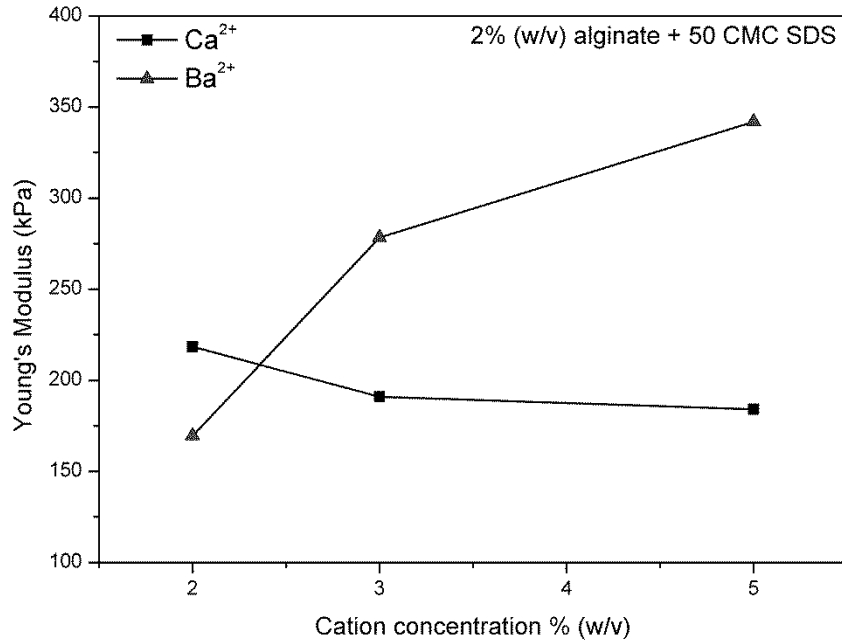


**Figure 3.5 :** Effect of crosslinker cation concentration on the Young's modulus of 2% (w/v) alginate beads containing 50 cmc of SDS.

### 3.4 Discussion

1. *Effect of alginate:* Most significant increase in Young's modulus is caused by increasing alginate concentrations. The increase in alginate from 1 to 4 % (w/v) leads to an increase in Young's modulus by a factor of about 5. Similar to the increase in viscosity of the alginate solutions, this increase is mainly caused by the densification of the polymer material in the beads. An additional cause might be the increased amount of aggregates formed between alginate chains via hydrogen bonding.

2. *Effect of surfactant:* Alginic acid is a copolymer of homopolymeric blocks of mannuronic acid and guluronic acid, and the  $pK_a$  values of these monomers are 3.2 and 3.6, respectively [60]. However,  $pK_a$  value of alginate is not definitely known. In a previous electrophoretic study, it was observed that alginate does not gain a noticeable electrophoretic mobility between  $pH = 3.5$  and  $8.5$  [53]. Alginate acted as a negatively charged molecule and gained an electrophoretic mobility when SDS was added to the medium above its cmc, showing an interaction between SDS and alginate [53]. This interaction is not expected to be electrostatic, it can be concluded that SDS half micelles were formed along the alginate chains via the hydrophobic interaction between non-charged parts of alginate and SDS. This half-micelles

increase the negative charge density of the alginate chain and the adsorption sites for the divalent cations enriches. Therefore, addition of SDS increases the crosslinking density and stiffness.

Nonionic Brij 35 probably interacts with alginate via hydrogen bonding via the head group association by the aliphatic chain. This could lead to covering of electron rich sites of alginate chain and a decrease in negative charge density. Therefore crosslinking density is decreased oppositely to the case with SDS.

Association via the head group could increase the hydrophobic character of the alginate chains and this could lead to an association between hydrophobic domains. Although this can lead to an increase in Young's modulus, this effect is probably minor or non-existent since Young's modulus values decreased with increasing amount of Brij 35. The effects of the surfactants were visualized in Figure 3.6.

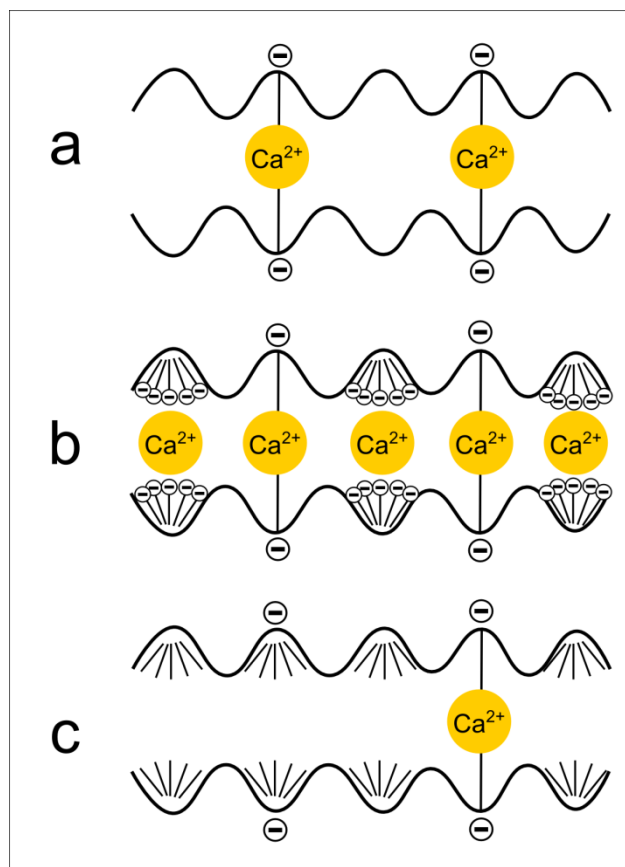


**Figure 3.6 :** Proposed structure for the interaction between surfactants and alginate chain (a) calcium alginate, (b) calcium alginate with SDS, (c) calcium alginate with Brij 35.

3. *Effect of cation type:* In literature, it is reported that affinity of alginate towards barium is higher than calcium [61,62] and stronger gel formation in the presence of

barium cations. Ionic radius values of calcium is 99 pm and barium is 135 pm, therefore the hydration shell around barium is smaller than calcium; making it easier for the negative groups of alginate to interact with barium. This causes to a stronger cross-linking in presence of barium. Since the crosslinking density increases, the increase in Young's modulus with increasing barium concentration can be expected; however the reason of the decrease in Young's modulus with increasing calcium concentration is unclear and it can be only speculated. The reason might be due to the screening of the charges in the presence of calcium ions, which might act like both a salt and a crosslinker, reducing the Young's modulus of the gels.

Since alginate gels are widely used in drug delivery studies, preparation of water purification agents, pharmaceutical applications and food industry, characterizing and modification of the mechanical properties of important. In this section, the variation of the Young's modulus of crosslinked gel beads by changing types or concentrations of surfactants and crosslinker cations. The effects of these variables on mechanical properties of beads were investigated by uniaxial compression measurements. Addition of nonionic Brij 35 decreases the Young's modulus of the beads while addition of negatively charged SDS showed the opposite. Therefore the type of association of SDS and Brij 35 to the alginate is different. Also, barium alginate beads have higher Young's modulus values than calcium alginate ones. It can be concluded that more rigid alginate beads can be obtained by the addition of SDS and crosslinking with barium, depending on the application area.

*Results of this chapter was published as "Surfactant and Metal Ion Effects on the Mechanical Properties of Alginate Hydrogels" in 2016, by H. Kaygusuz, G.A. Evingür, Ö. Pekcan, R. von Klitzing, F.B. Erim at International Journal of Biological Macromolecules 92 pp. 220-224.*

## 4 EFFECT OF ANIONIC SURFACTANT ON ALGINATE-CHITOSAN POLYELECTROLYTE MULTILAYERS

### 4.1 Introduction

Assembling the polyanions and polycations by physical sorption in order to form thin film structures is of interest and these materials are called as polyelectrolyte multilayers (PEM). [63,64]. Various forms of PEMs can be prepared by adsorption on planar interfaces [63], as particles [65] and free standing membranes [66]. PEMs can be constructed using layer-by-layer (LbL) technique. PEM growth by LbL technique is basically the alternating adsorption of oppositely charged polyelectrolytes on surfaces. Figure 4.1 shows the schematic of PEM construction using LbL technique. The binding on substrate can either be physical or chemical bonding.

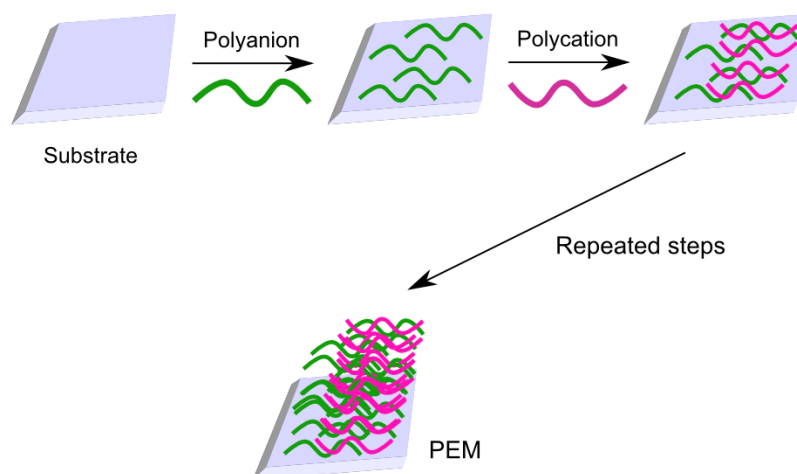
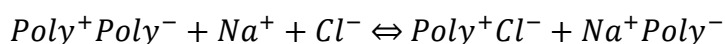


**Figure 4.1 :** Preparation of PEMs with LbL technique

The growth of the layers is based on the ion exchange when polyelectrolytes form complexes, hence effect of salt ions is critical in this manner [67–69]. Presence of salt ions affects thickness [64,70] and swelling [67,71] of the PEM and the cause of this critical effect is explained by the following chemical equation [68,72]:



In left-hand side of reaction,  $Poly^+Poly^-$  represents the polyelectrolyte-polyelectrolyte pair. Two results of great importance are as follows: Firstly, the amount of entrapped salt increases with salt concentration. Secondly, multilayered polyelectrolyte pairs

(PEMs) can be degraded with increasing salt concentration. Latter was proven by some studies [67,73].

Easy preparation of PEMs by LbL technique led the researchers to study on both synthetic and biopolymer based PEMs. In addition to the chemical properties of adsorbed polyelectrolytes, type of counterions [71,74,75], solvent [76], temperature [77,78] and charge density [68,79–81] are other parameters which modify the structural properties [64,82]. PEMs are sensitive to external stimuli, e.g. relative humidity [83], temperature [79,84] and pH [85].

Preparing PEMs based on biopolymers is of interest because of their biocompatible and non-toxic nature, in addition to the advantages of PEMs such as their good response to external stimuli. In this context, most commonly investigated biopolymers; alginate and chitosan were studied as PEM formulations also. Potential applications of PEMs based on alginate and chitosan are reported for antibody immobilization [86] and mesoporous nanoparticle coatings [87]. Alginate-chitosan PEMs were characterized by the means of the effect of biopolymer charge on PEM formation [88], crosslinking [89] and swelling behavior [90]. As presented and discussed in Chapter 2, effects of surfactants had significant effect on mechanical properties of alginate. Other reports in literature studied the effects of surfactants on alginate or chitosan systems. The interactions between alginate and SDS [55,56] are known. As discussed in Section 2, SDS binds to alginate chain via hydrophobic interactions. In addition to alginate, the strong interaction between chitosan and SDS [91] was characterized. The improvement of the mechanical properties of alginate formulations in the presence of surfactants attracted an attention to a possible alginate-chitosan PEM with surfactants as additives. To the best of our knowledge, no studies regarding the effects of surfactants on alginate-chitosan PEMs are reported. Therefore this section investigates the effect of SDS on alginate-chitosan PEM structure.

## **4.2 Materials and Methods**

Alginic acid sodium salt, low molecular weight chitosan, polyethyleneimine (PEI,  $M_w = 750$  kDa), Brij® 35 and sodium dodecyl sulfate (SDS) were purchased from Sigma-Aldrich (Germany). Sodium chloride was purchased from Merck (Germany)

and silicon wafers were obtained from Siltronic AG Siltron (South Korea). All reagents were used without further purification.

#### **4.2.1 Preparation of polyelectrolyte multilayers**

First step of the experimental part was to dissolve polyelectrolyte solutions. Alginate and PEI solutions were dissolved in 100 mmol/L sodium chloride solution. As chitosan is not soluble in neutral solutions, it was dissolved in 100 mmol/L acetic acid + 100 mmol/L sodium chloride solution. Sodium chloride was used as the supporting electrolyte. After complete dissolution, pH values of the solutions were adjusted to 5. pH adjustments were done using hydrochloric acid and sodium chloride solutions. All solutions were prepared in Milli Q water ( $22 \text{ M}\Omega\text{cm}^{-1}$ ). The concentrations of the biopolymers were 5 mg/mL and the concentration of PEI was 0.01 mol/L (per monomer unit). Before adsorption experiments, necessary amounts of surfactants (SDS or Brij 35) were added into alginate solution.

Silicon wafers need to be etched before polyelectrolyte deposition. Etching was done by  $\text{H}_2\text{SO}_4:\text{H}_2\text{O}_2$  (1:1) mixture for 30 minutes. This solution is extremely corrosive and needs to be used under very careful protection. After etching step, the wafers were rinsed with Milli-Q water and gently dried by  $\text{N}_2$  stream. Etched wafers should be used for dip-coating process just after the etching step.

Dip-coating process was done using an automatic dip-coater, which is programmable for each solution. PEM samples were prepared by dipping silicon substrate into the necessary solutions. First step in dip-coating was the adsorption of first layer, 0.01 mol/L PEI solution, which acts as the template for the rest of the PEM. Following procedure was used in automatic dip-coater, for all of the PEM formulations:

1. Dip the wafer into PEI solution (30 minutes)
2. Rinse with MilliQ water (1 minute), 3 times
3. Dip the wafer into alginate solution (20 minutes)
4. Rinse with MilliQ water (1 minute), 3 times
5. Dip the wafer into chitosan solution (20 minutes)
6. Rinse with MilliQ water (1 minute), 3 times.
7. Repeat steps 3-6

The procedure is visualized on Figure 4.2.

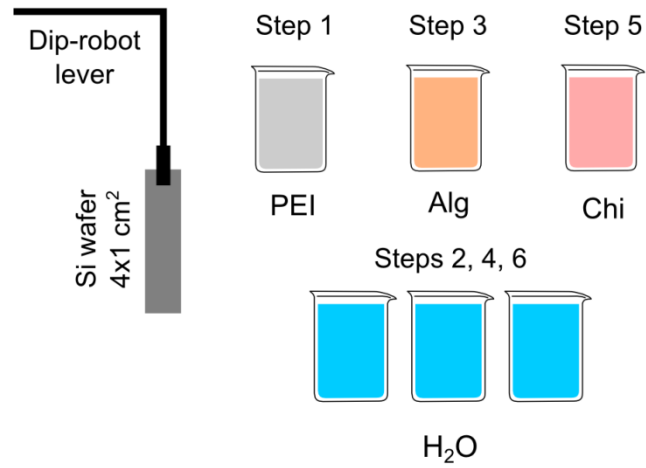


**Figure 4.2 :** Schematic representation of LbL procedure

One layer alginate and one layer of chitosan is called one double layer (DL) and 1 DL is prepared by steps 3-6. For example, a sample with 30 DL was prepared by repeating steps 3-6 by 30 times.

Crosslinking of the film structures was done by immersing dry PEM samples into aqueous solutions of  $\text{Ca}^{2+}$ ,  $\text{Ba}^{2+}$ ,  $\text{Zn}^{2+}$  and  $\text{Al}^{3+}$ , ranging from 0.1 and 1 mol/L, for 30 minutes. After 30 minutes, PEMs were taken out, washed with MilliQ water and gently dried using  $\text{N}_2$  gas.

#### 4.2.2 Characterization

Ellipsometry is an optical technique that is based on the measurement of the change of polarization of the sample-reflected light. Two parameters are vital in this measurement,  $\varphi$  and  $\Delta$ ; which are related to phase and amplitude of the light.  $\varphi$  is defined as follows [82]:

$$\tan\varphi = \frac{|E_p^r|/|E_p^i|}{|E_s^r|/|E_s^i|} \quad (4.1)$$

Where  $E$  is the amplitude of light. Letters p, s, i and r indicate parallel and perpendicular components of light, incoming and reflected beam, respectively.

On the other hand,  $\Delta$  is given in the following equation.

$$\Delta = (\delta_p^r - \delta_s^r) - (\delta_p^i - \delta_s^i) \quad (4.2)$$

$\delta$  is the phase of the light.

Since the reflection coefficients are expressed as follows,

$$r_p = \frac{|E_p^r|}{|E_p^i|} e^{i(\delta_p^r - \delta_p^i)} \quad (4.3)$$

$$r_s = \frac{|E_s^r|}{|E_s^i|} e^{i(\delta_s^r - \delta_s^i)} \quad (4.4)$$

The relation between  $\varphi$  and  $\Delta$  is:

$$\tan\varphi \cdot e^{i\Delta} = \frac{r_p}{r_s} \quad (4.5)$$

In this thesis, a null-ellipsometer with polarizer-compensator-sample-analyzer sequence setup was employed to measure the samples. Figure 4.3 shows a schematic representation of this type of ellipsometer. Unpolarized and monochromatic light, originated from light source, is converted into linearly polarized light. Secondly, polarized light passes through the compensator, which converts the linearly polarized light into elliptically polarized light; this light falls on sample and reflects with linear polarization. If an elliptically polarized light falls on a non-depolarizing sample, reflected beam is linearly polarized and vice versa. Finally, reflected light passes through the analyzer, which is actually a polarizer. Analyzer rotates the light to minimize the intensity of the light on detector. This step is also called as *nulling*.

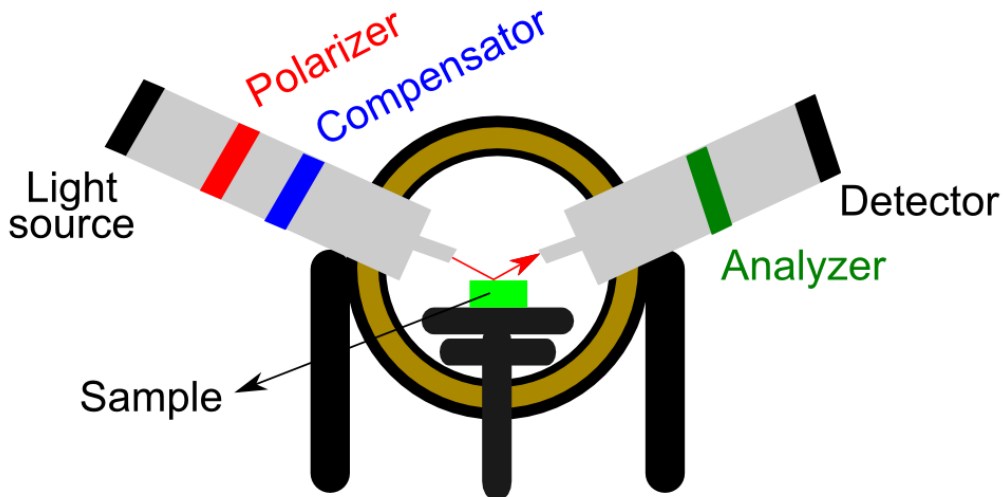


**Figure 4.3** : Schematic representation of ellipsometry

Thickness and refractive index values of the samples were measured using the Optrel GbR Null-ellipsometer (Germany) equipped with a red laser ( $\lambda = 632.8 \text{ nm}$ ) and polarizer-compensator-sample-analyzer setup. Thicknesses of the samples were measured under ambient conditions and 1% relative humidity (r.h.). 1% r.h. measurements were done in an isolated box and 1% r.h. was reached by streaming dry  $\text{N}_2$  gas. Minimum three points on the surface were measured for each sample and at least two samples of each formulation were measured. Ellipsometric parameters ( $\Delta$  and  $\Psi$ ) were modeled with a 4-layer model consisting of air, PEM, silicon oxide ( $n=1.46$ , thickness of 1.5 nm) and silicon substrate ( $n=3.8858$ ) layers, respectively.

X-ray reflectometry (XRR) was used for revealing the thickness and roughness profiles of the PEM samples. Measurements were carried out by a Bruker-AXS D8 Discover X-ray diffractometer (Germany) with  $\lambda_{\text{Cu-K}\alpha} = 0.1542 \text{ nm}$ . Minimum three points on the surface were measured for each sample and at least two samples of each formulation were measured. Reflectivity data were fitted using Igor Pro software (version 6.3.4.1., Wave Metrics Inc.) with Motofit package. After footprint correction, data was modeled using the following layer model: Silicon ( $\rho_e = 0.71 \text{ \AA}^{-3}$ ) as the backing, silicon oxide as the first layer (thickness of 1.5 nm,  $\rho_e = 0.71 \text{ \AA}^{-3}$ ) and air as the fronting ( $\rho_e = 0 \text{ \AA}^{-3}$ ). Using this model, it is possible to obtain thickness and roughness profiles of the PEM samples. Figure 4.4 shows a schematic representation of the X-ray reflectometry.

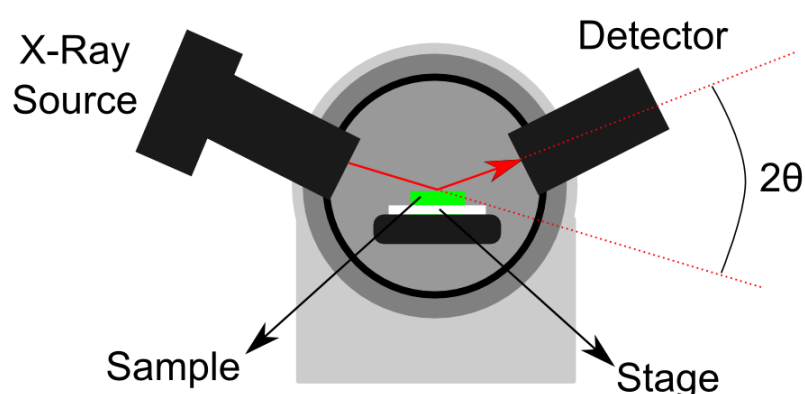


**Figure 4.4 :** Schematic representation of X-ray reflectometry

Another method for surface roughness characterization was atomic force microscopy (AFM). This technique measures the interactions between the sample surface and a probe. The movement and deflection of the probe during the surface scan is due to

van der Waals and electrostatic forces between the tip and surface. The probe tip is attached to the cantilever and the near-field forces between tip and sample surface causes the cantilever to bend. The change in cantilever position is monitored by a laser beam, which is reflected from the cantilever to detector, as illustrated in Figure 4.5.

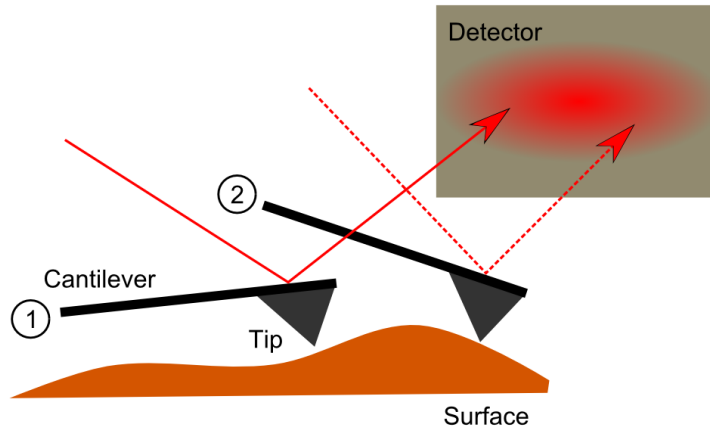


**Figure 4.5 :** Schematic representation of an AFM scan. The surface morphology is obtained from the change of the position of the reflected laser beam on the detector. Adapted from reference [82].

Asylum Research Cypher Scanning Probe Microscope (USA) was used in AFM measurements. AC air topography mode was selected as the measurement method and silicon microcantilevers (Olympus AC160TS) were employed. Image analyses were performed by Igor Pro software (version 6.3.4.1., Wave Metrics Inc.). Average root-mean-square roughness (RMS) values were calculated from at least three (1x1)  $\mu\text{m}^2$  surface areas of (5x5)  $\mu\text{m}^2$  scans. Scan speeds were between 0.5 and 1 Hz/s. Surface roughness was calculated as root mean square (rms):

$$rms = \sqrt{\frac{1}{n} \sum_i^n (y_i - \bar{y})^2} \quad (4.6)$$

Quartz Crystal Microbalance with Dissipation monitoring (QCM-D) technique was employed for characterization of polyelectrolyte adsorption. In this technique, the changes in oscillation frequency of a quartz crystal are detected, when a mass is adsorbed on a detection substrate. Excitation of the crystal is based on inverse piezoelectric effect, i.e. applying sinusoidal potential. As illustrated in Figure 4.6

Damped amplitude of the decaying oscillation is monitored when the potential is cut off [82]. The amplitude is

$$A(t) = A_0 e^{-\pi/\tau} \sin(2\pi f t + \varphi)$$

Where  $A_0$  is the initial amplitude of oscillation,  $\tau$  is the decay time constant,  $f$  is the resonance frequency and  $\varphi$  is the phase shift [92].

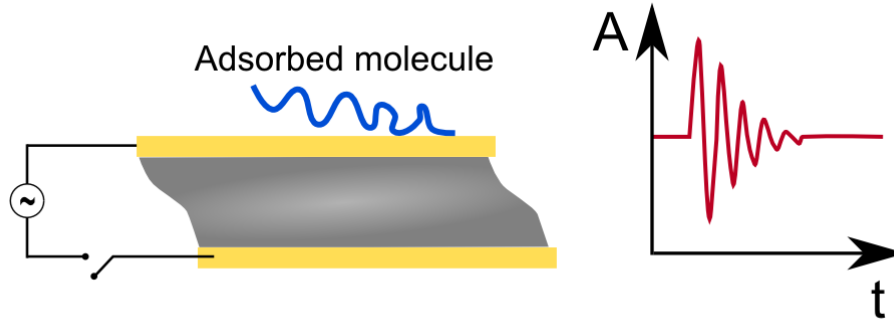


Figure 4.6 : Principle of QCM-D. Potential excites the crystal to oscillate at its resonance frequency and higher overtones. When the potential is cut off, the damping amplitude of oscillation ( $A$ ) is monitored in time ( $t$ ). Adapted from reference [82].

Shift of frequency and dissipation are given in the following equations, respectively:

$$\Delta f = f - f_0 \quad (4.7)$$

$$\Delta D = D - D_0 \quad (4.8)$$

$f_0$  is the frequency before adsorption.  $D$  and  $D_0$  are the dissipation energies at time  $t$  and 0.  $D$  is also defined as:

$$D = 1/\pi f \tau \quad (4.9)$$

The relation between adsorbed mass and the change in frequency is described by Sauerbrey [93]:

$$\Delta f = - \frac{2f_0^2}{A\sqrt{\rho_q\mu_q}} \Delta m \quad (4.10)$$

Where  $f_0$  is the fundamental frequency of quartz (4.95 MHz for this case),  $A$  is the piezoelectrical active area,  $\rho_q$  is the quartz density (2.648 g.cm<sup>-3</sup>) and  $\mu_q$  is the shear modulus of quartz (2.947.10<sup>-11</sup> g.cm<sup>-1</sup>.s<sup>-2</sup>). This model was originally for adsorbed

gas molecules onto a resonator, it is still used for the adsorption of rigid mass onto the substrate. Other models are Maxwell and Voigt models, which are valid for viscoelastic system. However, since the system in this thesis followed to a rigid film model, these models were not discussed in detail here.

The measurements were performed using quartz crystals (Q-Sense, Sweden). Before measurements, crystals need to be cleaned by the following procedure: Firstly, each crystal was cleaned by 2% (w/v) SDS solution for 30 minutes and carefully rinsed with Milli-Q water. After this, crystals were cleaned by plasma cleaning for 5 minutes. A schematic illustration of measurement setup is shown on Figure 4.7.

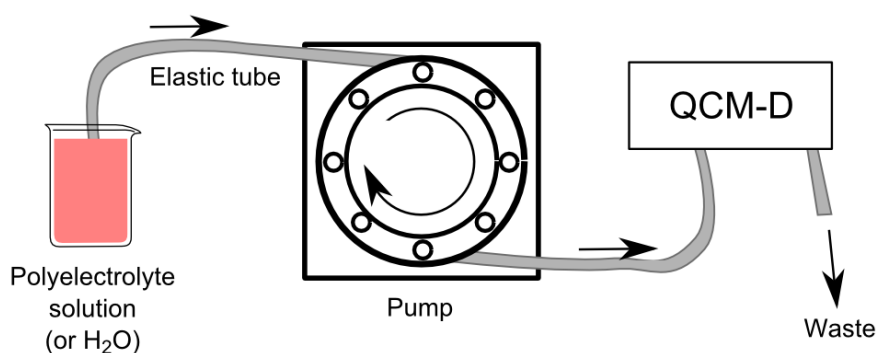


**Figure 4.7** : Schematic representation of QCM-D measurement setup.

Adsorption measurements in QCM-D were performed by a similar order with layer-by-layer assembly: A precursor layer of PEI was supplied to system for 30 minutes, followed by the rinsing step with Milli-Q water for 5 minutes. Then oppositely charged PEs (alginate and chitosan) were supplied for 20 minutes and after each PE step, crystal was rinsed with MilliQ water. Rinsing was done by supplying Milli-Q water to the system. Measurements were carried out at a constant flow rate of 0.1 mL/min.

### 4.3 Results

Preliminary LbL deposition experiments were made manually, i.e. dipping the etched wafer into polyelectrolyte solutions without using the dip-robot. PEMs up to 6 double layers were prepared by this method in order to observe the feasibility of LbL deposition of alginate and chitosan. These samples were characterized with ellipsometry.

Figure 4.8 shows the representation of Si wafer before and after LbL deposition experiments. Alginate-chitosan PEMs with and without SDS had similar appearance, transparent and darker than Si wafer. When Brij 35 was added to the formulation instead of SDS, films appeared as white opaque structures. When alginate-chitosan PEMs were crosslinked with cations, films turned into white-gray opaque structures with visible holes and defects on it. It should be noted that faint lines and color thickening at the bottom of the wafer may appear due to improper drying. This is due to improper drying after the LbL assembly. A drop of water from last rinsing step might remain at the bottom of the wafer for a long time and cause this alteration. In this case films should not be used for further measurements. In order to avoid this, films were carefully dried using N<sub>2</sub> stream.

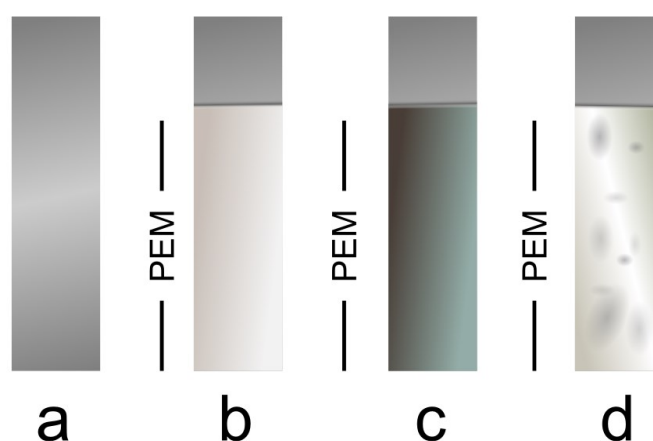


**Figure 4.8 :** Representation of (a) etched Si wafer, (b) alginate-chitosan PEMs with Brij 35, (c) alginate-chitosan PEMs with and without SDS, (d) alginate-chitosan PEMs crosslinked with cations.

Preliminary experiments were conducted for understanding the system and optimizing the formulations. Effects of sodium chloride concentration, surfactant type and concentration were investigated. Firstly, the increase in thickness when NaCl was added as the support electrolyte is shown in Table 4.1.

**Table 4.1** : Effect of sodium chloride concentration on thickness.

$C_{\text{NaCl}}$ (mmol/L)	DL	Thickness (nm)
0	2	$2.4 \pm 0.1$
	4	$3.3 \pm 0.1$
	6	$5.6 \pm 0.3$
5	2	$5.4 \pm 0.9$
	4	$8.2 \pm 0.2$
	6	$14.9 \pm 1.0$
100	2	$6.4 \pm 0.2$
	4	$12.7 \pm 0.6$
	6	$18.2 \pm 0.3$

Second investigation was the effect of surfactant type on formulations. However, when Brij 35 was added to alginate solution ( $C_{\text{Brij}} = 1$  mmol/L) and PEM samples were formed using this solution; resulting sample was opaque white, as represented in Figure 4.9. Moreover, it was not possible to obtain meaningful ellipsometric data from these samples. Therefore Brij 35 was not used in further formulations. Experiments were focused on the effect of SDS on PEM samples, which generated reproducible results. Table 4.2 shows the effect of SDS concentration on 6-DL PEM thickness. Concentration of sodium chloride was 100 mmol/L.

**Table 4.2** : Effect of SDS concentration on thickness of the 6-DL samples. $C_{\text{NaCl}} = 100$  mmol/L.

$C_{\text{SDS}}$ (mmol/L)	Thickness (nm)
0	$18.2 \pm 0.3$
0.1	$25.55 \pm 2.4$
1	$10.2 \pm 0.2$
2	9.8
10	-

Addition of 10 mmol/L of SDS into the system resulted in opaque PEMs which are not feasible to measure its properties. On the other hand, 0.1 mmol/L was found to have most significant effect on thickness, therefore 0.1 mmol/L was selected for further experiments. Critical micelle concentration of SDS in pure water is around 8

mmol/L. Since 0.1 mmol/L is well below the 8 mmol/L, a micelle formation at this concentration can be neglected.

First parameter in the characterization step was the thickness. Thickness profiles of the samples were studied by ellipsometry and XRR. Figure 4.9 indicates the thickness values versus number of deposited double layers for all sample formulations. Thickness values obtained from ellipsometry coincide with XRR.

Two-segment growth in thickness was observed for all formulations. The change in slope was appeared after 12 double layers, which means the increase changed its behavior after 12 double layers. Another interesting result was the change in thickness when the outermost layer is changed. Odd number of double layers indicates the films with alginate as the outermost layer and even number of double layers indicate the films with chitosan as the outermost layer. Addition of SDS into PEM structure caused a “zigzag” profile in thickness until 12 double layers and PEMs with odd number of double layers have less film thickness than the PEMs with even number of double layers.

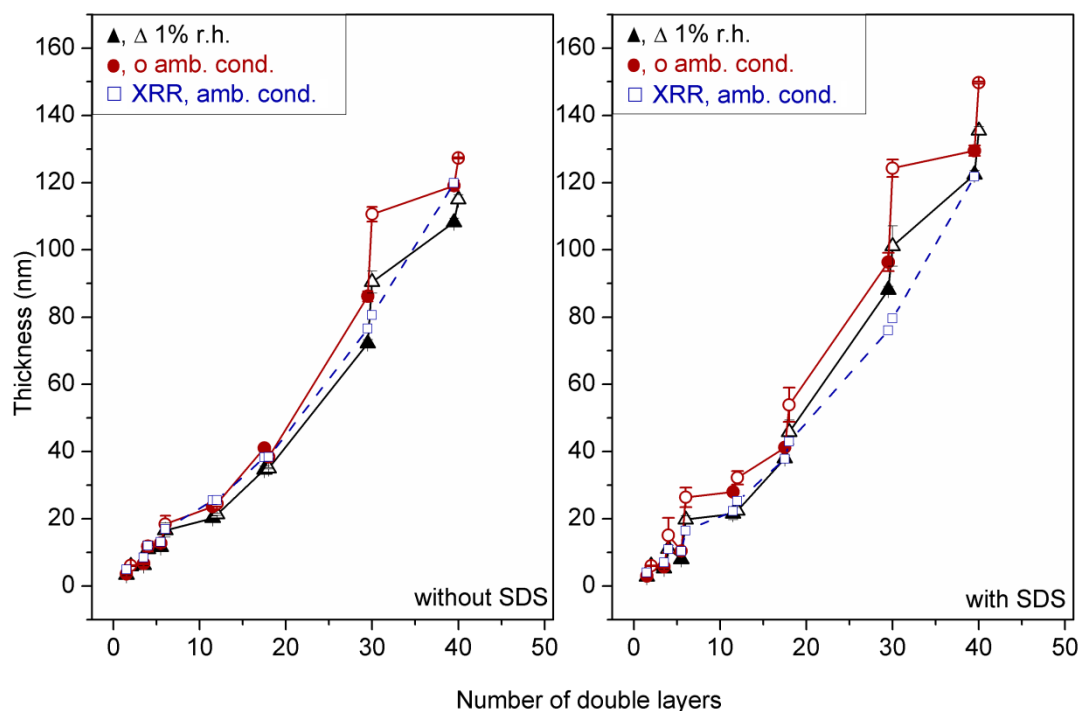


**Figure 4.9** : Thickness profiles of PEMs. Left: without SDS, Right: with 0.1 mmol/L SDS. Open symbols represent chitosan-terminated PEMs; filled symbols represent alginate-terminated PEMs. Black and red points indicate the thicknesses

**Figure 4.9 (continued):** calculated from ellipsometry data, under 1% r.h. and ambient conditions, respectively. Blue data represent the thickness values obtained from XRR data.

Decreasing the relative humidity caused a decrease in thickness for the PEMs. As can be seen from Figure 4.10, the thickness values were lower for PEMs under 1% r.h.. This behavior is expected since PEMs swell under humidity [94]. and both alginate and chitosan are hydrophilic polymers.

Second parameter was the refractive index of PEM samples. It is possible to determine both thickness and refractive index from the measured ellipsometric angles by ellipsometry. This approach is not valid for thinner films ( $< 20$  nm), because in this case only the change of phase can be obtained [95] which allows only one of the mentioned parameters to be calculated. Since thicknesses of some PEM samples were lower than 20 nm, this problem is avoided by fixing the refractive index of thick ( $> 20$  nm) samples to thinner ( $< 20$  nm) samples. Figure 4.10 represents the refractive indices ( $n$ ) of the samples and it can be seen that the values are in the range of 1.45 – 1.55. Refractive indices were found to be smaller for samples containing SDS. Similar to thickness profiles, an odd-even effect is present for samples up to 20 double layers. Samples with SDS show an irregular behavior, the change was not directly related to number of double layers.

Roughness values of the samples were calculated from XRR and AFM. Figure 4.11 shows the roughness profiles of the samples. PEMs with SDS have a higher surface roughness when compared to films without SDS, and it was not possible to measure the PEM roughness with AFM for films higher than 18 double layers, because the surface had some globules on it as shown in Figure 4.12. This behavior was described as local alginate and chitosan complexes and previously reported for alginate and chitosan films [86]. Thus, roughness profiles obtained from AFM were not reported for samples with higher than 18 double layers. Similar to thickness and refractive index results, an odd-even effect was observed in roughness values.

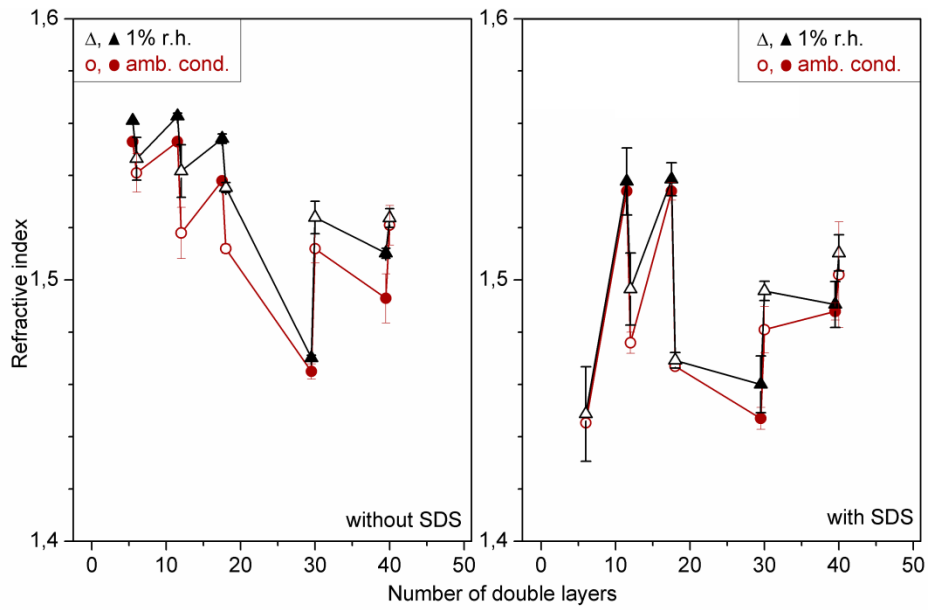


**Figure 4.10** : Refractive indices of the samples, calculated from ellipsometry data. Left: without SDS, Right: with 0.1 mmol/L SDS. Open symbols represent chitosan-terminated PEMs; filled symbols represent alginate-terminated PEMs.

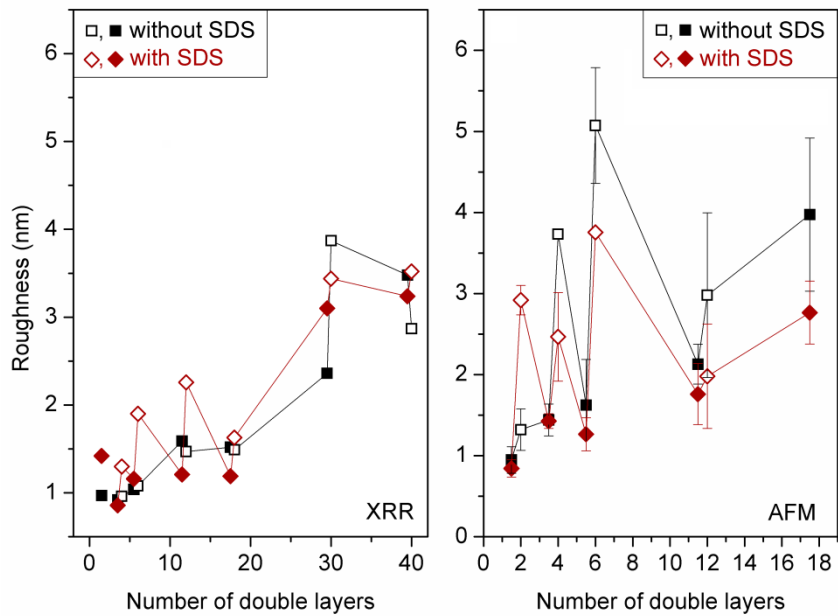


**Figure 4.11** : Roughness values of the samples, calculated from Left: XRR, Right: AFM. Open symbols represent chitosan-terminated PEMs; filled symbols represent alginate-terminated PEMs.

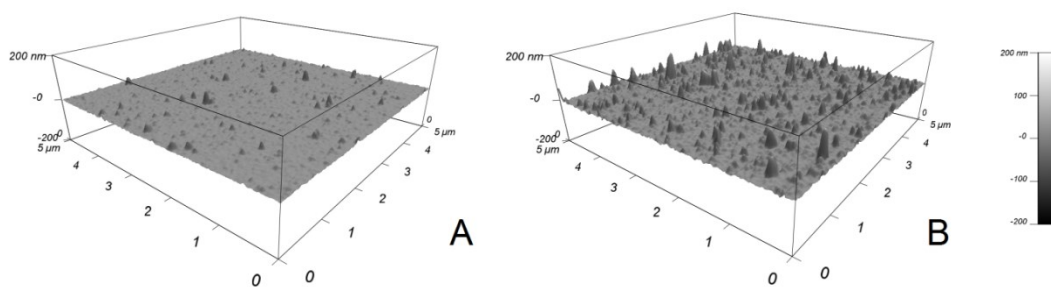


**Figure 4.12** : AFM images of 18 DL samples (A) without SDS, (B) with 0.1 mmol/L SDS.

The system was assumed to be elastic, therefore total sensed mass ( $\Delta m$ ) related to the shift of resonance frequency ( $\Delta f$ ) from QCM-D data was modeled using the Sauerbrey relation (Equation 4.10).

Here,  $f_0$  is the fundamental frequency of quartz (4.95 MHz for AT cut quartz sensors),  $A$  is the piezoelectrically active area,  $\rho_q$  is the density of quartz ( $2.648 \text{ g.cm}^{-3}$ ) and  $\mu_q$  is the shear modulus of quartz ( $2.947 \cdot 10^{-11} \text{ gcm}^{-1}\text{s}^{-2}$ ). The measurement was done for first 6 layers and the result is shown on Figure 4.13. Total adsorbed mass increased linearly with the increasing number of layers. The increase in PEMs with SDS was higher for PEMs without SDS, which is in accordance with thickness profiles as presented before.

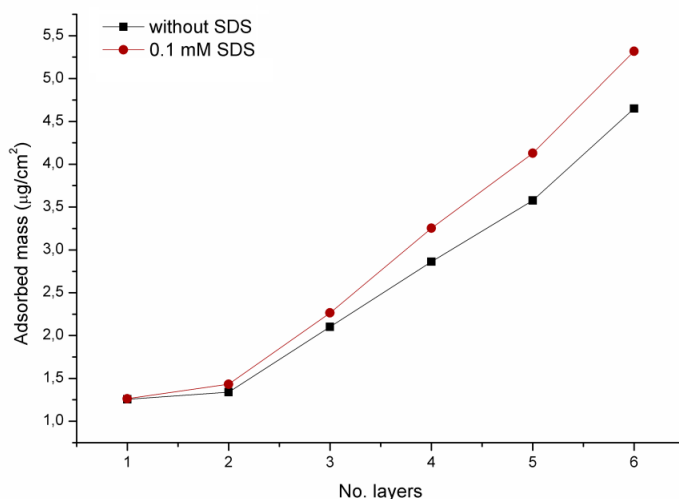


**Figure 4.13** : Adsorbed mass vs number of layers, calculated from QCM-D data.

Crosslinking of alginate structures cause a shrinking [22]. In this study, PEMs were crosslinked with calcium, barium, zinc and aluminum cations. After crosslinking, PEM samples turned into opaque white, irregular structures which can be directly seen by naked eye. The deformation in film structure was also measured with AFM

and can be seen in Figure 4.14 as a surface with high roughness. This can be caused by either salt effect of the cations or directly by crosslinking of alginate chain. However, as the alginate chains were already crosslinked with chitosan in PEM formulations, the crosslinking might not occur and the destruction of PEM due to crosslinking can be negligible.

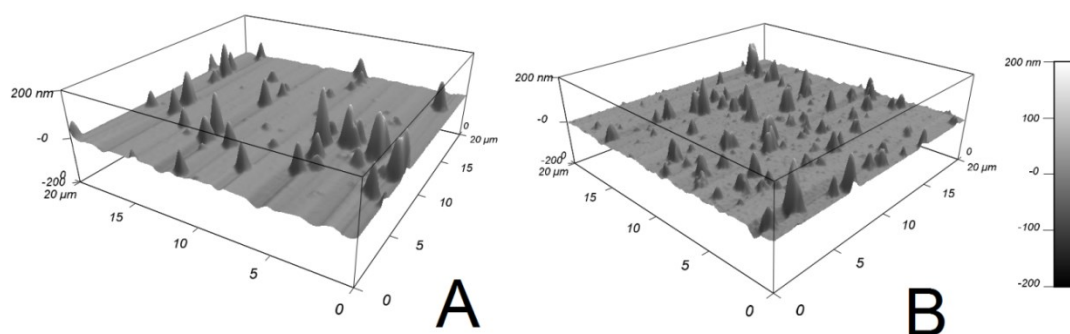


**Figure 4.14** : AFM images of PEM samples crosslinked with 1 mol/L  $\text{Ca}^{2+}$ , A: 49.5 double layers, B: 50 double layers, without SDS.

#### 4.4 Discussion

Addition of SDS increased the thickness of the alginate-chitosan PEMs and the type of the growth was found to be linear with some “zigzag” behavior. Hydrophilic alginate and chitosan are hydrophilic polymers and their multilayer structures show swelling behavior (Maurstad 2008), which is expectable under humidity. Swelling ratio ( $SR$ ) of the samples were calculated according to the following equation:

$$SR = \frac{(t_h - t_0)}{t_0} \quad (4.11)$$

Where  $t_h$  and  $t_0$  are defined as the thickness under ambient conditions and 1% r.h., respectively.

Swelling ratio of the PEM formulations were calculated for all formulations and listed in Appendix. It can be seen that swelling ratio of the PEMs are not related to the presence of SDS and number of double layers.

The increase in the adsorbed mass for PEMs containing SDS was significant. This can be explained by the higher amount of chitosan adsorption, which is due to the increased ionic interactions with the addition of SDS to alginate solution. Oppositely charged chitosan and alginate attract each other, as well as chitosan and SDS

(Lundin, 2008). Therefore the interaction between alginate and chitosan becomes stronger in the presence of SDS. As shown in Section 2 SDS is found to be bind to the alginate chain via hydrophobic-hydrophobic interaction and increase the surface charge of the alginate chain. Therefore here the increase in thickness and adsorbed mass is expected.

PEM films with SDS are found to be thicker for chitosan-terminated samples when compared to alginate-terminated ones. This was might be due to the shrinking when the outermost layer is alginate and SDS, which may result in more electrostatic interaction between previous chitosan layer.

*Results of this chapter is under review as “Effect of anionic surfactant on alginate-chitosan polyelectrolyte multilayer thickness”*

## 5 PREPARATION OF CERIUM ALGINATE–CHITOSAN FILMS AS POTENT WOUND DRESSING AGENTS

### 5.1 Introduction

As discussed in earlier sections, alginate has many advantages in material science and technology, thanks to its abundance, low toxicity and its easily modifiable properties. One of the applications of alginate is in the wound dressing area. Efficient alginate based wound dressing material is reported in literature [96] and commercial products can be found in market. These wound dressings appear as white flat pads and are placed on skin wounds. Main principle of alginate based wound dressings is the absorption of liquid from the open wound due to hydrophilic nature of alginate gels. Although being sterilized, alginate dressings often require an additional woundcare product, since alginate is not antiseptic itself. Chitosan has the advantage over alginate in this sense, since antimicrobial properties of chitosan are well-known [97]. Wound dressing formulations based on chitosan are reported in literature [97–99] and commercially available. Chitosan based wound dressings both absorb the exudate and inhibits the growth of the bacteria. An efficient wound dressing shows good inhibition against bacteria, keeps the wound moist, flexible, low-cost [100] and, if possible, biodegradable. An example illustration to application of a wound dressing on an-open wound is given in Figure 5.1.

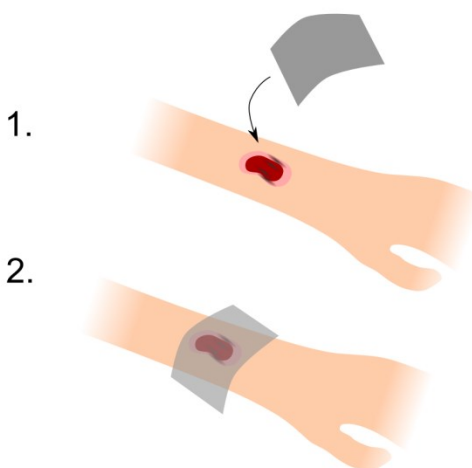


**Figure 5.1 :** Application of a wound dressing on a wound. Wound dressing should be flexible and cover the lesion.

Antibacterial properties of cerium(III) nitrate are utilized in antibacterial and topical burn treatment formulations based on cerium(III) [101–103]. It is effectively used in

a combination with silver sulfadiazine in burn treatment. The median lethal dose (LD50) of cerium nitrate in rats is 49.6 mg/kg [104] and no attributable toxicity to cerium was observed [102]. Besides antimicrobial activity, cerium nitrate binds and denatures a lipid protein complex on burned skin, which causes immunosuppression [97,103].

In the past two sections, structural and mechanical properties of calcium alginate, barium alginate, alginate-surfactant, alginate-chitosan and alginate-chitosan-surfactant formulations were investigated. In this section, the aim was to put together the advantages of alginate, chitosan and cerium nitrate in order to prepare a promising wound & burn dressing and show the feasibility of biopolymers in application areas. For this purpose, cerium(III) alginate and cerium(III) alginate-chitosan films were fabricated. Chemical and physical properties of the films were characterized and the results were compared with calcium alginate films.

## **5.2 Materials and Methods**

Alginic acid sodium salt (viscosity of 2% solution ~250 cps), chitosan (low molecular weight, with a degree of deacetylation 75–85%, viscosity 20–300 cP) and cerium(III) nitrate hexahydrate were purchased from Sigma-Aldrich (USA). Calcium chloride dihydrate, glycerol and glacial acetic acid were from Merck (Germany). All reagents were used without further purification.

### **5.2.1 Preparation of the film samples**

Alginate was dissolved in a solution of 5% (w/v) glycerol to give a 1% (w/v) solution. Glycerol was used as plasticizer for the films. After complete dissolution of the alginate, a 30 mL aliquot was carefully poured into plastic Petri dishes of 9 cm diameter and dried at 40°C for 24 h. After drying, transparent alginate films were obtained. These films were used for further crosslinked experiments. If films contain some surface defects or trapped air bubbles, these films were not used and disposed.

In order to crosslink the films, four different formulations were used: Ca<sup>2+</sup>, Ce<sup>3+</sup>, Ca<sup>2+</sup> with chitosan and Ce<sup>3+</sup> with chitosan. Calcium was selected for comparison, because crosslinking with calcium is very common. Concentrations of the crosslinker cations were 0.031, 0.076 and 0.15 mol/L. Concentrations of chitosan were 0, 0.25 and 1% (w/v). After preliminary experiments, the concentration of crosslinker

cations were set as 0.076 mol/L (approximately 2.5 % (w/v) cerium nitrate). Samples were named as Ca, Ce, Ca-Chi and Ce-Chi. Crosslinker solutions were prepared by dissolving necessary amounts of calcium chloride dehydrate or cerium(III) nitrate hexahydrate in deionized water or 1% (w/v) chitosan solution, depending on formulation. As chitosan is not soluble in neutral pH, chitosan solutions were prepared in 1% (v/v) acetic acid.

Crosslinking step was done by pouring the 30 mL crosslinker solutions on dried alginate films. Crosslinking starts immediately results in wrinkling of the alginate film. This was not acceptable in further measurements. Therefore, rings made of glass (9 cm diameter) were placed in Petri dishes to avoid crosslinking. After 12 h of crosslinking, films turned into opaque films (Figures 5.2 and 5.3). After 12 h, excess crosslinking solution was removed and films were washed with deionized water. These samples were kept under 75% relative humidity in order to avoid wrinkling.

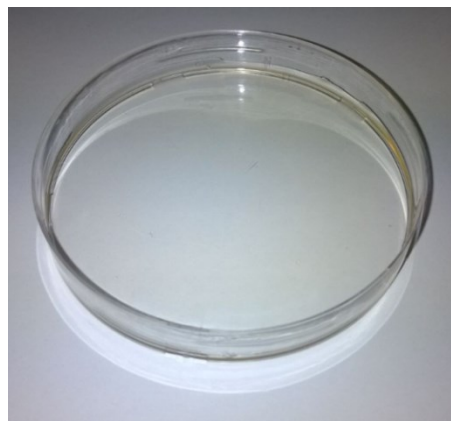


**Figure 5.2 :** Sodium alginate film



**Figure 5.3 :** Crosslinked cerium alginate-chitosan film

### 5.2.2 Preparation of inoculums

Lyophilized cultures of Gram-negative *Escherichia coli* (ATCC 25922) and Gram-positive *Staphylococcus aureus* (ATCC 6538) were obtained from Microbiologics Inc. (USA). Stock cultures were stored in brain heart infusion broth (Merck, Germany) supplemented with 20% glycerol at -18°C. Working cultures were grown in nutrient agar slants (Merck, Germany) and kept at 4°C. Microorganism suspensions were prepared and adjusted to cell density of approximately  $5 \times 10^6$  CFU/mL in 1/500 nutrient broth (Merck Germany). These were used as inoculum in in-vitro antibacterial activity assay experiments.

### 5.2.3 Characterization

Film samples were characterized by Fourier transform infrared spectroscopy (FTIR) using a Perkin-Elmer Spectrum One FTIR spectrometer (USA). Morphological properties were investigated using a JEOL-JSM-5919LV scanning electron microscope (SEM, Japan). In order to measure the cross-sections of the film samples, films were cut using cutting instruments. Light transmittance measurements were done using a Shimadzu UV-1800 spectrometer (Japan).

Swelling properties were gravimetrically characterized by placing certain amounts of crosslinked dry films in deionized water and pH 5.5 citrate-phosphate buffer (CPB). Mixtures were shaken at 37°C and 100 rpm in a Nüve ST-402 shaking water bath (Turkey). Films were taken out after 3 h, excess surface water was gently removed using a filter paper and film samples were accurately weighed. Swelling ratio (*SR*) was defined by Equation 5.1:

$$SR = (m - m_0)/m_0 \quad (5.1)$$

Where  $m_0$  and  $m$  are defined as the masses before and after swelling measurement, respectively.

Mechanical properties of the film samples were investigated by tensile measurements. An Instron 3345 universal testing device (USA) attached with a 10 N force transducer was employed in measurements. Speed was set to 0.5 mm/min at 25°C. Figure 5.4 represents the experimental setup for mechanical stretching measurements.

Water vapor transmission rate (*WVTR*) measurements of the samples were done according to the wet cup method (described by ASTM E96-95) [105]. Measurement was done as follows: A Petri dish was filled with distilled water and this Petri dish was completely covered by the film sample. The loss in water mass over time was recorded using a Labthink TSY-T3 water vapor permeability testing device (PR China) at 38°C and under 80% relative humidity. Water vapor permeability values (*WVP*) were reported using the following equation:

$$WVP = (WVTR \times d) / \Delta P \quad (5.2)$$

Where *d* is the thickness of the film in mm and  $\Delta P$  is the partial water vapor pressure gradient. *WVP* has the unit of g.mm/h.m<sup>2</sup>.Pa. The wet cup method was illustrated in Figure 5.5.

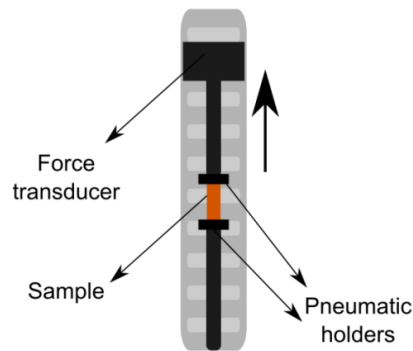


**Figure 5.4 :** Illustration of experimental setup for stretching measurements. Film sample was carefully held by pneumatic holders.

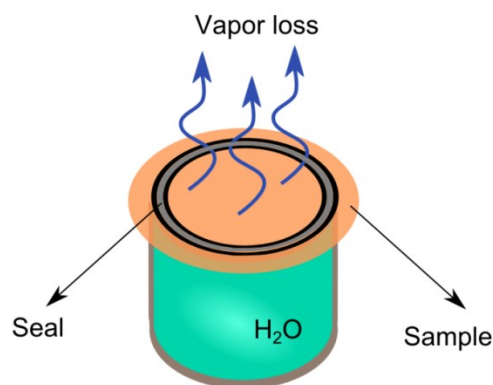


**Figure 5.5 :** Wet-cup method for WVTR determination. A vessel is filled with water and the cup is completely sealed with film sample. The loss of the mass due to escaped vapor through film is recorded over time.

#### 5.2.4 Antibacterial activity

Antibacterial activity measurements were done according to ISO 22196 standard [106]. The activities were determined by quantifying the amount of survived bacteria. The plain PP film was used as the control. Film samples (50 mm x 50 mm) were sterilized by UV treatment, placed into sterile Petri dishes and an aliquot (200  $\mu$ L) of test inoculums were pipetted onto film samples. After that, inoculated film samples were covered with a UV sterilized plain PP film (40 mm x 40 mm). Petri dishes with inoculated samples were (for 1, 2 and 3 hours) incubated at 35°C and under relative humidity above 90%. Survived populations of bacteria enumerated on tryptic soy agar (Lab M, Burry, UK). Colonies grown on the plates were counted and reported as logarithm colony-forming unit per mass of sample (log *CFU*/g sample).

### 5.3 Results and Discussion

#### 5.3.1 Characterization

Modulus of elasticity values were obtained from the linear regions of the stress-strain curves. Moduli of elasticity and *SR* of the samples are given in Table 5.1. Elastic modulus values were increased when films were crosslinked with chitosan. Cerium-crosslinked samples were found to be more flexible than films crosslinked with calcium. On the other hand, addition of chitosan decreased the flexibility. Swelling properties of Ce and Ce-Chi were less than Ca and Ca-Chi, and addition of chitosan into film structure caused an increase in *SR* values.

**Table 5.1** Mechanical properties and *SR* values of the samples

	Elastic modulus (kPa)	Elongation at break (%)	<i>SR</i> in water	<i>SR</i> in CPB
Ca	2.96 $\pm$ 0.3	23.7 $\pm$ 0.3	193 $\pm$ 9	268 $\pm$ 22
Ca- Chi	3.51 $\pm$ 0.7	20.2 $\pm$ 2.8	437 $\pm$ 88	540 $\pm$ 66
Ce	25.1 $\pm$ 2.4	35.4 $\pm$ 4.4	11 $\pm$ 4	109 $\pm$ 12
Ce- Chi	40.3 $\pm$ 1.4	26.1 $\pm$ 1.9	7 $\pm$ 2	211 $\pm$ 22

FTIR spectra of Ce and Ce-Chi samples were compared in Figure 5.6. The increased absorption band around  $1300\text{ cm}^{-1}$  indicates the presence of chitosan due to C-N stretching in Ce-Chi. Since the structures of the both formulations are almost similar, no major difference was observed in their FTIR spectra.

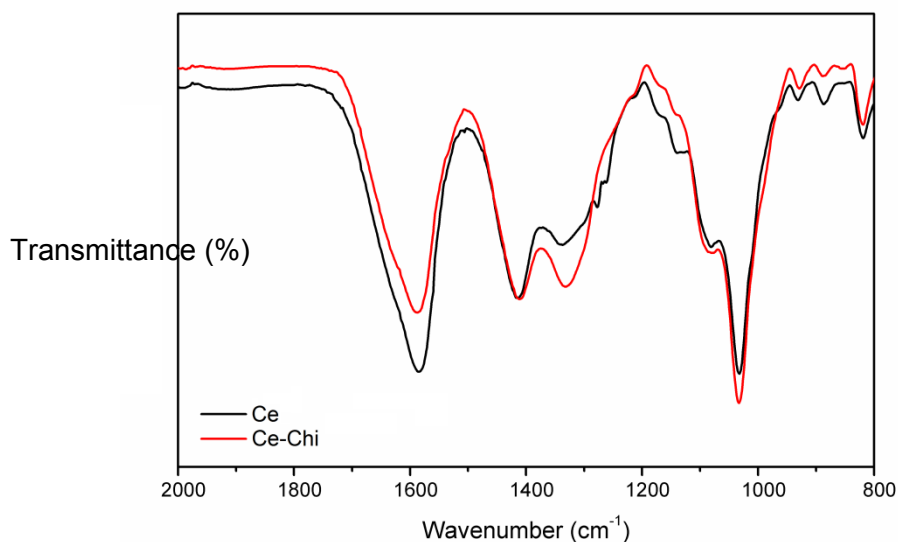


**Figure 5.6 :** FTIR spectra of Ce and Ce-Chi samples.

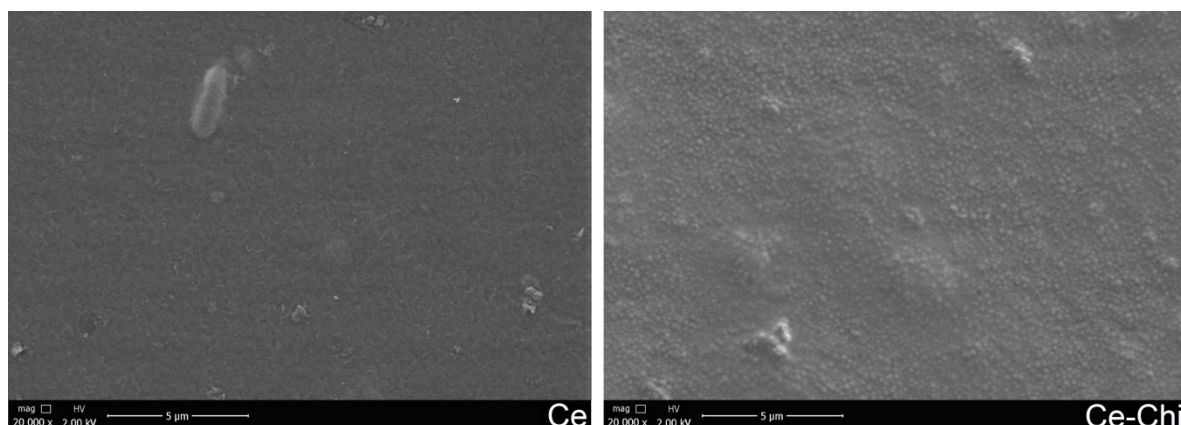


**Figure 5.7 :** Surface images of Ce and Ce-Chi samples.

Scanning electron microscopy (SEM) was used to characterize the surface morphology and cross-section of the samples. Figure 5.7 shows the SEM pictures of Ce and Ce-C. Surface of Ce was the typical alginate film structure [107,108]. Effect of chitosan was appeared as bubble-like structures on Ce-Chi. These structures were also observed in the study of Akter et al. when they added chitosan into starch-based films [109]. On the other hand, cross-sections of the samples were shown in Figure 5.8. Cross-sections of all formulations were dense, however Ce and Ce-Chi showed more compact structure. Two-layered membrane-like structure which might indicate chitosan coating was not observed. This structure was not expected, since chitosan

was added at the same time with crosslinker cation. It can be assumed that chitosan diffuse into alginate structure during crosslinking.

Light transmittance profiles of the film samples are shown in Figure 5.9. Almost no UV transmittance was observed for all samples between 200 and 300 nm, and up to 30% transmittance between 300 and 400 nm. In visible region, Ca and Ca-Chi were almost opaque. Addition of chitosan into film structure increased the transmittances for both calcium and cerium crosslinked films.

*WVTR* values of the samples were calculated as 1849, 2182, 2284 and 2578  $\text{g/m}^2\cdot\text{day}$  for Ca, Ca-Chi, Ce and Ce-Chi, respectively. Queen et al. recommend a rate of 2000 to 2500  $\text{g/m}^2\cdot\text{day}$  as the *WVTR* without wound dehydration [110]. In vitro and in vivo study by Xu et al. also suggest a *WVTR* range of approximately 1800-2300  $\text{g/m}^2\cdot\text{day}$  is able to maintain optimal moisture content [111]. Except the small deviations, *WVTR* values of the samples are found to be fall in this range.

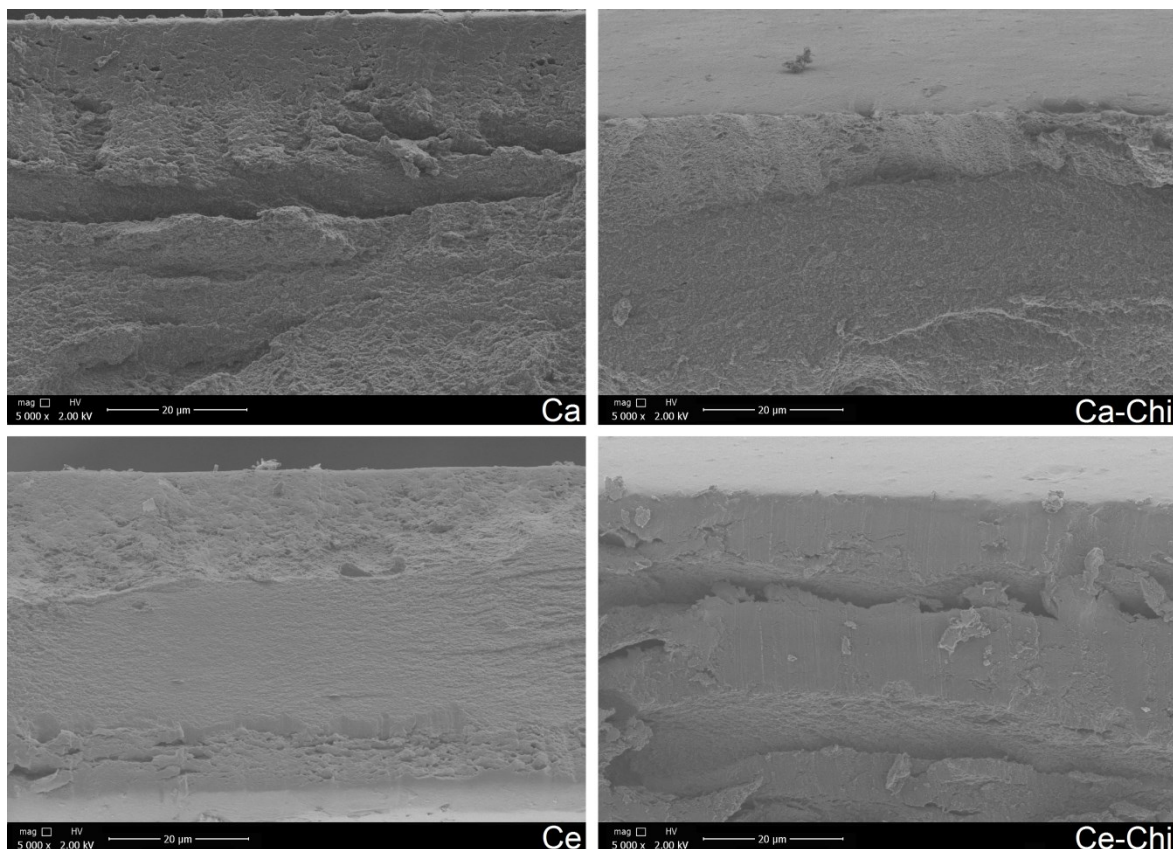


**Figure 5.8** : Cross-section images of Ca, Ca-Chi, Ce and Ce-Chi samples.

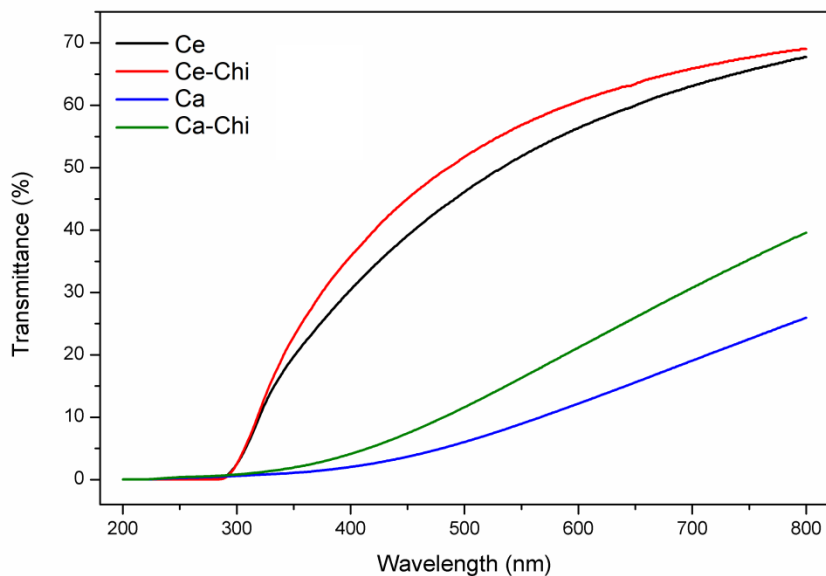


**Figure 5.9 :** UV-VIS transmittance spectra of the Ce, Ce-Chi, Ca and Ca-Chi samples.

### 5.3.2 Antibacterial activities

Antibacterial activities of the samples are shown in Figure 5.10 as log CFU/g sample against exposure time (h) for *E. coli* and *S. aureus*.

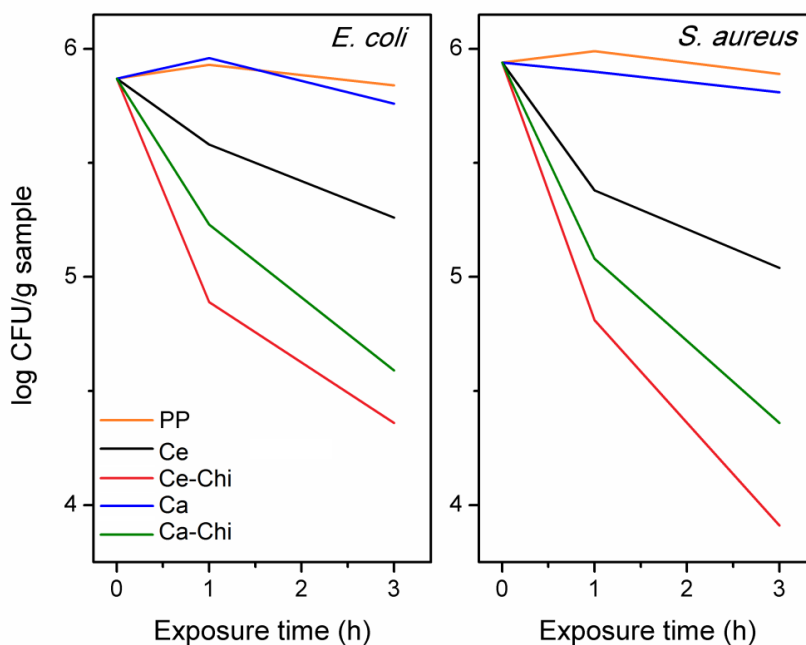


**Figure 5.10 :** Antibacterial activity (log CFU/g sample vs exposure time in h) of the samples and polypropylene film (PP) against *E. coli* and *S. aureus*.

Results indicate that Ce, Ce-Chi and Ca-Chi result in a reduction in the counts of microorganisms when to PP control film after 3 h exposure. Ca film had no

antibacterial activity against *E. Coli* and *S. Aureus*. Best result was obtained for Ce-Chi, which reached to 4.3 and 3.9 log CFU/g sample, for *E. Coli* and *S. Aureus*, respectively. Therefore it can be concluded that crosslinking with cerium and chitosan into structure both increased the antibacterial property. Effect of chitosan is dominant than effect of cerium, when Ca-Chi and Ce are compared.

In this part of the thesis, potential wound dressings were developed made of cerium/chitosan crosslinked alginate.  $Ce^{3+}$  and chitosan are known for their antimicrobial properties, and these features were also observed for Ce-Chi film. In addition to this, cerium crosslinked films were more stiff. Ce-Chi has the potential to be used as wound dressings. In future, *in vivo* studies can be conducted to improve the results in this area.

*Results of this chapter is accepted for publication as “Antimicrobial cerium ion-chitosan crosslinked alginate biopolymer films: A novel and potential wound dressing” in International Journal of Biological Macromolecules.*

## 6 BIBLIOGRAPHY

- [1] H. Tamura, T. Furuike, Chitin and Chitosan, in: *Encycl. Polym. Nanomater.*, Springer Berlin Heidelberg, Berlin, Heidelberg, 2015: pp. 386–389. doi:10.1007/978-3-642-29648-2\_322.
- [2] H. Tamura, H. Nagahama, S. Tokura, Preparation of Chitin Hydrogel Under Mild Conditions, *Cellulose*. 13 (2006) 357–364. doi:10.1007/s10570-006-9058-z.
- [3] H. Braconnot, Sur la nature des champignons, *Ann. Chim.* 79 (1811) 261–304.
- [4] M.C. Rouget, Des substances amylacées dans les tissus des animaux; spécialement des Articulés (chitine), *Comp. Rend.* 48 (1859) 792–795.
- [5] G.A.F. Roberts, *Chitin Chemistry*, Macmillan Education UK, London, 1992. doi:10.1007/978-1-349-11545-7.
- [6] V. Zargar, M. Asghari, A. Dashti, A Review on Chitin and Chitosan Polymers: Structure, Chemistry, Solubility, Derivatives, and Applications, *ChemBioEng Rev.* 2 (2015) 204–226. doi:10.1002/cben.201400025.
- [7] J.. Ko, H.. Park, S.. Hwang, J.. Park, J.. Lee, Preparation and characterization of chitosan microparticles intended for controlled drug delivery, *Int. J. Pharm.* 249 (2002) 165–174. doi:10.1016/S0378-5173(02)00487-8.
- [8] A. Rampino, M. Borgogna, P. Blasi, B. Bellich, A. Cesàro, Chitosan nanoparticles: Preparation, size evolution and stability, *Int. J. Pharm.* 455 (2013) 219–228. doi:10.1016/j.ijpharm.2013.07.034.
- [9] R.S. Mello, G.C. Bedendo, F. Nome, H.D. Fiedler, M.C.M. Laranjeira, Preparation of chitosan membranes for filtration and concentration of compounds under high pressure process, *Polym. Bull.* 56 (2006) 447–454. doi:10.1007/s00289-006-0513-7.
- [10] S.M. Ojagh, M. Rezaei, S.H. Razavi, S.M.H. Hosseini, Effect of chitosan coatings enriched with cinnamon oil on the quality of refrigerated rainbow trout, 120 (2010) 193–198. doi:10.1016/j.foodchem.2009.10.006.
- [11] K.I. Draget, O. Smidsrød, G. Skjåk-Bræk, K.I. Draget, O. Smidsrød, G. Skjåk-Bræk, Alginates from Algae, in: E.J. Vandamme, S. De Baets, A. Steinbüchel (Eds.), *Biopolym. Online*, Wiley-VCH Verlag GmbH & Co. KGaA, Weinheim, Germany, 2005. doi:10.1002/3527600035.bpol6008.
- [12] F.G. Fischer, H. Dörfel, Die Polyuronsäuren der Braunalgen (Kohlenhydrate der Algen I), *Hoppe-Seyler's Zeitschrift Für Physiol. Chemie.* 302 (1955) 186–203. doi:10.1515/bchm2.1955.302.1-2.186.
- [13] K.Y. Lee, D.J. Mooney, Alginate: properties and biomedical applications., *Prog. Polym. Sci.* 37 (2012) 106–126. doi:10.1016/j.progpolymsci.2011.06.003.
- [14] G.T. Grant, E.R. Morris, D.A. Rees, P.J.C. Smith, D. Thom, Biological interactions between polysaccharides and divalent cations: The egg-box model, *FEBS Lett.* 32 (1973) 195–198. doi:10.1016/0014-5793(73)80770-7.
- [15] B.J. Kvam, H. Grasdalen, O. Smidsrød, T. Anthonsen, R. Kivekäs, NMR Studies of the Interaction of Metal Ions with Poly(1,4-hexuronates). VI.

- Lanthanide(III) Complexes of Sodium (Methyl alpha-D-galactopyranosid)uronate and Sodium (Phenylmethyl alpha-D-galactopyranosid)uronate., *Acta Chem. Scand.* 40b (1986) 735–739. doi:10.3891/acta.chem.scand.40b-0735.
- [16] H.H. Tønnesen, J. Karlsen, Alginate in Drug Delivery Systems, *Drug Dev. Ind. Pharm.* 28 (2002) 621–630. doi:10.1081/DDC-120003853.
- [17] F. Tuğcu-Demiröz, F. Acartürk, S. Takka, Ö. Konuş-Boyunağa, Evaluation of alginate based mesalazine tablets for intestinal drug delivery, *Eur. J. Pharm. Biopharm.* 67 (2007) 491–497. doi:10.1016/j.ejpb.2007.03.003.
- [18] S. Takka, F. Acartürk, Calcium alginate microparticles for oral administration: I: effect of sodium alginate type on drug release and drug entrapment efficiency, *J. Microencapsul.* 16 (1999) 275–290. doi:10.1080/026520499289013.
- [19] M. George, T.E. Abraham, Polyionic hydrocolloids for the intestinal delivery of protein drugs: Alginate and chitosan — a review, *J. Control. Release.* 114 (2006) 1–14. doi:10.1016/j.jconrel.2006.04.017.
- [20] C.V. Liew, L.W. Chan, A.L. Ching, P.W.S. Heng, Evaluation of sodium alginate as drug release modifier in matrix tablets, *Int. J. Pharm.* 309 (2006) 25–37. doi:10.1016/j.ijpharm.2005.10.040.
- [21] N. Dürüst, A. Kayansalan, Potentiometric determination of some food additives and their binding to a polycationic species using polyion sensors, *Turkish J. Chem.* 37 (2014) 308–315. doi:10.3906/KIM-1208-10.
- [22] H. Kaygusuz, F.B. Erim, Alginate/BSA/montmorillonite composites with enhanced protein entrapment and controlled release efficiency, *React. Funct. Polym.* 73 (2013) 1420–1425. doi:10.1016/j.reactfunctpolym.2013.07.014.
- [23] H. Kaygusuz, M. Uysal, V. Adımcılar, F.B. Erim, Natural alginate biopolymer montmorillonite clay composites for vitamin B2 delivery, *J. Bioact. Compat. Polym.* 30 (2015) 48–56. doi:10.1177/0883911514557014.
- [24] H. Kaygusuz, F.B. Erim, Ö. Pekcan, G. Akin Evingür, Cation effect on slow release from alginate beads: A fluorescence study, *J. Fluoresc.* 24 (2014) 161–167. doi:10.1007/s10895-013-1282-y.
- [25] G. Akin Evingür, H. Kaygusuz, F.B. Erim, Ö. Pekcan, Effect of Calcium Ion Concentration on Small Molecule Desorption from Alginate Beads, *J. Macromol. Sci. Part B.* 53 (2014) 1157–1167. doi:10.1080/00222348.2014.895625.
- [26] V. Rocher, J.-M. Siaugue, V. Cabuil, A. Bee, Removal of organic dyes by magnetic alginate beads, *Water Res.* 42 (2008) 1290–1298. doi:10.1016/j.watres.2007.09.024.
- [27] I. Alemzadeh, S. Nejati, Removal of Phenols with Encapsulated Horseradish Peroxidase in Calcium Alginate, *Iran. J. Chem. Chem. Eng.* 28 (2009) 43–49.
- [28] S. Uzaşçı, F. Tezcan, F.B. Erim, Removal of hexavalent chromium from aqueous solution by barium ion cross-linked alginate beads, *Int. J. Environ. Sci. Technol.* 11 (2013) 1861–1868. doi:10.1007/s13762-013-0377-y.
- [29] World Health Organization, Fluoride in Drinking-water, 2006.

- [30] M. Mohapatra, S. Anand, B.K. Mishra, D.E. Giles, P. Singh, Review of fluoride removal from drinking water, *J. Environ. Manage.* 91 (2009) 67–77. doi:10.1016/j.jenvman.2009.08.015.
- [31] A. Bhatnagar, E. Kumar, M. Sillanpää, Fluoride removal from water by adsorption—A review, *Chem. Eng. J.* 171 (2011) 811–840. doi:10.1016/j.cej.2011.05.028.
- [32] K. Biswas, K. Gupta, A. Goswami, U.C. Ghosh, Fluoride removal efficiency from aqueous solution by synthetic iron(III)–aluminum(III)–chromium(III) ternary mixed oxide, *Desalination.* 255 (2010) 44–51. doi:10.1016/j.desal.2010.01.019.
- [33] A. Teutli-Sequeira, M. Solache-Ríos, P. Balderas-Hernández, Modification Effects of Hematite with Aluminum Hydroxide on the Removal of Fluoride Ions from Water, *Water, Air, Soil Pollut.* 223 (2012) 319–327. doi:10.1007/s11270-011-0860-3.
- [34] H. Kaygusuz, S. Uzaşçı, F.B. Erim, Removal of Fluoride from Aqueous Solution Using Aluminum Alginate Beads, *CLEAN - Soil, Air, Water.* 43 (2015) 724–730. doi:10.1002/clen.201300632.
- [35] H. Kaygusuz, M.H. Çoşkunırmak, N. Kahya, F.B. Erim, Aluminum Alginate–Montmorillonite Composite Beads for Defluoridation of Water, *Water, Air, Soil Pollut.* 226 (2015) 2257. doi:10.1007/s11270-014-2257-6.
- [36] A. Idris, N.S.M. Ismail, N. Hassan, E. Misran, A.-F. Ngomsik, Synthesis of magnetic alginate beads based on maghemite nanoparticles for Pb(II) removal in aqueous solution, *J. Ind. Eng. Chem.* 18 (2012) 1582–1589. doi:10.1016/j.jiec.2012.02.018.
- [37] S. Ben Hammouda, N. Adhoum, L. Monser, Synthesis of magnetic alginate beads based on Fe<sub>3</sub>O<sub>4</sub> nanoparticles for the removal of 3-methylindole from aqueous solution using Fenton process, *J. Hazard. Mater.* 294 (2015) 128–136. doi:10.1016/j.jhazmat.2015.03.068.
- [38] Z. Jiang, S. Xu, Y. Lu, W. Yuan, H. Wu, C. Lv, Nanotube-doped alginate gel as a novel carrier for BSA immobilization., *J. Biomater. Sci. Polym. Ed.* 17 (2006) 21–35.
- [39] J. Mongkolkajit, J. Pullsirisombat, S. Limtong, M. Phisalaphong, Alumina-doped alginate gel as a cell carrier for ethanol production in a packed-bed bioreactor, *Biotechnol. Bioprocess Eng.* 16 (2011) 505–512. doi:10.1007/s12257-010-0404-5.
- [40] M. Ionita, M.A. Pandele, H. Iovu, Sodium alginate/graphene oxide composite films with enhanced thermal and mechanical properties, *Carbohydr. Polym.* 94 (2013) 339–344. doi:10.1016/j.carbpol.2013.01.065.
- [41] Y. Zhuang, F. Yu, J. Chen, J. Ma, Batch and column adsorption of methylene blue by graphene/alginate nanocomposite: Comparison of single-network and double-network hydrogels, *J. Environ. Chem. Eng.* 4 (2016) 147–156. doi:10.1016/j.jece.2015.11.014.
- [42] Y. Zhuang, F. Yu, H. Chen, J. Zheng, J. Ma, J. Chen, Alginate/graphene double-network nanocomposite hydrogel beads with low-swelling, enhanced mechanical properties, and enhanced adsorption capacity, *J. Mater. Chem. A.*

- 4 (2016) 10885–10892. doi:10.1039/C6TA02738E.
- [43] K. Sultana, G. Godward, N. Reynolds, R. Arumugaswamy, P. Peiris, K. Kailasapathy, Encapsulation of probiotic bacteria with alginate–starch and evaluation of survival in simulated gastrointestinal conditions and in yoghurt, *Int. J. Food Microbiol.* 62 (2000) 47–55. doi:10.1016/S0168-1605(00)00380-9.
- [44] D.A. Bichara, X. Zhao, N.S. Hwang, H. Bodugoz-Senturk, M.J. Yaremchuk, M.A. Randolph, et al., Porous Poly(vinyl alcohol)-Alginate Gel Hybrid Construct for Neocartilage Formation Using Human Nasoseptal Cells, *J. Surg. Res.* 163 (2010) 331–336. doi:10.1016/j.jss.2010.03.070.
- [45] E.K. Solak, O. Şanlı, Use of Sodium Alginate-Poly(vinyl pyrrolidone) Membranes for Pervaporation Separation of Acetone/Water Mixtures, *Sep. Sci. Technol.* 45 (2010) 1354–1362. doi:10.1080/01496391003608256.
- [46] M. Beyer, J. Reichert, E. Heurich, K.D. Jandt, B.W. Sigusch, Pectin, alginate and gum arabic polymers reduce citric acid erosion effects on human enamel, *Dent. Mater.* 26 (2010) 831–839. doi:10.1016/j.dental.2010.04.008.
- [47] Z. Li, H.R. Ramay, K.D. Hauch, D. Xiao, M. Zhang, Chitosan–alginate hybrid scaffolds for bone tissue engineering, *Biomaterials.* 26 (2005) 3919–3928. doi:10.1016/j.biomaterials.2004.09.062.
- [48] C. Ouwerx, N. Velings, M. Mestdagh, M.A. Axelos, Physico-chemical properties and rheology of alginate gel beads formed with various divalent cations, *Polym. Gels Networks.* 6 (1998) 393–408. doi:10.1016/S0966-7822(98)00035-5.
- [49] G. Kaklamani, D. Cheneler, L.M. Grover, M.J. Adams, J. Bowen, Mechanical properties of alginate hydrogels manufactured using external gelation., *J. Mech. Behav. Biomed. Mater.* 36 (2014) 135–42. doi:10.1016/j.jmbbm.2014.04.013.
- [50] C.X. Wang, C. Cowen, Z. Zhang, C.R. Thomas, High-speed compression of single alginate microspheres, *Chem. Eng. Sci.* 60 (2005) 6649–6657. doi:10.1016/j.ces.2005.05.052.
- [51] E.-S. Chan, T.-K. Lim, W.-P. Voo, R. Pogaku, B.T. Tey, Z. Zhang, Effect of formulation of alginate beads on their mechanical behavior and stiffness, *Particuology.* 9 (2011) 228–234. doi:10.1016/j.partic.2010.12.002.
- [52] J. Yang, J. Zhao, Y. Fang, Calorimetric studies of the interaction between sodium alginate and sodium dodecyl sulfate in dilute solutions at different pH values., *Carbohydr. Res.* 343 (2008) 719–25. doi:10.1016/j.carres.2007.12.010.
- [53] N. Öztekin, S. Başkan, F.B. Erim, Determination of alginate copolymer in pharmaceutical formulations by micellar electrokinetic chromatography, *J. Chromatogr. B.* 850 (2007) 488–492. doi:10.1016/j.jchromb.2006.12.025.
- [54] J. Yang, S. Chen, Y. Fang, Viscosity study of interactions between sodium alginate and CTAB in dilute solutions at different pH values, *Carbohydr. Polym.* 75 (2009) 333–337. doi:10.1016/j.carbpol.2008.07.037.
- [55] J. Yang, J. Zhao, Y. Fang, Calorimetric studies of the interaction between sodium alginate and sodium dodecyl sulfate in dilute solutions at different pH

values., Carbohydr. Res. 343 (2008) 719–25. doi:10.1016/j.carres.2007.12.010.

- [56] H. Bu, A.-L. Kjøniksen, A. Elgsaeter, B. Nyström, Interaction of unmodified and hydrophobically modified alginate with sodium dodecyl sulfate in dilute aqueous solution, *Colloids Surfaces A Physicochem. Eng. Asp.* 278 (2006) 166–174. doi:10.1016/j.colsurfa.2005.12.016.
- [57] H. Hertz, Über die Berührung fester elastischer Körper, *J. Für Die Reine Und Angew. Math.* 92 (1881) 156–171.
- [58] K. Kim, J. Cheng, Q. Liu, X.Y. Wu, Y. Sun, Investigation of mechanical properties of soft hydrogel microcapsules in relation to protein delivery using a MEMS force sensor., *J. Biomed. Mater. Res. A.* 92 (2010) 103–13. doi:10.1002/jbm.a.32338.
- [59] R Core Team, R: A language and environment for statistical computing, (2013). <http://www.r-project.org>.
- [60] S.J. Horn, E. Moen, K. Østgaard, Direct determination of alginate content in brown algae by near infra-red (NIR) spectroscopy, *J. Appl. Phycol.* 11 (1999) 9–13. doi:10.1023/A:1008024009954.
- [61] A. Haug, O. Smidsrød, Selectivity of Some Anionic Polymers for Divalent Metal Ions, *Acta Chem. Scand.* 24 (1970) 843–854.
- [62] Y.A. Mørch, I. Donati, B.L. Strand, G. Skjåk-Braek, Effect of Ca<sup>2+</sup>, Ba<sup>2+</sup>, and Sr<sup>2+</sup> on alginate microbeads., *Biomacromolecules.* 7 (2006) 1471–80. doi:10.1021/bm060010d.
- [63] G. Decher, Fuzzy Nanoassemblies: Toward Layered Polymeric Multicomposites, *Science* (80-. ). 277 (1997) 1232–1237. doi:10.1126/science.277.5330.1232.
- [64] R. von Klitzing, Internal structure of polyelectrolyte multilayer assemblies., *Phys. Chem. Chem. Phys.* 8 (2006) 5012–33. doi:10.1039/b607760a.
- [65] G.B. Sukhorukov, E. Donath, H. Lichtenfeld, E. Knippel, M. Knippel, A. Budde, et al., Layer-by-layer self assembly of polyelectrolytes on colloidal particles, *Colloids Surfaces A Physicochem. Eng. Asp.* 137 (1998) 253–266. doi:10.1016/S0927-7757(98)00213-1.
- [66] L. Krasemann, B. Tieke, Highly Efficient Composite Membranes for Ethanol-Water Pervaporation, *Chem. Eng. Technol.* 23 (2000) 211–213. doi:10.1002/(SICI)1521-4125(200003)23:3<211::AID-CEAT211>3.0.CO;2-7.
- [67] D. Volodkin, R. von Klitzing, Competing mechanisms in polyelectrolyte multilayer formation and swelling: Polycation–polyanion pairing vs. polyelectrolyte–ion pairing, *Curr. Opin. Colloid Interface Sci.* 19 (2014) 25–31. doi:10.1016/j.cocis.2014.01.001.
- [68] J.B. Schlenoff, S.T. Dubas, Mechanism of polyelectrolyte multilayer growth: Charge overcompensation and distribution, *Macromolecules.* 34 (2001) 592–598. doi:10.1021/ma0003093.
- [69] R.A. Ghostine, M.Z. Markarian, J.B. Schlenoff, Asymmetric Growth in Polyelectrolyte Multilayers, *J. Am. Chem. Soc.* 135 (2013) 7636–7646. doi:10.1021/ja401318m.

- [70] J.J. Harris, M.L. Bruening, Electrochemical and in situ ellipsometric investigation of the permeability and stability of layered polyelectrolyte films, *Langmuir*. 16 (2000) 2006–2013. doi:10.1021/la990620h.
- [71] S. Dodoo, R. Steitz, A. Laschewsky, R. von Klitzing, Effect of ionic strength and type of ions on the structure of water swollen polyelectrolyte multilayers, *Phys. Chem. Chem. Phys.* 13 (2011) 10318. doi:10.1039/c0cp01357a.
- [72] J.B. Schlenoff, H. Ly, M. Li, Charge and Mass Balance in Polyelectrolyte Multilayers, *J. Am. Chem. ....* 7863 (1998) 7626–7634. doi:10.1021/ja980350.
- [73] L. Han, Z. Mao, H. Wuliyasu, J. Wu, X. Gong, Y. Yang, et al., Modulating the Structure and Properties of Poly(sodium 4-styrenesulfonate)/Poly(diallyldimethylammonium chloride) Multilayers with Concentrated Salt Solutions, *Langmuir*. 28 (2012) 193–199. doi:10.1021/la2040533.
- [74] S.T. Dubas, J.B. Schlenoff, Factors controlling the growth of polyelectrolyte multilayers, *Macromolecules*. 32 (1999) 8153–8160. doi:10.1021/ma981927a.
- [75] L. Ghimici, S. Dragan, Behaviour of cationic polyelectrolytes upon binding of electrolytes: effects of polycation structure, counterions and nature of the solvent, *Colloid Polym. Sci.* 280 (2002) 130–134. doi:10.1007/s003960100575.
- [76] E. Poptoshev, B. Schoeler, F. Caruso, Influence of solvent quality on the growth of polyelectrolyte multilayers, *Langmuir*. 20 (2004) 829–834. doi:10.1021/la035485u.
- [77] K. Büscher, K. Graf, H. Ahrens, C. A. Helm, Influence of Adsorption Conditions on the Structure of Polyelectrolyte Multilayers, (2002). doi:10.1021/LA011682M.
- [78] P. Nestler, S. Block, C.A. Helm, Temperature-Induced Transition from Odd–Even to Even–Odd Effect in Polyelectrolyte Multilayers Due to Interpolyelectrolyte Interactions, *J. Phys. Chem. B*. 116 (2012) 1234–1243. doi:10.1021/jp208837m.
- [79] R. Steitz, V. Leiner, K. Tauer, V. Khrenov, R. von Klitzing, Temperature-induced changes in polyelectrolyte films at the solid-liquid interface, *Appl. Phys. A Mater. Sci. Process.* 74 (2002) s519–s521. doi:10.1007/s003390201782.
- [80] A. Garg, J.R. Heflin, H.W. Gibson, R.M. Davis, Study of Film Structure and Adsorption Kinetics of Polyelectrolyte Multilayer Films: Effect of pH and Polymer Concentration, *Langmuir*. 24 (2008) 10887–10894. doi:10.1021/la8005053.
- [81] K. Glinel, A. Moussa, A.M. Jonas, A. Laschewsky, Influence of polyelectrolyte charge density on the formation of multilayers of strong polyelectrolytes at low ionic strength, *Langmuir*. 18 (2002) 1408–1412. doi:10.1021/la0113670.
- [82] S. Micciulla, Organic and inorganic coatings of polymer brushes: mutual effects on structural and stimuli responsive properties, Technische Universität Berlin, 2016.

- [83] J.E. Wong, F. Rehfeldt, P. Hänni, M. Tanaka, R. von Klitzing, Swelling Behavior of Polyelectrolyte Multilayers in Saturated Water Vapor, *Macromolecules*. 37 (2004) 7285–7289. doi:10.1021/ma0351930.
- [84] K. Köhler, D.G. Shchukin, H. Möhwald, G.B. Sukhorukov, Thermal behavior of polyelectrolyte multilayer microcapsules. 1. The effect of odd and even layer number., *J. Phys. Chem. B*. 109 (2005) 18250–9. doi:10.1021/jp052208i.
- [85] D. Yoo, S.S. Shiratori, M.F. Rubner, Controlling Bilayer Composition and Surface Wettability of Sequentially Adsorbed Multilayers of Weak Polyelectrolytes, *Macromolecules*. 31 (1998) 4309–4318. doi:10.1021/ma9800360.
- [86] W. Yuan, H. Dong, C.M. Li, X. Cui, L. Yu, Z. Lu, et al., pH-controlled construction of chitosan/alginate multilayer film: characterization and application for antibody immobilization., *Langmuir*. 23 (2007) 13046–52. doi:10.1021/la702774a.
- [87] W. Feng, W. Nie, C. He, X. Zhou, L. Chen, K. Qiu, et al., Effect of pH-responsive alginate/chitosan multilayers coating on delivery efficiency, cellular uptake and biodistribution of mesoporous silica nanoparticles based nanocarriers., *ACS Appl. Mater. Interfaces*. 6 (2014) 8447–60. doi:10.1021/am501337s.
- [88] A. Acevedo-Fani, L. Salvia-Trujillo, R. Soliva-Fortuny, O. Martín-Belloso, Modulating Biopolymer Electrical Charge to Optimize the Assembly of Edible Multilayer Nanofilms by the Layer-by-Layer Technique., *Biomacromolecules*. 16 (2015) 2895–903. doi:10.1021/acs.biomac.5b00821.
- [89] N.M. Alves, C. Picart, J.F. Mano, Self assembling and crosslinking of polyelectrolyte multilayer films of chitosan and alginate studied by QCM and IR spectroscopy., *Macromol. Biosci*. 9 (2009) 776–85. doi:10.1002/mabi.200800336.
- [90] G. Maurstad, Y.A. Morch, A.R. Bausch, B.T. Stokke, Polyelectrolyte layer interpenetration and swelling of alginate–chitosan multilayers studied by dual wavelength reflection interference contrast microscopy, *Carbohydr. Polym*. 71 (2008) 672–681. doi:10.1016/j.carbpol.2007.07.019.
- [91] M. Thongngam, D.J. McClements, Characterization of interactions between chitosan and an anionic surfactant., *J. Agric. Food Chem*. 52 (2004) 987–91. doi:10.1021/jf034429w.
- [92] M. Rodahl, B. Kasemo, A simple setup to simultaneously measure the resonant frequency and the absolute dissipation factor of a quartz crystal microbalance,  
[http://oasc12039.247realmedia.com/RealMedia/ads/click\\_lx.ads/www.aip.org/pt/adcenter/pdfcover\\_test/L-37/804729140/x01/AIP-PT/MCL\\_RSIArticleDL\\_022217/MCL\\_banner.jpg/434f71374e315a556e61414141774c75?x](http://oasc12039.247realmedia.com/RealMedia/ads/click_lx.ads/www.aip.org/pt/adcenter/pdfcover_test/L-37/804729140/x01/AIP-PT/MCL_RSIArticleDL_022217/MCL_banner.jpg/434f71374e315a556e61414141774c75?x). (1998). doi:10.1063/1.1147494.
- [93] G. Sauerbrey, Verwendung von Schwingquarzen zur Wägung dünner Schichten und zur Mikrowägung, *Zeitschrift Für Phys*. 155 (1959) 206–222. doi:10.1007/BF01337937.
- [94] M. Zerboll, A. Laschewsky, R. von Klitzing, Swelling of Polyelectrolyte

- Multilayers: The Relation Between, Surface and Bulk Characteristics, *J. Phys. Chem. B.* 119 (2015) 11879–11886. doi:10.1021/acs.jpcc.5b04350.
- [95] S. Micciulla, P.A. Sánchez, J. Smiatek, B. Qiao, M. Segal, A. Laschewsky, et al., Layer-by-Layer Formation of Oligoelectrolyte Multilayers: A Combined Experimental and Computational Study, *Soft Mater.* 12 (2014) S14–S21. doi:10.1080/1539445X.2014.930046.
- [96] B. Balakrishnan, M. Mohanty, P.R. Umashankar, A. Jayakrishnan, Evaluation of an in situ forming hydrogel wound dressing based on oxidized alginate and gelatin, *Biomaterials.* 26 (2005) 6335–6342. doi:10.1016/j.biomaterials.2005.04.012.
- [97] T. Dai, Y.Y. Huang, S.K. Sharma, J.T. Hashmi, D.B. Kurup, M.R. Hamblin, Topical antimicrobials for burn wound infections., *Recent Pat. Antiinfect. Drug Discov.* 5 (2010) 124–51.
- [98] R. Jayakumar, M. Prabakaran, P.T. Sudheesh Kumar, S.V. Nair, H. Tamura, Biomaterials based on chitin and chitosan in wound dressing applications, *Biotechnol. Adv.* 29 (2011) 322–337. doi:10.1016/j.biotechadv.2011.01.005.
- [99] N. Levi-Polyachenko, R. Jacob, C. Day, N. Kuthirummal, Chitosan wound dressing with hexagonal silver nanoparticles for hyperthermia and enhanced delivery of small molecules, *Colloids Surfaces B Biointerfaces.* 142 (2016) 315–324. doi:10.1016/j.colsurfb.2016.02.038.
- [100] V. Jones, J.E. Grey, K.G. Harding, Wound dressings., *BMJ.* 332 (2006) 777–80. doi:10.1136/bmj.332.7544.777.
- [101] R. Yin, Y. Huang, C. Huang, Y. Tong, N. Tian, Preparation and characterization of novel gelatin/cerium (III) fiber with antibacterial activity, 2009. doi:10.1016/j.matlet.2009.03.014.
- [102] W.W. Monafo, S.N. Tandon, V.H. Ayvazian, J. Tuhschmidt, A.M. Skinner, F. Deitz, Cerium nitrate: a new topical antiseptic for extensive burns., *Surgery.* 80 (1976) 465–73.
- [103] J.P. Garner, P.S.J. Heppell, Cerium nitrate in the management of burns, *Burns.* 31 (2005) 539–547. doi:10.1016/j.burns.2005.01.014.
- [104] T.J. Haley, *Pharmacology and Toxicology of the Rare Earth Elements*, *J. Pharm. Sci.* 54 (1965) 663–670. doi:10.1002/jps.2600540502.
- [105] ASTM E96-95, Standard test methods for water vapor transmission of materials, in: *Annu. B. ASTM Stand.*, American Society for Testing Materials, Philadelphia, PA, USA, 1994.
- [106] ISO, 22196:2007 Plastics -- Measurement of antibacterial activity on plastics surfaces, 2007.
- [107] K. Kashima, M. Imai, Advanced Membrane Material from Marine Biological Polymer and Sensitive Molecular-Size Recognition for Promising Separation Technology, in: *Adv. Desalin., InTech*, 2012. doi:10.5772/50734.
- [108] A.A. Santana, T.G. Kieckbusch, Physical evaluation of biodegradable films of calcium alginate plasticized with polyols, *Brazilian J. Chem. Eng.* 30 (2013) 835–845. doi:10.1590/S0104-66322013000400015.
- [109] N. Akter, R.A. Khan, M.O. Tuhin, M.E. Haque, M. Nurnabi, F. Parvin, et al.,

Thermomechanical, barrier, and morphological properties of chitosan-reinforced starch-based biodegradable composite films, *J. Thermoplast. Compos. Mater.* 27 (2014) 933–948. doi:10.1177/0892705712461512.

- [110] N. Sone, M. Sekimachi, E. Kutoh, Identification and properties of a quinol oxidase super-complex composed of a bc1 complex and cytochrome oxidase in the thermophilic bacterium PS3., *J. Biol. Chem.* 262 (1987) 15386–15391. doi:10.1063/1.2358685.
- [111] R. Xu, H. Xia, W. He, Z. Li, J. Zhao, B. Liu, et al., Controlled water vapor transmission rate promotes wound-healing via wound re-epithelialization and contraction enhancement, *Sci. Rep.* 6 (2016) 24596. doi:10.1038/srep24596.

## APPENDICES

### APPENDIX A: SUPPORTING INFORMATION FOR CHAPTER 3

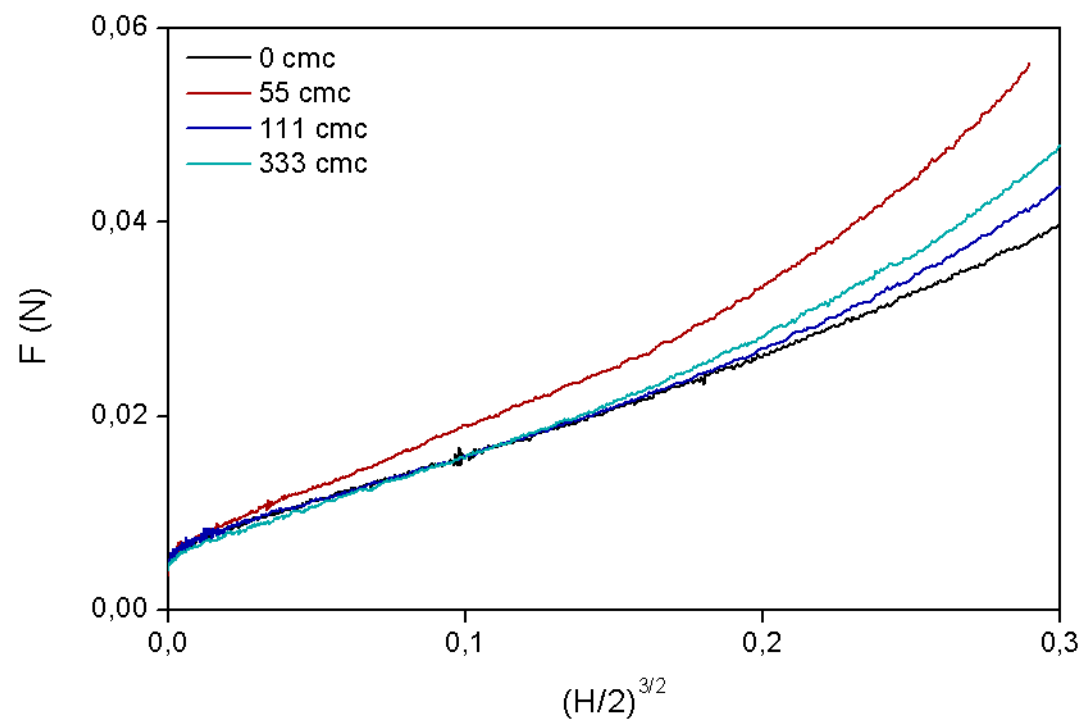


**Figure A.1 :** Force (N) versus  $(H)^{3/2}$  curves for beads with 1% (w/v) alginate beads crosslinked with 3% (w/v)  $\text{Ca}^{2+}$ ; doped with Brij 35

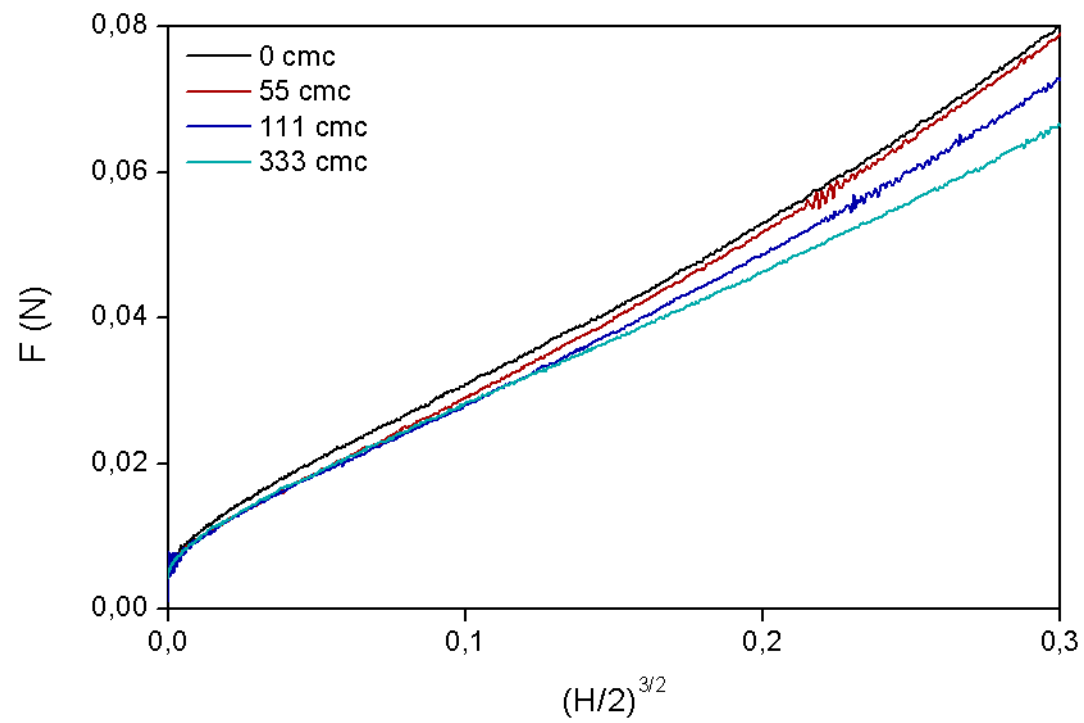


**Figure A.2 :** Force (N) versus  $(H)^{3/2}$  curves for beads with 2% (w/v) alginate beads crosslinked with 3% (w/v)  $\text{Ca}^{2+}$ ; doped with Brij 35

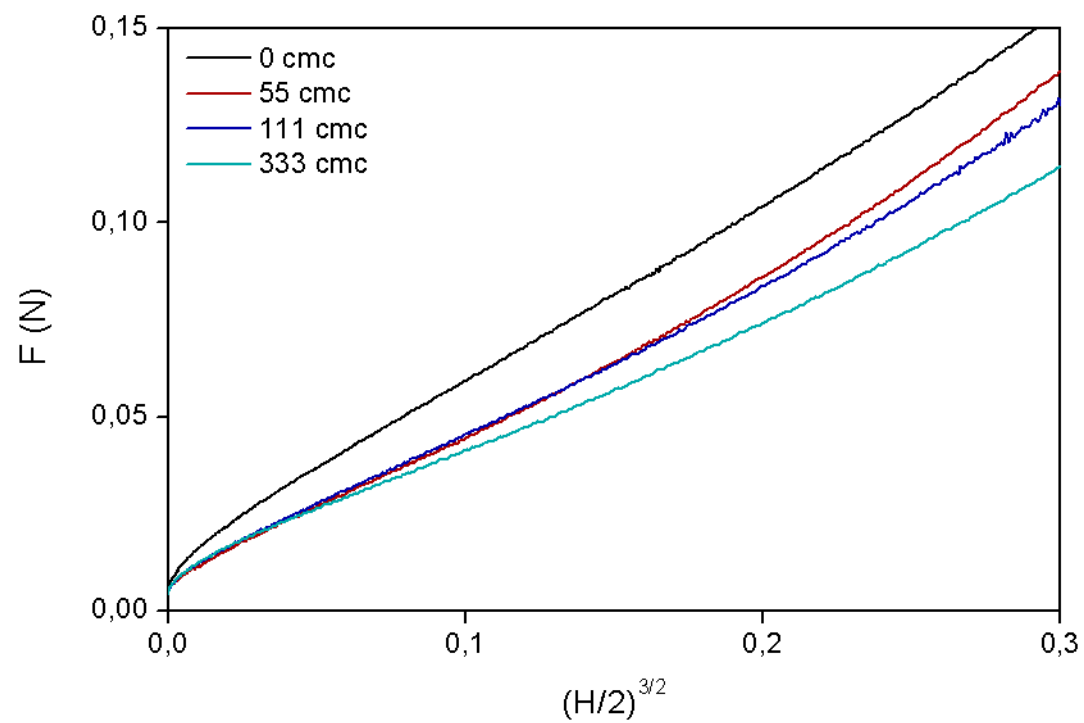


**Figure A.3 :** Force (N) versus  $(H)^{3/2}$  curves for beads with 3% (w/v) alginate beads crosslinked with 3% (w/v)  $\text{Ca}^{2+}$ ; doped with Brij 35

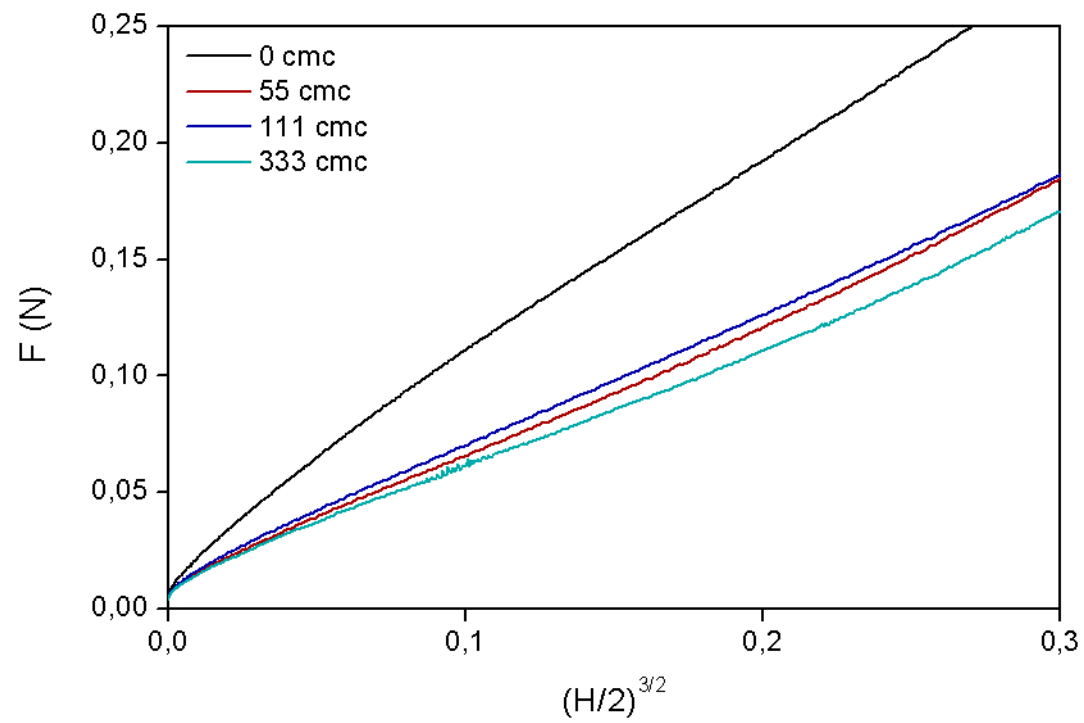


**Figure A.4 :** Force (N) versus  $(H)^{3/2}$  curves for beads with 4% (w/v) alginate beads crosslinked with 3% (w/v)  $\text{Ca}^{2+}$ ; doped with Brij 35

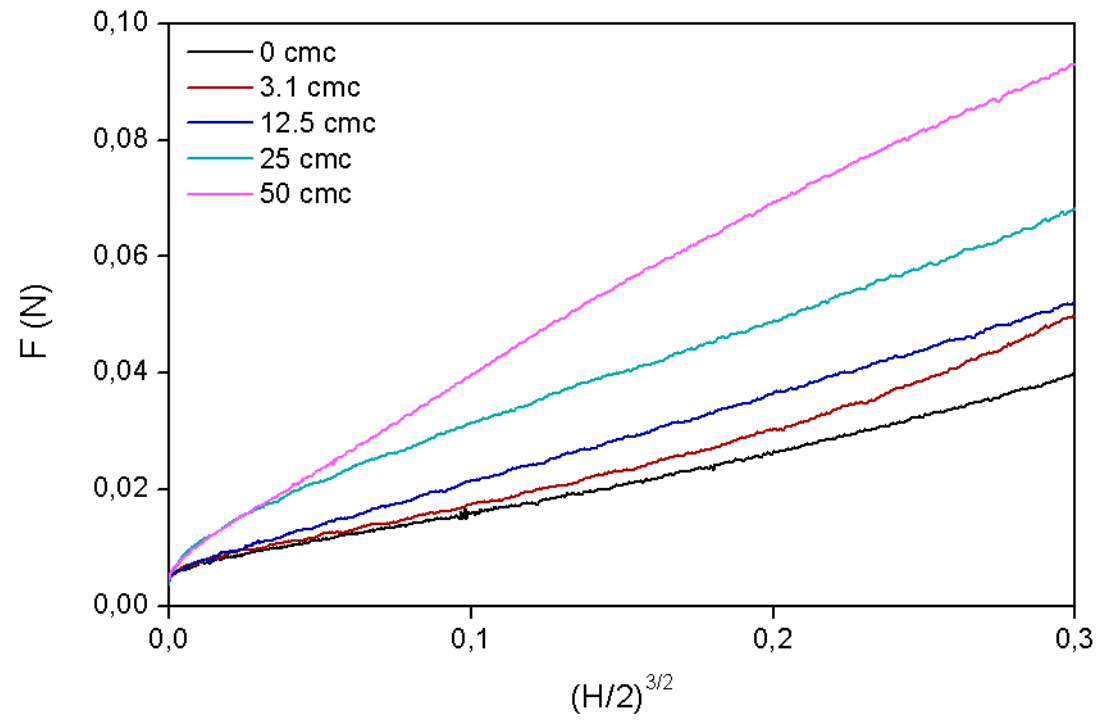


**Figure A.5** : Force (N) versus  $(H)^{3/2}$  curves for beads with 1% (w/v) alginate beads crosslinked with 3% (w/v)  $\text{Ca}^{2+}$ ; doped with SDS

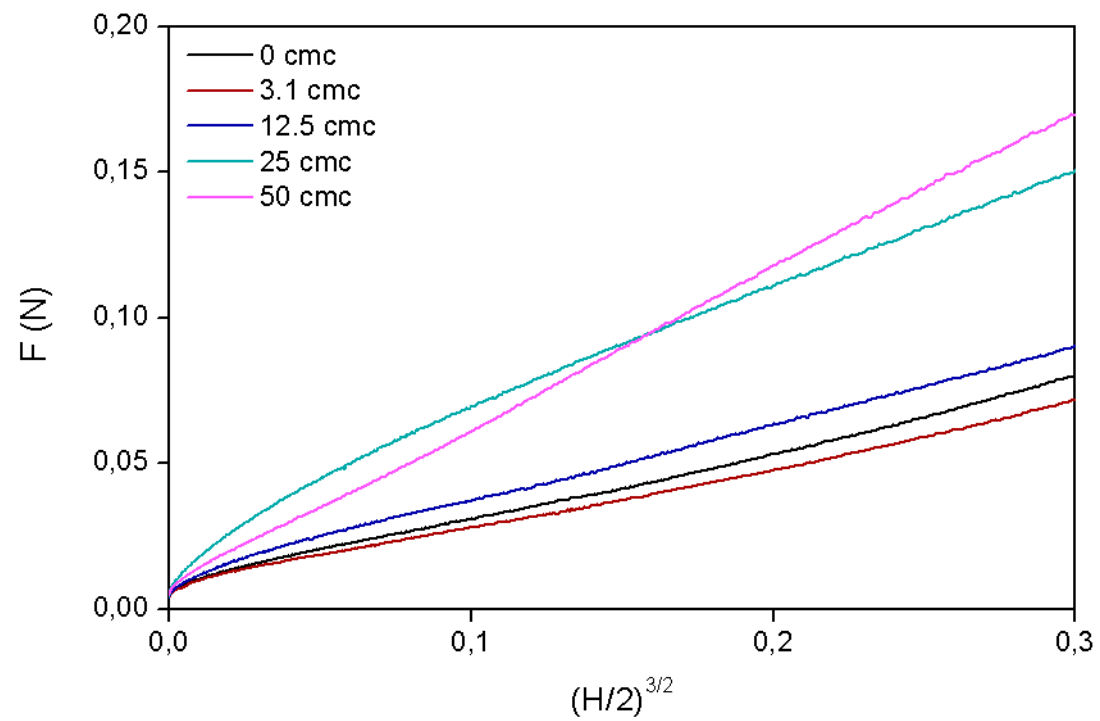


**Figure A.6** : Force (N) versus  $(H)^{3/2}$  curves for beads with 2% (w/v) alginate beads crosslinked with 3% (w/v)  $\text{Ca}^{2+}$ ; doped with SDS

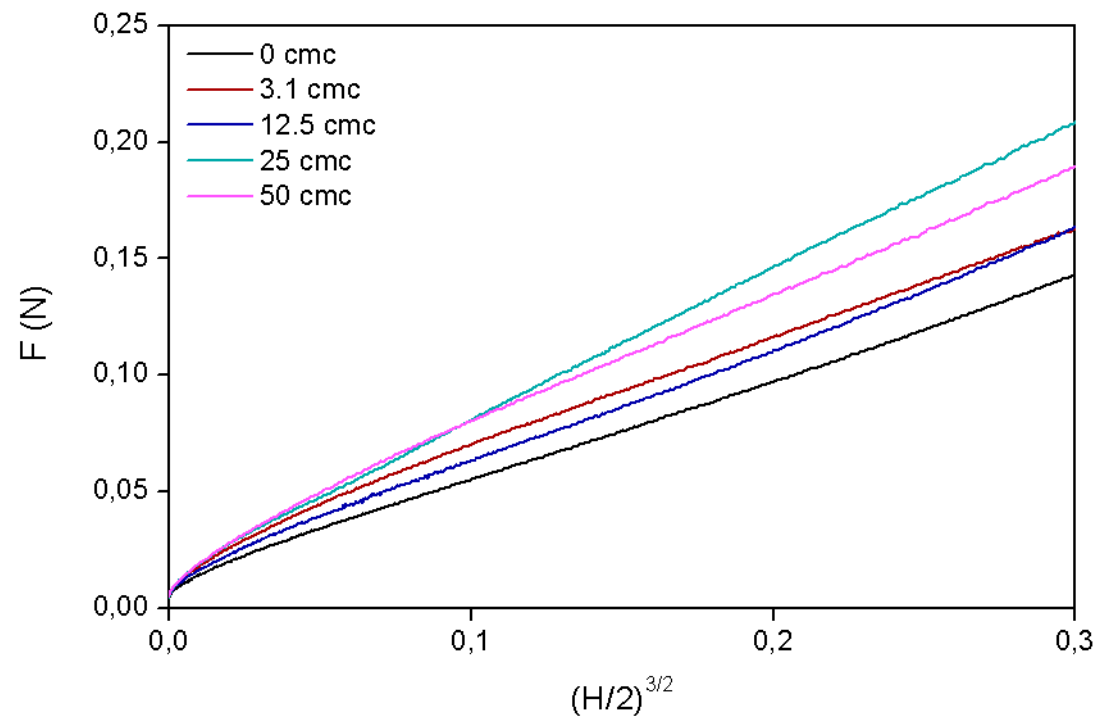


**Figure A.7 :** Force (N) versus  $(H)^{3/2}$  curves for beads with 3% (w/v) alginate beads crosslinked with 3% (w/v)  $\text{Ca}^{2+}$ ; doped with SDS

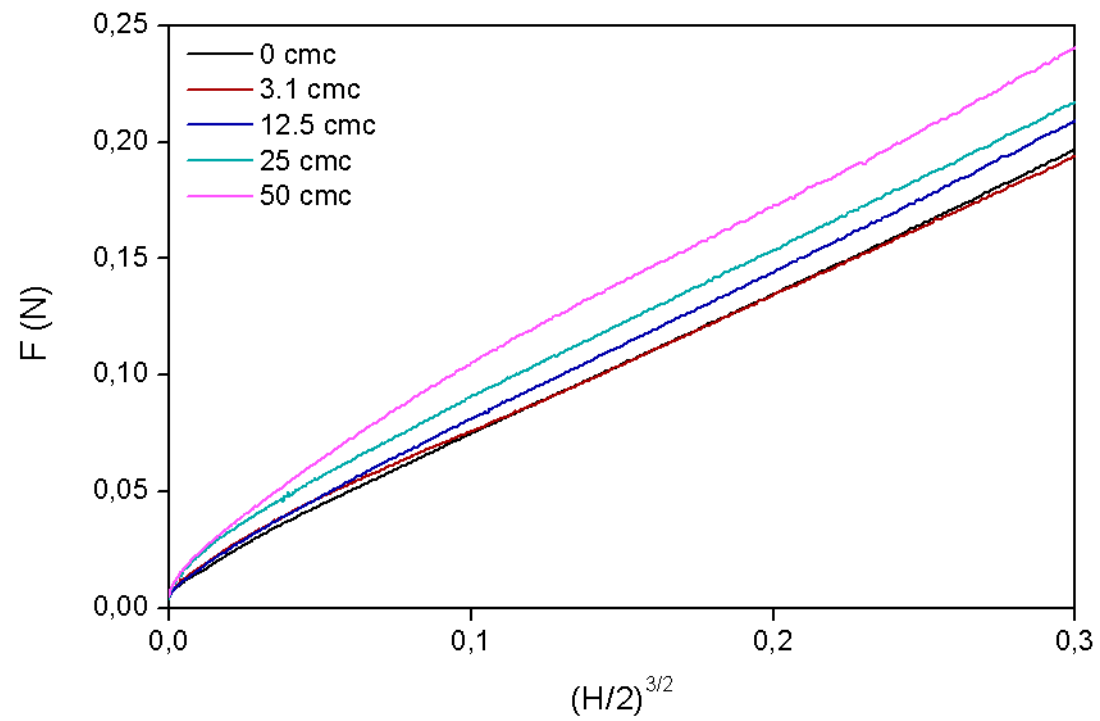


**Figure A.8** : Force (N) versus  $(H)^{3/2}$  curves for beads with 4% (w/v) alginate beads crosslinked with 3% (w/v)  $\text{Ca}^{2+}$ ; doped with SDS

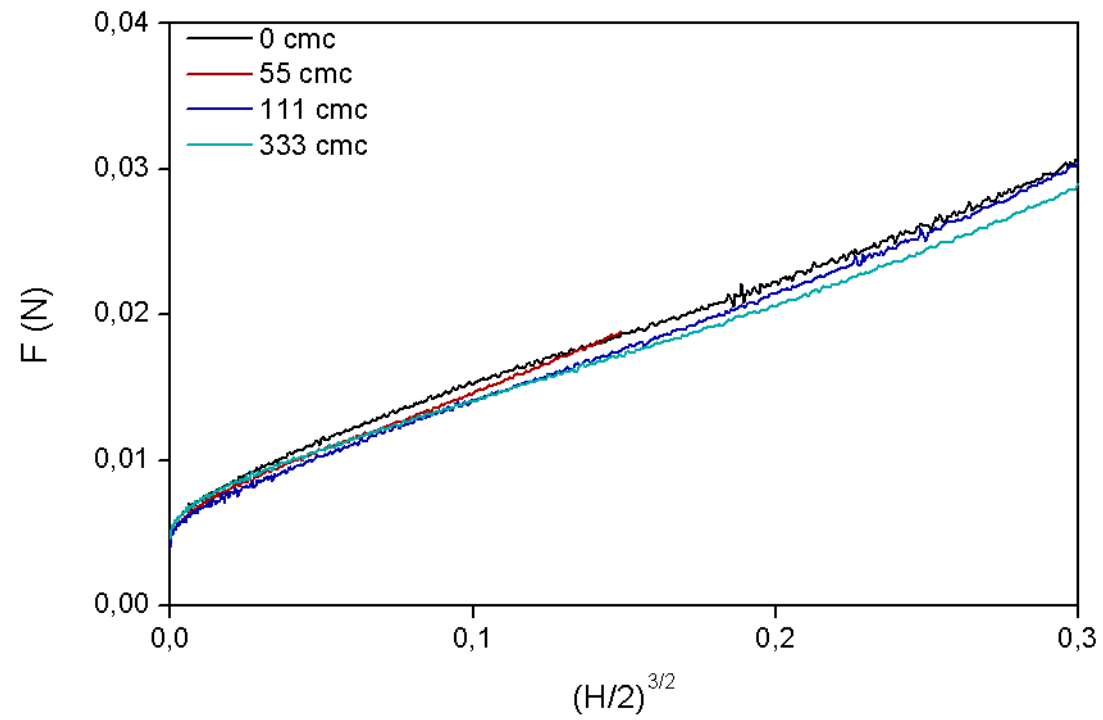


**Figure A.9 :** Force (N) versus  $(H)^{3/2}$  curves for beads with 1% (w/v) alginate beads crosslinked with 3% (w/v)  $Ba^{2+}$ ; doped with Brij 35

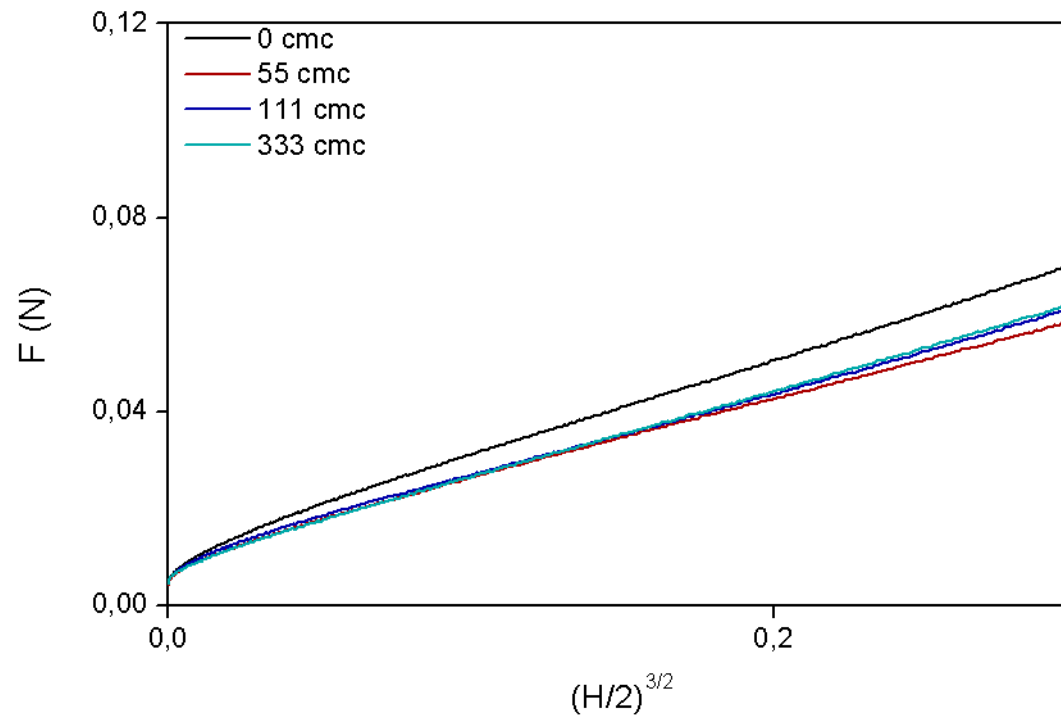


**Figure A.10** : Force (N) versus  $(H)^{3/2}$  curves for beads with 2% (w/v) alginate beads crosslinked with 3% (w/v)  $Ba^{2+}$ ; doped with Brij 35

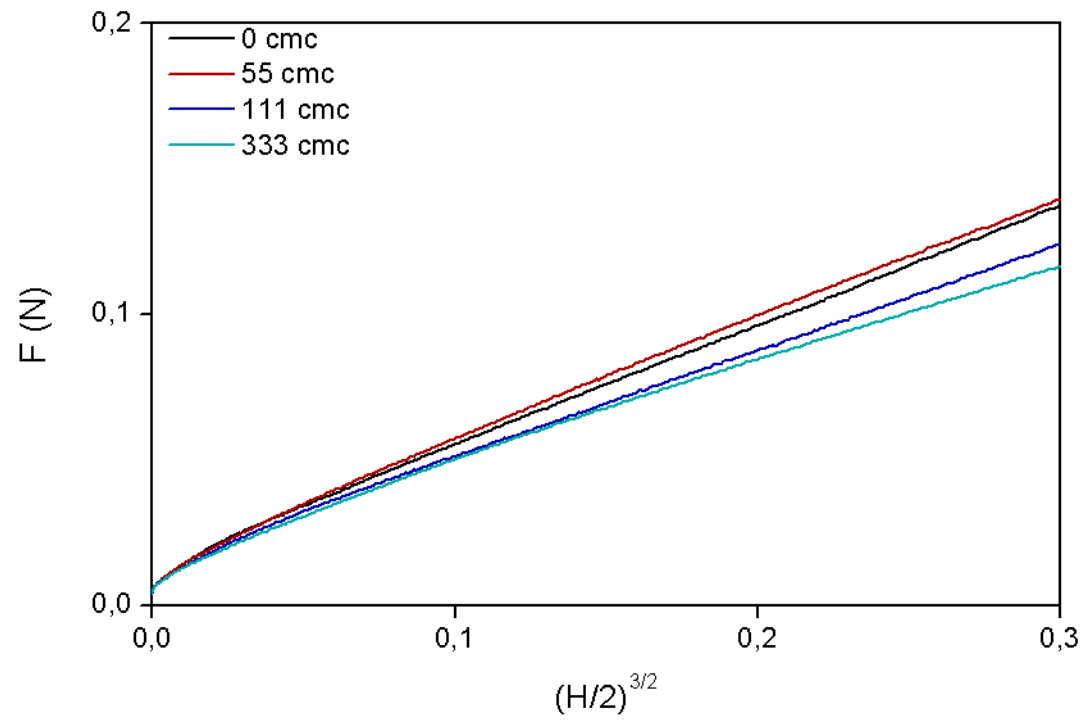


**Figure A.11** : Force (N) versus  $(H)^{3/2}$  curves for beads with 3% (w/v) alginate beads crosslinked with 3% (w/v)  $Ba^{2+}$ ; doped with Brij 35

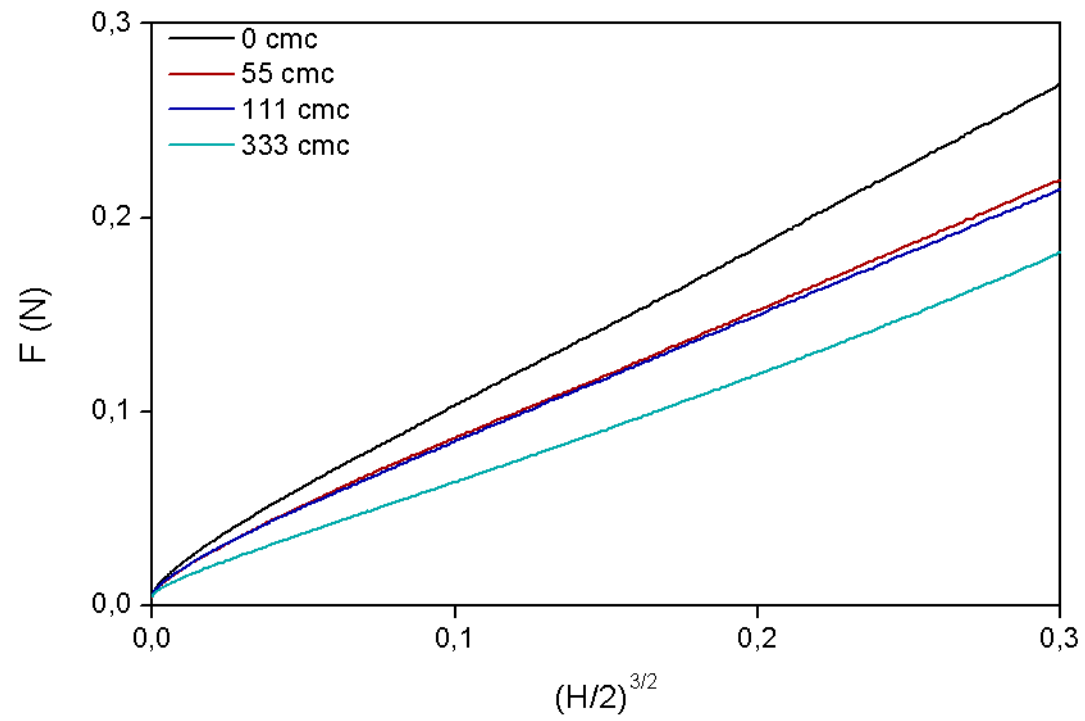


**Figure A.12** : Force (N) versus  $(H)^{3/2}$  curves for beads with 4% (w/v) alginate beads crosslinked with 3% (w/v)  $Ba^{2+}$ ; doped with Brij 35

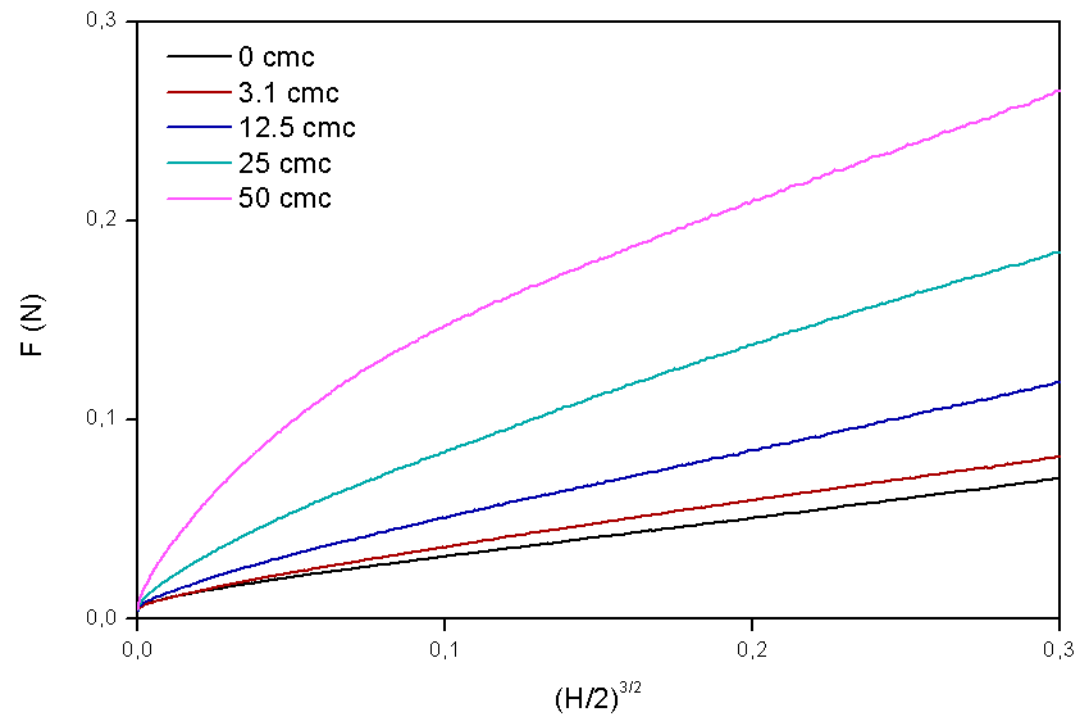


**Figure A.13** : Force (N) versus  $(H)^{3/2}$  curves for beads with 2% (w/v) alginate beads crosslinked with 3% (w/v)  $Ba^{2+}$ ; doped with SDS

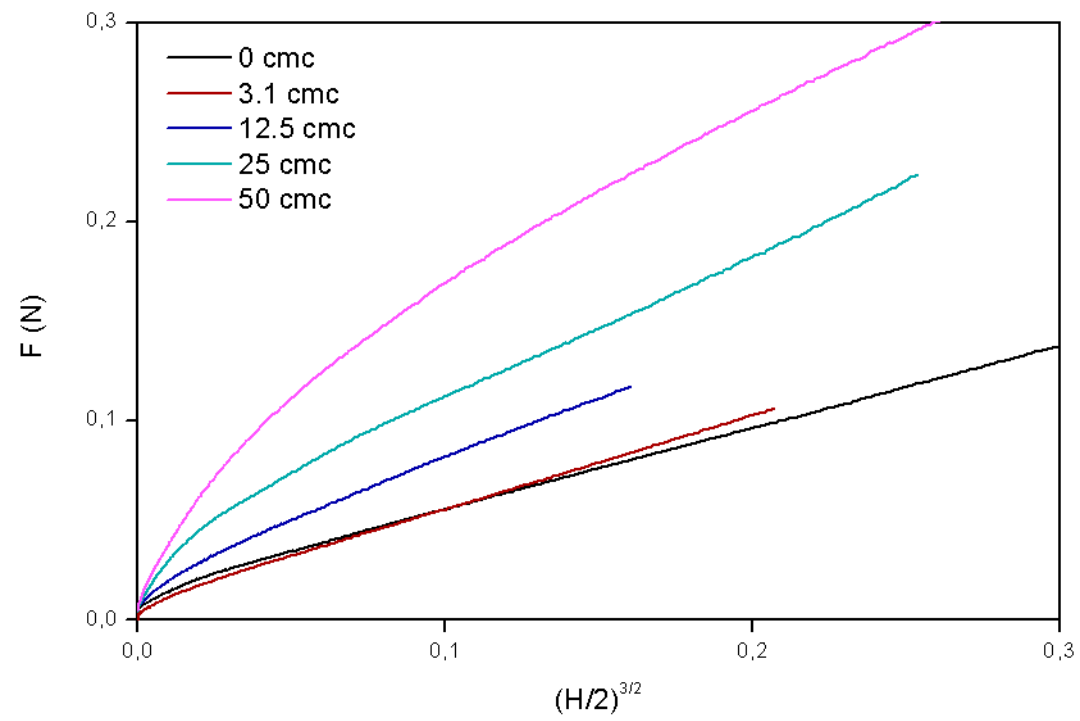


**Figure A.14 :** Force (N) versus  $(H)^{3/2}$  curves for beads with 3% (w/v) alginate beads crosslinked with 3% (w/v)  $Ba^{2+}$ ; doped with SDS

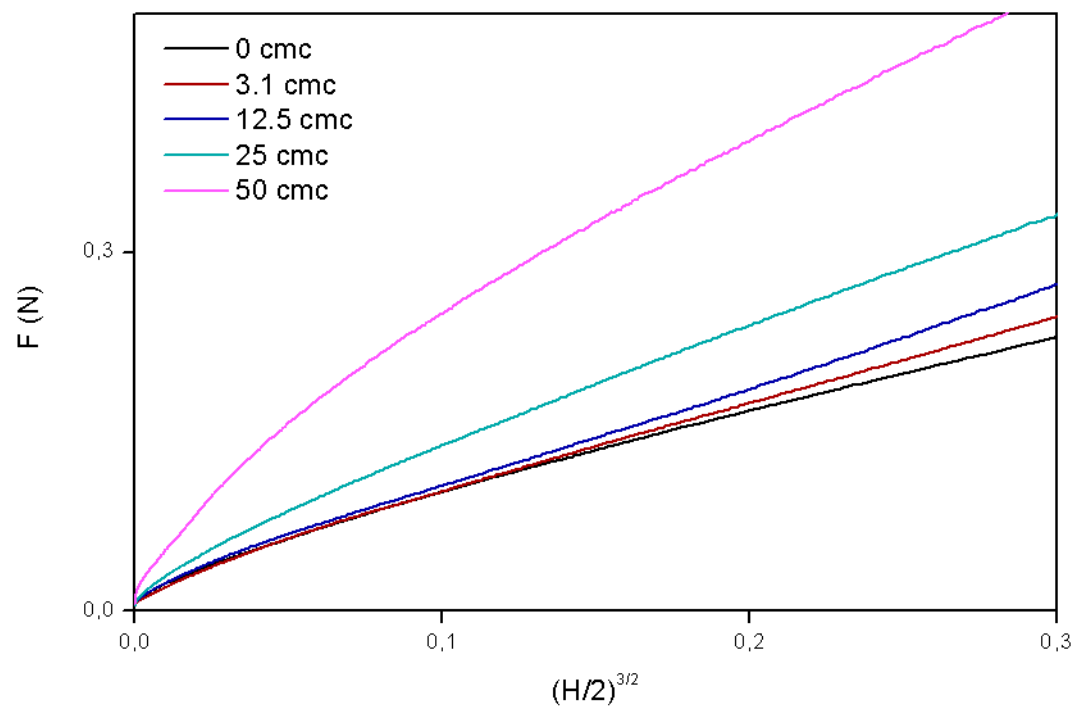


**Figure A.15** : Force (N) versus  $(H)^{3/2}$  curves for beads with 4% (w/v) alginate beads crosslinked with 3% (w/v)  $Ba^{2+}$ ; doped with SDS

**APPENDIX B: SUPPORTING INFORMATION FOR CHAPTER 4**

**Table B.1 :** Thickness values of the all PEM samples (calculated from ellipsometry data)

Without SDS					With SDS				
No. DL	Thickness (nm)		Thickness (nm)		No. DL	Thickness (nm)		Thickness (nm)	
	S. dev.		S. dev.			S. dev.		S. dev.	
	1% r.h.		Ambient conditions			1% r.h.		Ambient conditions	
1.5	3.3	0.2	3.6	0.2	1.5	2.8	0.2	3	0.2
2	5.9	0.2	6.1	0.1	2	6	0.1	6	0.1
3.5	6.2	0.2	6.7	0.2	3.5	5.2	0.2	5.7	0.3
4	10.9	1.2	11.8	1.5	4	11.1	1	15.1	5.2
5.5	11.6	0.5	12.7	0.6	5.5	8	0.5	10.4	0.1
6	16.6	2.1	18.4	2.5	6	19.8	1.1	26.4	2.9
11.5	20.2	0.6	23.6	1.1	11.5	21.5	1.8	28.0	0.4
12	21.3	0.3	24.5	0.9	12	22.4	1.2	32.2	2
17.5	34.6	1.1	41.1	0.2	17.5	38	0.9	41.2	0.3
18	35.0	0.2	38.4	0.6	18	45.8	3.6	53.9	5.1
29.5	72.2	1.1	86.2	1.5	29.5	88.1	1	96.4	2.7
30	90.4	3.3	110.6	2.2	30	101.1	6	124.3	2.6
39.5	108.2	1.2	119.1	1.5	39.5	122.4	1.2	129.5	1.5
40	115.0	1.4	127.3	0.2	40	135.5	1.1	149.7	0.3

**Table B.2** : Parameters of XRR fits.

	SiO <sub>2</sub> layer	Backing (Si)
Thickness (Å)	1.5	Infinite
SLD	18.91	20.15
Roughness	3	3

**Table B.3** : Swelling ratio (SR) values of the PEM samples

No. DL	SR (%)	
	Without SDS	With SDS
1.5	9.09	7.14
2	3.39	-
3.5	8.06	9.62
4	8.26	36.04
5.5	9.48	30.00
6	10.84	33.33
11.5	16.83	30.23
12	15.02	43.75
17.5	18.79	8.42
18	9.71	17.69
29.5	19.39	9.42
30	22.35	22.95
39.5	10.07	5.80
40	10.70	10.48

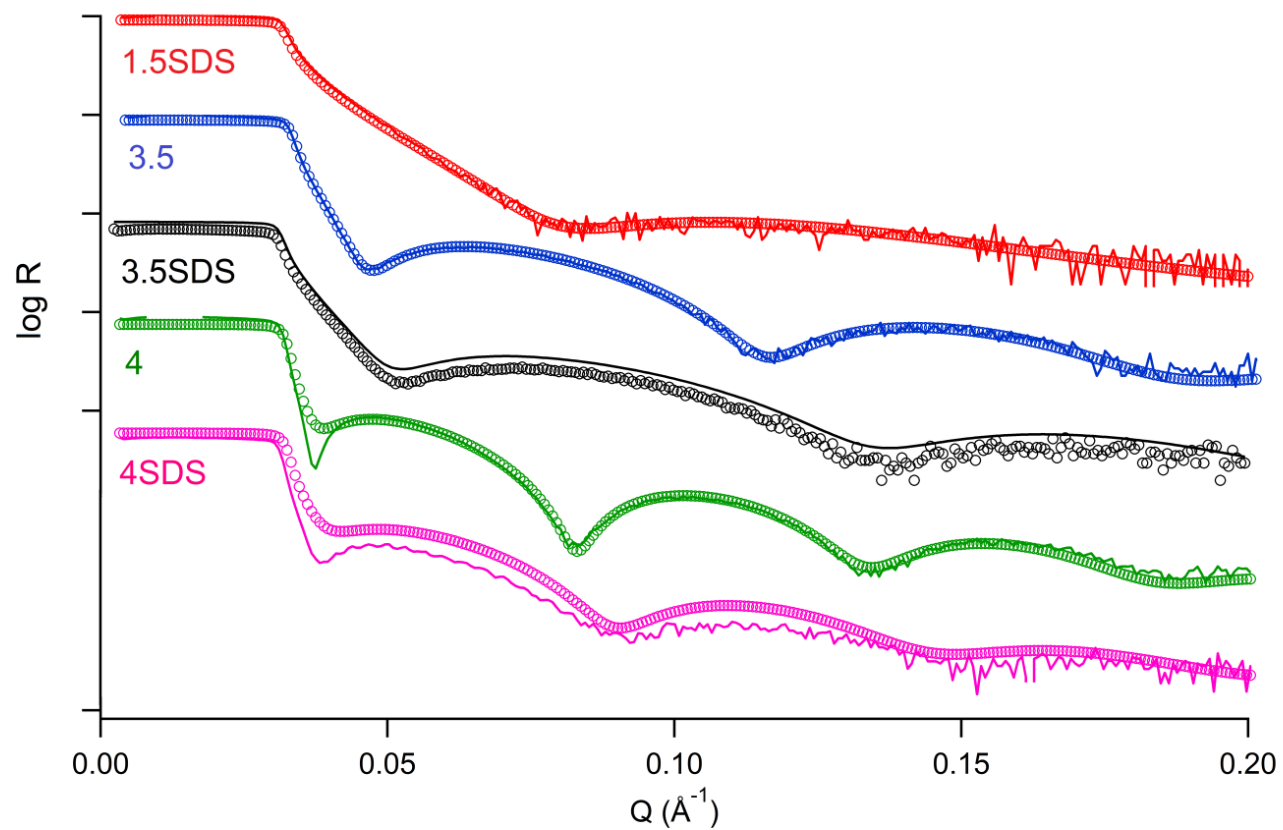


**Figure B.1** : XRR data and fit of PEM samples measured at ambient conditions. Dots indicate fits and lines are experimental data.

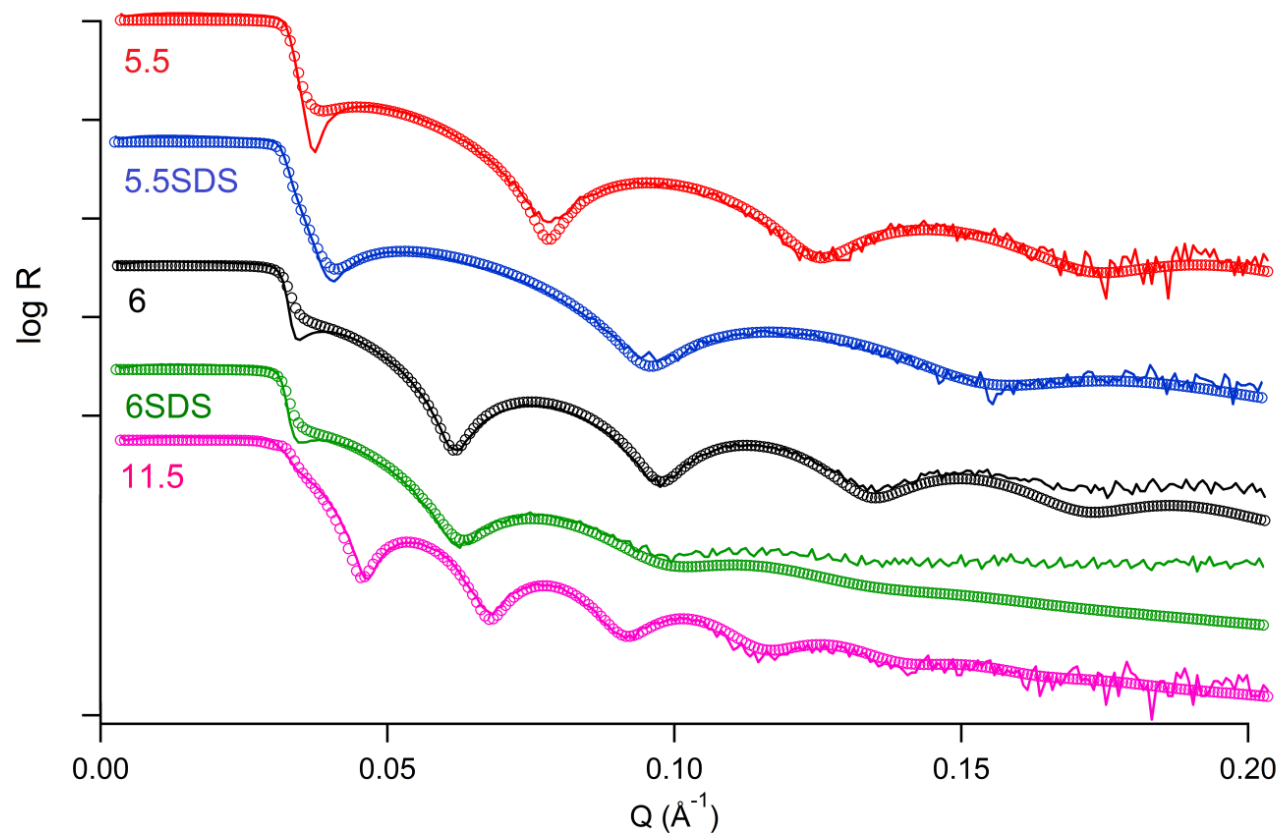


**Figure B.2** : XRR data and fit of PEM samples measured at ambient conditions. Dots indicate fits and lines are experimental data.

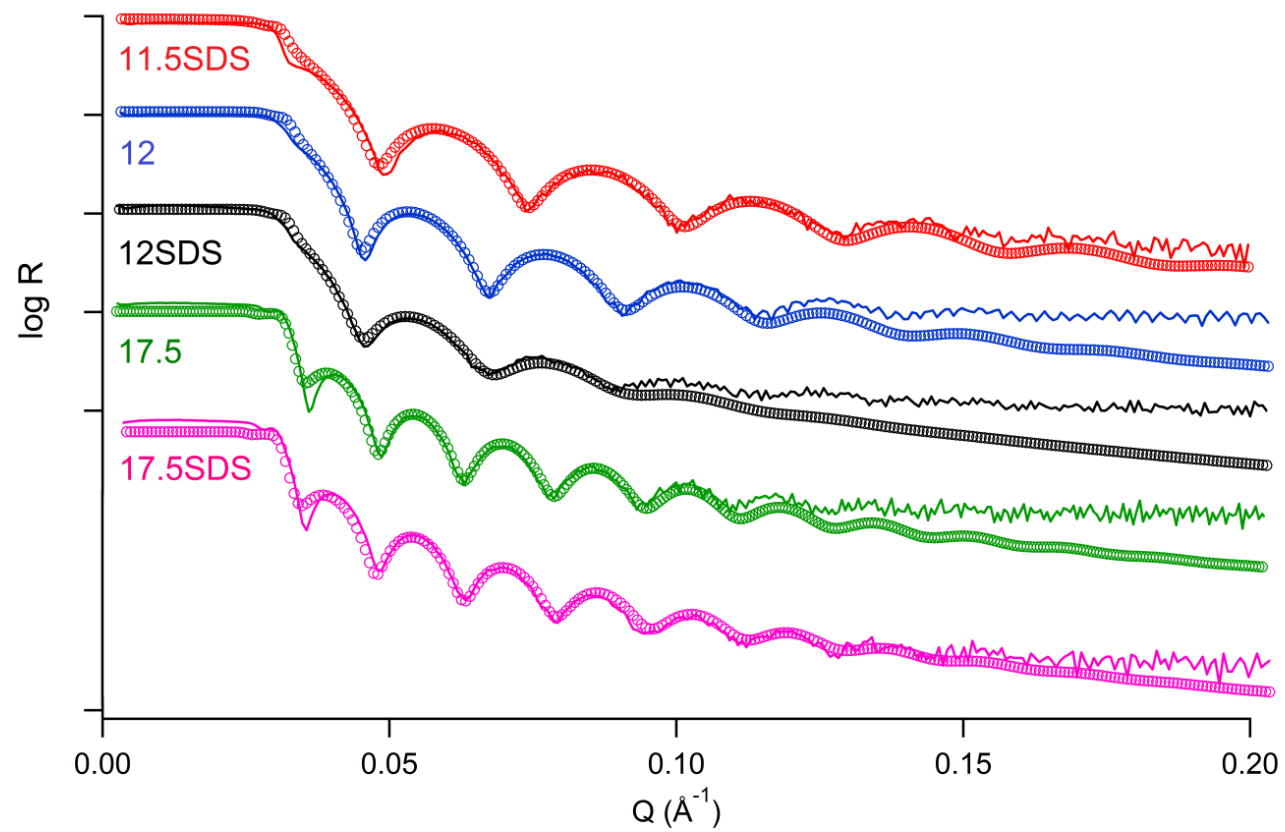


**Figure B.3 :** XRR data and fit of PEM samples measured at ambient conditions. Dots indicate fits and lines are experimental data.

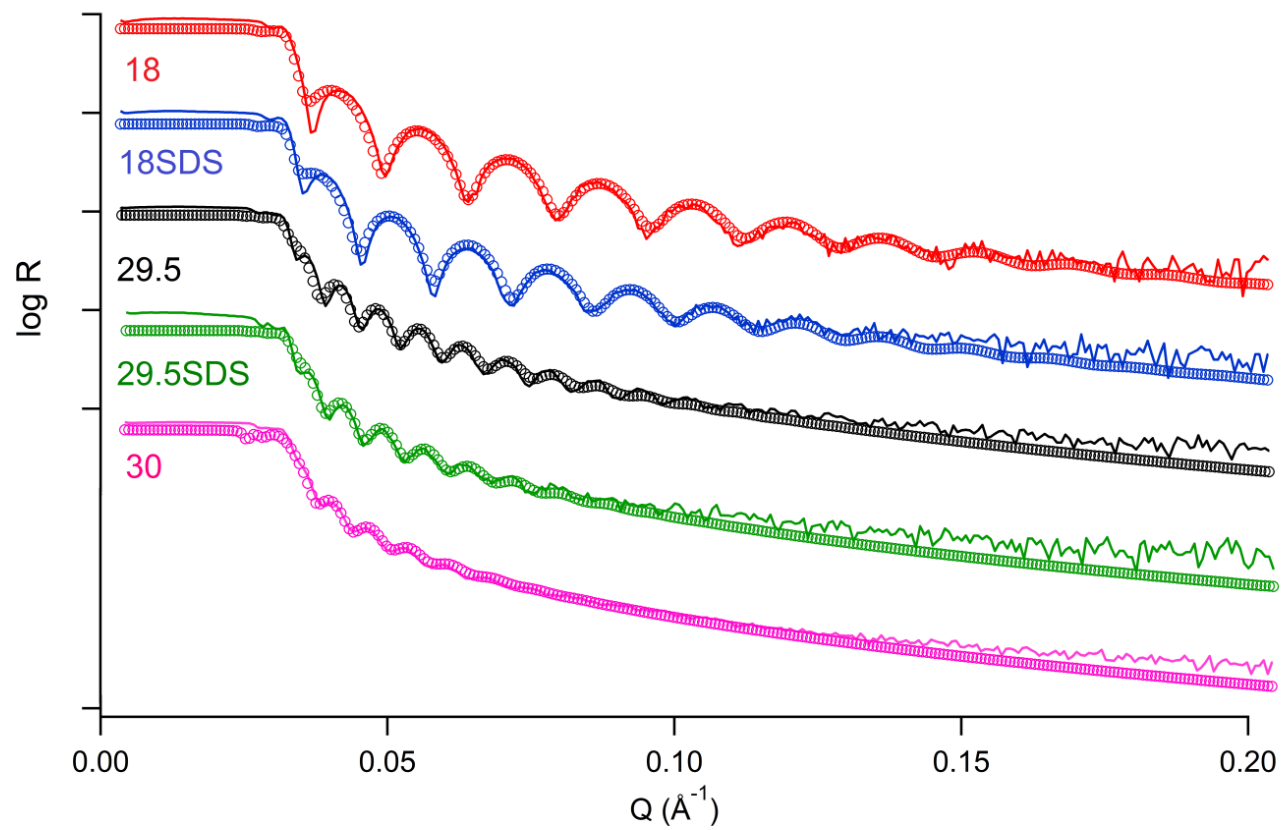


**Figure B.4 :** XRR data and fit of PEM samples measured at ambient conditions. Dots indicate fits and lines are experimental data.

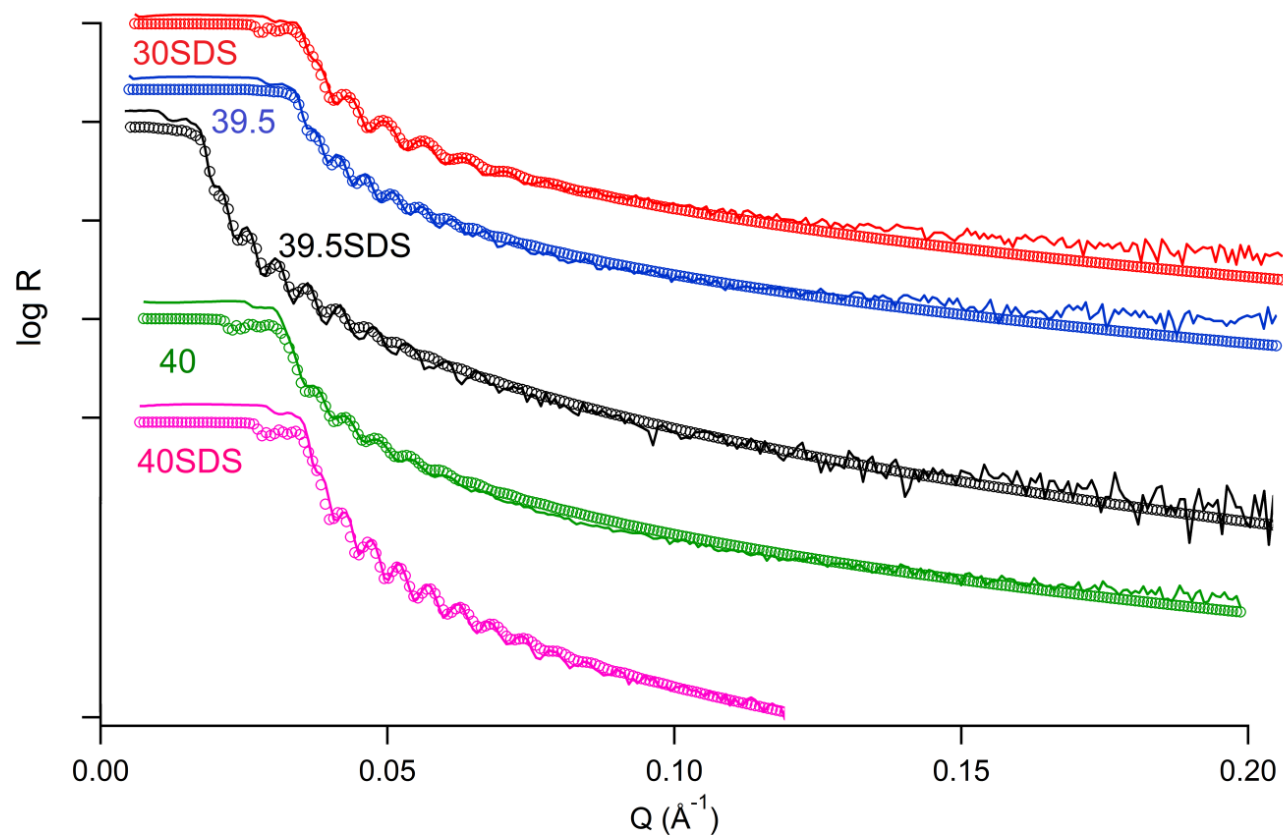


**Figure B.5 :** XRR data and fit of PEM samples measured at ambient conditions. Dots indicate fits and lines are experimental data.

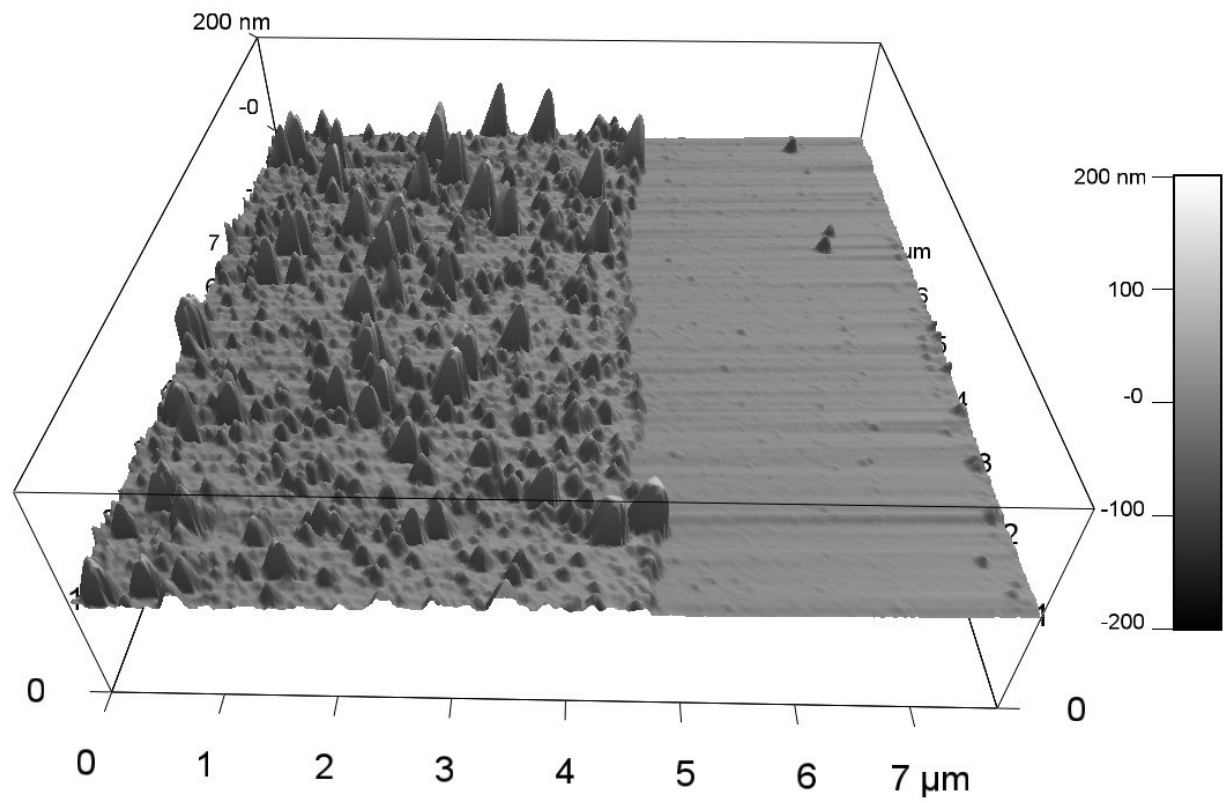


**Figure B.6** : Surface of a chitosan PEM film, imaged by AFM. Right hand side of the image is the Si wafer, left side is the PEM.

APPENDIX C: SUPPORTING INFORMATION FOR CHAPTER 5

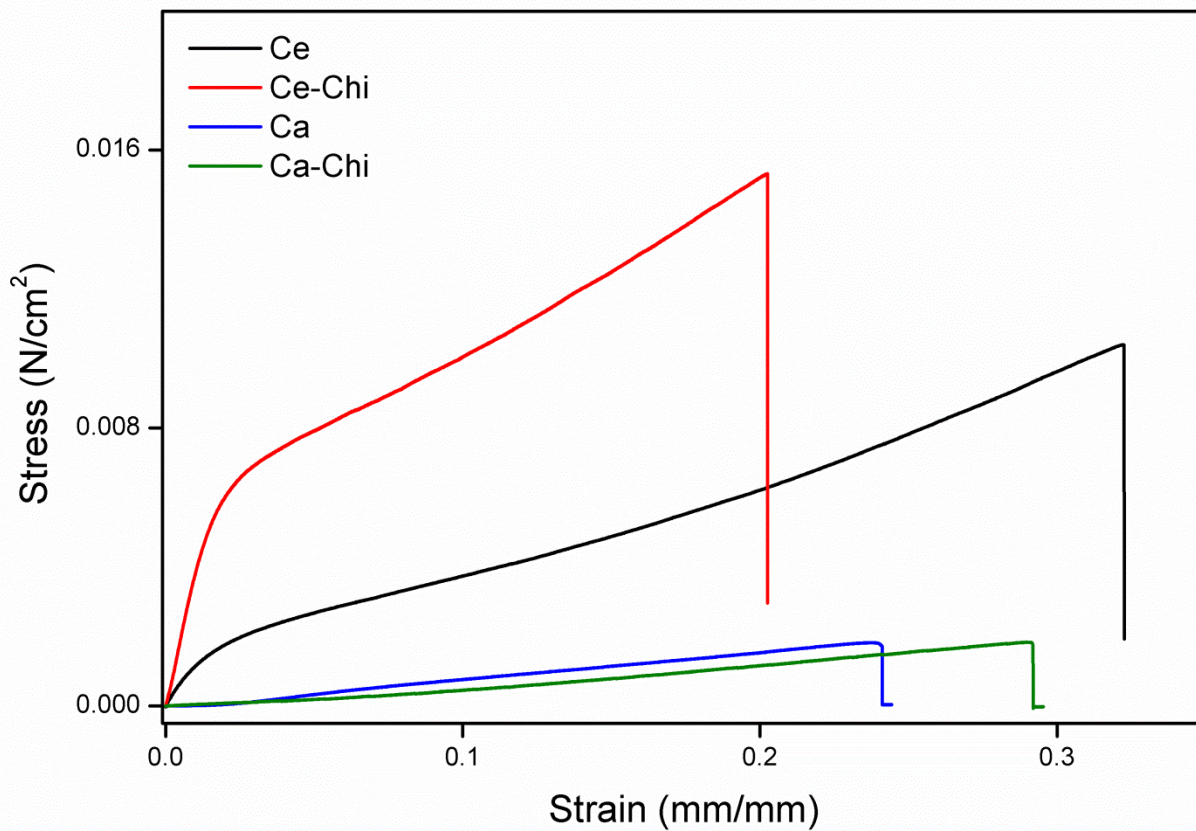


Figure C.1 : Stress-strain curves for equally shaped film samples.

## PUBLICATIONS AND PRESENTATIONS ON THE THESIS:

- **Paper I: H. Kaygusuz, G.A. Evingür, Ö. Pekcan, R. von Klitzing and F.B. Erim** 2016: Surfactant and metal ion effects on the mechanical properties of alginate hydrogels, *International Journal of Biological Macromolecules*, 92, 220-224
- **Paper II: H. Kaygusuz, S. Micciulla, F.B. Erim and R. von Klitzing** Effect of anionic surfactant on alginate-chitosan polyelectrolyte multilayer thickness, *under review*
- **Paper III: H. Kaygusuz, E. Torlak, G.A Evingür, İ. Özen, R. von Klitzing and F.B. Erim** Antimicrobial cerium ion-chitosan crosslinked alginate biopolymer films: A novel and potent wound dressing, *International Journal of Biological Macromolecules*, accepted.
- **H. Kaygusuz, F. Bedia Erim and R. von Klitzing** 2015. Alginate - chitosan multilayer films and their properties, *79th Annual Meeting of the DPG and DPG Spring Meeting*, Berlin, 15-20 March 2015.
- **H. Kaygusuz, F. Bedia Erim and R. von Klitzing** 2013. Aljinat-kitosan çoklu tabaka filmleri ve özellikleri, *19th National Liquid State Symposium*, Istanbul, 19 December 2015.

Hereby I declare that the manuscripts and this thesis were written by myself under the guidance of Prof. Dr. F. Bedia Erim Berker and Prof. Dr. Regine von Klitzing. All experiments and data analysis were carried out by myself with the following exceptions:

Paper I: Mechanical measurements and related data analysis were conducted with the support of Dr. Gülşen Akın Evingür and Prof. Dr. Önder Pekcan at Piri Reis University and Kadir Has University.

Paper II: Detailed data analysis for ellipsometry and QCM-D were performed with support of Dr. Samantha Micciulla at TU Berlin.

Paper III: Antimicrobial measurements were carried out by Dr. Emrah Torlak at Necmettin Erbakan University, Konya. Water vapor transmission rate experiments were carried out by Dr. İlhan Özen at Erciyes University. Mechanical measurements were done with the guidance of Dr. Gülşen Akın Evingür at Piri Reis University.